INFORMATION TO USERS

This manuscript has been reproduced from the microfilm master. UMI films the text directly from the original or copy submitted. Thus, some thesis and dissertation copies are in typewriter face, while others may be from any type of computer printer.

The quality of this reproduction is dependent upon the quality of the copy submitted. Broken or indistinct print, colored or poor quality illustrations and photographs, print bleedthrough, substandard margins, and improper alignment can adversely affect reproduction.

In the unlikely event that the author did not send UMI a complete manuscript and there are missing pages, these will be noted. Also, if unauthorized copyright material had to be removed, a note will indicate the deletion.

Oversize materials (e.g., maps, drawings, charts) are reproduced by sectioning the original, beginning at the upper left-hand corner and continuing from left to right in equal sections with small overlaps. Each original is also photographed in one exposure and is included in reduced form at the back of the book.

Photographs included in the original manuscript have been reproduced xerographically in this copy. Higher quality 6" x 9" black and white photographic prints are available for any photographs or illustrations appearing in this copy for an additional charge. Contact UMI directly to order.

UMI

A Bell & Howell Information Company
300 North Zeeb Road, Ann Arbor MI 48106-1346 USA
313/761-4700 800/521-0600

PART 1: RAMAN SPECTROSCOPY OF MASS SELECTED METAL CLUSTERS
AND
PART 2: CONFORMATIONAL STUDIES OF TURNS IN PEPTIDES BY VIBRATIONAL CD

By

Qinwei Zhou

A dissertation submitted to the Graduate Faculty in Chemistry in partial fulfillment of the requirement for the degree of Doctor of Philosophy, The City University of New York.

1996

This manuscript has been read and accepted for the Graduate Faculty in Chemistry in satisfaction of dissertation requirement for the degree of Doctor of Philosophy.

NOV 6, 1995
Date

Chair of Examining Committee

Nov. 7, 1995
Date

Executive Officer

Supervisory Committee

The City University of New York

ABSTRACT

PART1: RAMAN SPECTROSCOPY OF MASS SELECTED METAL CLUSTERS AND PART2: SYNTHESIS AND CONFORMATIONAL STUDIES OF TURNS IN PEPTIDES BY VIBRATIONAL CIRCULAR DICHROISM

By

Qinwei Zhou

Adviser: Professor Max Diem and Professor John Lombardi

This dissertation includes two parts of work which were done in two different labs. The first part is focused on Raman Spectroscopy of Mass Selected Metal Clusters in Argon Matrices. The second part is concentrated on Synthesis and Conformational Studies of Turns in Peptides by Vibrational Circular Dichroism.

A principal goal of metal cluster research is a better understanding of the structural properties of these species as a function of cluster size and metal type. In order to achieve this, an ion sputtering cluster deposition source has been successfully built in the lab. Three different clusters (Vanadium dimers, Niobium dimer and Ziroconium dimer) in argon matrices have been studied by both Raman Spectroscopy and Scattering Depletion Spectroscopy. We have observed the first absorption spectra of these dimers which are free from interference from atoms or

higher mass clusters. Raman spectra obtained throughout the blue-green and red region are in good accord with the optical absorption data.

Vibrational spectroscopy has become one of the common techniques to determine the structure and dynamics of biological molecules and to monitor their conformational changes. Several model peptides are designed with two cysteine residues on both N- and C- terminals which can be cyclized by ringclosure of the S-S disulfide bond between cysteines. Both linear and cyclized peptides are synthesized by step-wise Solid Phase Peptide Synthesis. Conformational changes of these small peptides with both different amino acids between two cysteines and various chemical environment are monitored by VCD. The variety of solvent properties can be used as a probe, which can help us to understand the driving force in peptide folding. The conformation difference between linear and cyclized peptides have been studied. Furthermore, the factor whether D- or L- amino acid residue in peptides have been proven to play a major role in determining the conformation of peptides. Structures from such an analysis consist with that from other techniques. The computed spectra based on Coupled Oscillator Model further confirmed structures from observed VCD.

To my wife, Peixian Lu

Her encouragement made the completion of this work possible.

To my little son, Charles, L. Zhou

And to my father, Goofu Zhou and mother, Fengyi Chen as well as my mother in law, Xiuying Jiang

And to my sister and brother

for their encouraging words and help.

Acknowledgments

I wish to express my appreciation to Professor Max Diem, my mentor, for his guidance throughout the entire work, and for his encouragement and his patience during my transferring from City college.

I would especially like to thank Dr. Nicholas Giorgio, my boss in Imclone Systems Inc., without his help, I would never achieve this goal. I also like to thank Mr. John Ye in United Biomedical Inc. for his support during the early stage.

I would like to express my respect here to Prof. John Lombardi and Prof. Derek Lindsay, my former mentor in City College of New York. Under their friendship and guidance, I entered the United States to pursue my further education.

I also like to thank my friend Dr. Dingjiang Liu for his help in NMR measurements and my colleagues Dr. Zhendong Hu, Dr. Sheryl Birk, and Mr. Luis Chiriboga and Ismailu Agbaje.

Finally, I really want to thank Dr. Ping Xie, his great support and help during my entire research on this project. All of that will definitely be remembered.

PREFACE

" It is indeed a pleasure to acquire knowledge and, as you go on acquiring, to put into practice what you have acquired. A greater pleasure still is when friends of congenial minds come from afar to seek you because of your attainments. But he is truly a wise and good man who feels no discomposure even when he is not noticed by man. "

Confucius

A central goal of biochemistry has been to obtain an understanding of the physical/chemical basis for biological activity and information transfer in biological systems. This information is dependent on conformational and dynamic properties: conformation because biological systems exist in 3D chiral space; dynamics because conformational changes in time are essential to living systems. Thus various spectroscopies (Raman, CD, VCD, IR, NMR), X-ray crystallography, model building, and computational methods to examine peptide conformation and dynamics, as well as binding and bioassay data (thermodynamics and kinetics) are used to provide insights into the conformational, topographical, and dynamic properties that are critical to molecular recognition and biological activity. In recent years, there has been tremendous interests in cyclic peptides which are conformational constraint by stabilization of secondary structure. There are five major advantages: 1) improved metabolic stability in cells;

2) better receptor selectivity;

3) controlled bioavailability;

4) ease of conformational investigation;

5) moldeling / "locking" secondary structure in protein folding.

It goes without saying that chemical synthesis is of central importance in peptide research. The remarkable developments in peptide chemistry during the past 50 years, especially the developments of solid-phase synthesis pioneered by Merrifield (1) and its optimization, makes peptide chemistry the most quantitative synthetic methodology available to organic chemistry.

One of essential differences between chemistry of living and nonliving systems is the greater structural complexity of biological macromolecules. We shall not unravel chemistry of life in molecular detail without knowing the structure of biological macromolecules, especially the proteins at atomic resolution.

The structure of protein has not yielded a simple and all-embracing explanation of the relation between protein structure and function. We know the three-dimensional structure of some 400 different proteins, yet we are still unable to formulate a set of general rules that predict three-dimensional structure from amino acid sequence of its polypeptide chains. It is perhaps not surprising that protein structures are so much more complex than those of DNA. Proteins are built up from twenty different amino acids compared with the four nucleotides of DNA. Moreover, proteins fulfill a much wider range of biological functions than DNA, and functional diversity dictates structural diversity.

By comparison with molecular genetics, progress in research on protein structure has been painfully slow, not only because of the great diversity that protein structures have, but also because of the simple technical problem of obtaining protein crystals. Until now there has been no technique that is perfect for structural studies of peptides and proteins. The best way to do that is by using multiple techniques.

The varieties of bioactivities of proteins or peptides is due mostly to the varieties of their conformations in different environments. These conformations exhibit chirality, which may be monitored by measurement of vibrational optical activity (VOA). Natural optical activity is one of the most structurally sensitive molecular properties available for spectroscopic probing, and, as such its measurement has been exploited extensively in stereochemical analyses. Most spectroscopic techniques (for example, infrared and Raman spectroscopies) sense detailed aspects of molecular geometry only via perturbation of energy levels and selection rules. However, molecular optical activity originates as a direct consequence of the geometrical arrangement and interaction of atoms in a molecule. In other words, the observable optical activity can be considered to have a first-order dependence on the molecular geometry. In recent years, the standard technique for assessing optical activity has been circular dichroism(CD) spectroscopy, or measurement of the differential absorption of left and right circular polarized light ($\Delta\varepsilon = \varepsilon_L - \varepsilon_R$). Circular dichroism is related to the previously used measurement of optical rotatory dispersion (ORD).

Conventional CD is a study of transitions to excited electronic states only a few of which, such as the $\pi^* \leftarrow \pi$ and $\pi^* \leftarrow$ n of aromatics and carbonyls, are accessible for UV-CD in proteins and nucleic acids. These transitions usually also involve overlapping, broad, featureless spectral bands that consequently have interfering CD signals. This interference has compromised the results, for example, in cases where aromatic side chains provide a significant contribution to the spectrum.

In the vibrational region of the spectrum, infrared and Raman transitions are typically much better resolved and are more straightforward to assign and interpret than are electronic transitions. The nature and polarization of various characteristic vibrations have been established firmly in many cases. Extensive

infrared and Raman studies have demonstrated that certain spectral features are characteristic in frequency or intensity for expected structural aspects of either proteins or nucleic acids. However, in ordinary infrared and Raman spectroscopies, the spectral differences between related structures are quite small; so, even though a great amount of spectral detail is available, sensitivity to conformational changes is limited.

Vibrational circular dichroism studies combine the advantages of each of these techniques by providing the detail of infrared data with the added conformational sensitivity of CD. The extension of measurements of circular dichroism into the infrared region has been a long-sought goal for many scientists. It utilizes the combination of the sensitivity of CD and the specificity of infrared spectroscopy to solve a variety of problems in molecular stereochemistry. Technical obstacles made the goal impractical until the early 1970's. The infrared circular dichroism became reality, thanks to technical advances on several fronts, such as highly sensitive IR detectors, personal computers and, especially, photoelastic modulators in the IR region.

Biological molecules such as peptides, proteins, oligonucleatides and others usually retain their biological activity only in solution, in most cases, in water. Therefore, it is very important to get to know the solution conformation of these molecules. But unfortunately, people have much more knowledge of molecules in gas phase and solid phase than in solution. This is also true in metal clusters. The two extreme, the free atom and the bulk metal are quite well understood, much less is known about the transition region in between which is cluster. We should not attempt to solve the problems in these fields, but rather to be able to participate in these research areas. We hope that this dissertation can serve as a building block to the fields if possible.

The research project in this dissertation has divided into two parts. The first part mainly deal with the design, construction and testing of the Mass Selected Cluster Deposition Apparatus in CCNY. Absorption and Raman Spectra of various metal dimers have been studied in that system. The second part is concentrated on design, synthesis and conformational study by VCD of small peptides which are both linear and cyclized.

This thesis contains two parts and six chapters. Chapter one summarizes the absorption and Raman spectroscopy of mass selected metal clusters in argon matrices which were done in CCNY. Chapter two mainly discusses the peptide synthesis by SPPS and purification by HPLC which were done both in United Biomedical, Inc. and Imclone Systems, Inc.. In chapter three we focus on the theoretical background of optical activity and computation models of circular dichroism which is the "Coupied Oscillator Model" in this thesis. We also concentrate on the instrumental aspect of vibrational circular dichroism (VCD). This chapter contains the discussion of circular polarized light, photoelastic modulator and the measurement of VCD.

In chapter four, five, and six, we deal exclusively with the applications of conformational studies of peptides, especially with that of small peptides. The model peptides, tetramers (Cys-Pro-Xxx-Cys), trimers (Cys-Xxx-Cys), and octamer (Phe-Cys-Phe-Trp-Lys-Thr-Cys-Thr) are specifically designed peptides that all have two Cys in both C-terminal and N-terminal which can be covalently forced into a turn. The molecules are forced into a turn by formation of an internal sulfur- sulfur linkage between the two cysteines. These typical examples show that VCD is significantly sensitive to conformations and their changes when peptides are in different chemical environments. The VCD is an enormously sensitive tool for monitoring the conformation of peptides and proteins.

REFERENCES

I. Shan S. Wong, (1991) " Chemistry of protein conjugation and cross-linking " CRC PRESS; NY.

II. E. Atherton and R. C. Sheppard, (1989) " Solid phase peptide synthesis, a practical approach " IRL PRESS; Oxford.

III. Max Diem,(1993) " Introduction Modern Vibrational Spectroscopy" John Wiley and Son,-Interscience; NY.

IV. Stinson, S.C., (1985) *Chemical & Eng. News*, Nov. 11, 21.

V. Applequest, (1987) *J., American Scientist*, 75, 58.

VI. Robert C. Bohinski, (1987) " Modern concepts in Biochemistry " Allyn and Bacon; Boston.

TABLE OF CONTENTS

Chapter Two: Synthesis and Modification of Peptides

Chapter Three: Optical Activity of Molecules and Vibrational Circular Dichroism

Chapter Four: Conformational Studies of β-Turns in Cyclic Peptides by Vibrational CD

List of Tables

List of Figures

Abbreviations

AC- alternating current

CD - circular dichroism

COM - coupled oscillator model.

CPL - circularly polarized light.

DC - direct current.

ESR - electron Spin Resonance

FT - Fourier transform.

HPLC - high performance liquid chromatography.

IR - infrared spectroscopy.

LD - linear dichroism.

PEM - photoelastic modulator.

PLL - poly-L -lysine.

PMT - photomultiplier tube

SDS - scattering Deletion spectroscopy

SPPS - solid phase peptide synthesis

VCD - vibrational circular dichroism.

Symbols

$A(\nu)$ - absorbance of sample.

$A_+(\nu)$ - absorbance of sample toward right CPL.

$A_-(\nu)$ - absorbance of sample toward left CPL.

C - concentration, in mole/ L.

D - dipole strength or dipole moment.

g - anisotropy, or dissymetric factor.

$I(\nu)$ - light intensity.

$J_n(x)$ - n th order Bessel function.

k - light wave vector, $k = (2\pi\nu/c)\varepsilon_K$

l - sample cell pathlength.

m - magnetic dipole operator.

m_j - mass of particle j.

p_j - momentum of particle j.

Q - nuclear coordinates.

q - electron coordinates.

R - rotational strength.

r_j - position of particle j.

$V(\nu)$ - signal output of detector.

$V_{DC}(\nu)$ - transmission signal which is not modulated by PEM.

$V_{AC}(\nu)$ - signal modulated by PEM.

$\varepsilon(\nu)$ - molar extinction coefficient, L. $mole^{-1}.cm^{-1}$.

ε_U - unit vector in direction U.

λ- light wavelength.

ν- light frequency, c / λ in Hz.

μ- electric dipole operator.

θ - initial phase of light.

Θ- quadruple transition moment.

Ψ - molecular wavefunction.

PART 1

CHAPTER ONE

RAMAN SPECTROSCOPY OF MASS SELECTED METAL CLUSTERS IN ARGON MATRICES

1.1 INTRODUCTION:

The nature, importance and potential applications of metal clusters are issues attracting wide attention by a large number of people working in quite diverse areas of research. This is especially evident from a lot of specialized symposia [1-1,2,3,4,5] and review articles [1-6,7,8,9], where contributions have ranged from nuclear and solid state physics through materials science, surface science and catalysis. Thus, while the two extremes, the free atom and the bulk metal are quite well understood, much less is known about the transition region in between. One experimental approach (more favored by applied researchers) involves growing increasingly smaller particles and looking for the appearance of "quantum size" effects. A second, complementary method (adopted first by chemists) is to start with the atom and then synthesize progressively larger cluster sizes, attempting to find the "onset" of bulk properties such as band structure, plasma resonances, ionization behavior, phase transitions, crystalline habit. From the industrial views, in order to fully understand the mechanism of catalysis, therefore the process can

be manipulated, one has to understand the structure of catalyst in atomic scale i.e. clusters. This will be described more detailed later on.

Such investigations raise a host of rather intriguing questions. How in detail does the progression from atom through molecule to macroscopic sample take place? In what ways do the molecular and solid state descriptions of matter merge? At what size does a metal cluster think it is a solid? Do clusters possess special properties (e. g. shell and "supershell" structures), not to be found in molecules or bulk materials? Might such properties be of practical importance, as for instance in ultraminiaturized electronic circuits? Could particular molecular arrangements, observed in cluster beams be a means of manufacturing macroscopic components or materials, for example as sources for epitaxial growth? Can nanophase materials and quantum dot devices be assembled using clusters or even on an atom-by-atom basis? Particularly exciting are the Fullerene molecules, first characterized by molecular beam studies but recently synthesized on macroscopic scale[1-4]. Possible applications for this new allotrope of carbon include superconductivity, lubrication, energy storage devices, composite materials and catalysis.

Parallel to and interactive with these more fundamental concerns has been a search for applications of these novel compounds. In fact, much of the early interest in cluster chemistry was driven by the realization that catalytic behavior is

related largely or in part to the properties of small metal particles[1-10]. The majority of present day industrial catalysts are heterogeneous in nature. Often these consist of small particles supported on an inert substrate. In many cases the active site may be a molecular sized cluster or "raft". For certain "demanding" reactions, catalytic activity is markedly improved as the degree of dispersion (ratio of atoms present in the surface to the total number of atoms) is increased[1-11,12]. This effect arises not just from an increase in surface area, but also because small metal particles (< 50 Å) show a much greater activity than do larger particles. Certain bimetallic catalysts have a dispersion approaching unity, with particle sizes as small as 5 -10 Å [1-11]. Very recently [1-13], a Pt_3Ru_6 cluster complex has been shown to be an effective catalyst for hydrogenation reactions. Small Ag and Au clusters are essential to the photographic process. These latter species are formed photolytically and subsequently act as catalysts in the development of photographic materials. It has been demonstrated that approximately four atoms of silver and two atoms of gold constitute the minimum cluster size for effective catalytic behavior[1-14]. A related effect is the observation[1-15] that smooth, perfectly grown Pt surfaces are relatively inactive as catalysts. However, Pt surfaces prepared with a large number of kinks, terraces and other irregularities show enhanced activity. It is not, therefore, the structure of the bulk solid or whole crystalline plane which is important to study. Rather, it is the nature of the imperfections on the surface, a class of features which in many ways mimic small metal clusters. As models for chemically active sites, small metal clusters appear as a common theme to surface

science, to heterogeneous catalysis and to the properties of polynuclear organometallic compounds. Most recently, a new discovered Bose-Einstein condensate state will have a lot of influence to the cluster researches.

While it is relatively easy to produce and mass analyze cluster beams, direct structural information has been much harder to obtain. With some important polyatomic exceptions, vibrationally resolved spectra have only been obtained for a relatively few diatomic metal molecules[1-7]. The principal difficulties are: (1) distinguishing the spectral features of one cluster species from another, (2) rotationally and/or vibrationally cooling theses complex molecules and (3) the apparent widespread availability of non-radioactive channels which has largely limited conventional fluorescence techniques to diatomic species. Owing to their relative insensitivity, direct absorption measurements have not generally been applied to gas-phase cluster studies. Two photo ionization (TPI) techniques combined with supersonic expansion can, in some cases, overcome these difficulties[1-1]. Complicating these experiments are spectral congestion (the " vibronic scoup ") and predissociation. The latter phenomenon can be taken advantage of by recording photofragmentation and photodepletion spectra[1-1,16], or by monitoring atomic emission features as in the case of the bound-free transitions[1-8] observed for Na_3 and K_3. In cases where the parent mass peak is not observed, photodepletion or TPI spectra may no longer be mass selective. It should be noted that most of the reported spectral constants pertain to cluster

excited states and that ground state information is generally available only through the observation of hot bands.

Most early spectroscopic studies of metal clusters employed matrix isolation methods (often in conjunction with absorption spectroscopy) which permit the preparation of stable samples containing large numbers of clusters at cold temperatures[1-8]. Matrix Raman and Electron Spin Resonance (ESR)[1-6,7] techniques are most successful in determining cluster structures and spectroscopic constants. Thus, Raman spectra have been reported for[71-78] Li_3, Cu_3, Ag_3, Ni_3, Pb_3, Cr_3, Sc_3, Mn_3 and Sb_4. Well resolved vibrational progressions have been analyzed to give accurate spectroscopic constants for these cluster molecules. Since different n-mers were generally identified by their behavior under annealing or by intensity versus concentration studies, there was often considerable controversy as to the spectral carrier, even for sizes as small as dimer. Only with the recent advent of mass-selected cluster deposition techniques, has it become possible to overcome these assignment problems[1-17]. The importance of mass-selection is illustrated by the elegant experiments of Honea et al[1-18], who have recently reported matrix Raman measurements on Si_4, Si_6 and Si_7 and are able to predict cluster geometries by comparison of their observed spectra with frequencies from calculated structures.

1.2. EXPERIMENTS:

A principal goal of metal cluster research is a better understanding of the structural properties of these species as a function of cluster size and metal type. One means of achieving this goal is through cluster vibrational spectra which directly probe properties such as bending and stretching frequencies, force constants, bond energies, vibronic interactions, etc. Commonly used techniques are absorption, excitation, fluorescence, and Raman spectroscopy. Most often these measurements are carried out in conjunction with matrix isolation methods which ensure large numbers of absorbers at relatively low temperatures. Moreover, the vibrational frequencies of matrix isolated species are quite close to the corresponding gas-phase values, when known[1-19]. However, matrix absorption spectra do not usually show vibrational structure and many, if not most, cluster species have very low fluorescence quantum yields. Raman spectroscopy, by contrast, has proved to be a powerful technique for obtaining vibrational information on small metal clusters[1-8]. Thus, preresonance and/or resonance Raman spectra have been reported for numerous metal diatomics and for about eight triatomic cluster species [1-8]. The principal problem with such measurements, especially for the larger clusters, is the assignment of the carrier of the Raman spectrum. As described elsewhere[1-17,20,21,22], assignment problems can be overcome by preparing monodispersed (or at least highly enriched) matrix samples, using a mass-selected cluster ion beam as deposition source. These studies, however, exploited the fairly sensitive detection techniques of excitation and fluorescence

spectroscopy. We will demonstrate the feasibility of Raman measurements on a matrix sample (V_2 in Ar) prepared by the mass-selected ion deposition technique.

1.2.1 CLUSTER DEPOSITION METHOD:

The cluster deposition source, shown schematically in Fig.1.1, is similar in several aspects to that described by Harbich, Lindsay et al. in refs. 1-17 and 20. An intense (typically 10 mA at 25 keV) argon ion beam from a " CORDIS " ion source (Rokion Ionenstrahl-Technologie, Darmstadt, Germany)[1-23] sputters vanadium cluster ions from a water cooled, vanadium target (Aesar, 99.5%). The primary beam was collimated by an 8 mm aperture (denoted A1 in Fig.1.1) which also serves to separate the ion source from the rest of the apparatus. The ion source was pumped indirectly, through and around A1, by a 500 l/s turbomolecular pump (Balzers TPU 510) which supports the specially designed sputtering chamber (MDC Vacuum Products). The 50^0 inclination between the primary and secondary beam lines correspond closely to the optimum ejection angle for material sputtered from a metal surface[1-24].

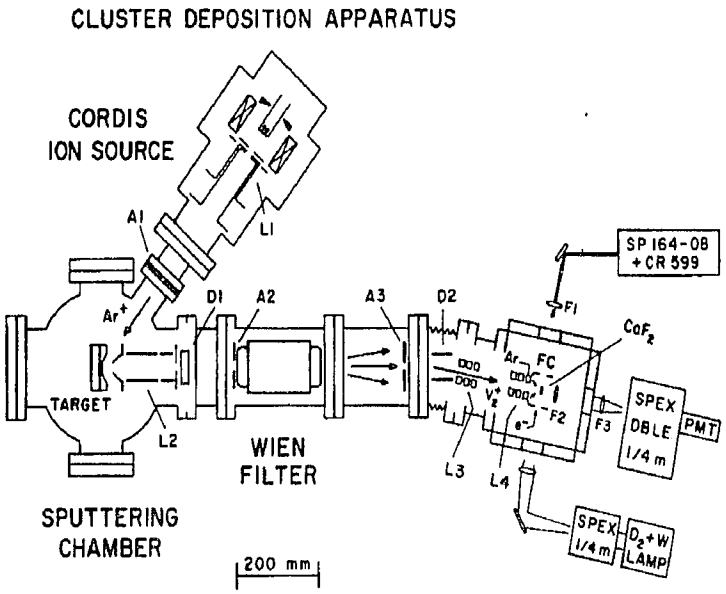

FIG. 1. Schematic of the cluster deposition source.

Fig.1.1. Schematic of the cluster deposition source.

Cluster cations sputtered from the target (normally maintained at 700 V) were extracted with a modified Colutron model 200-B lens system (L2 in Fig.1.1). The secondary ions were mass selected by a Wien filter (Colutron 600-B) in conjunction with an approximately 175 mm long drift space and a 6.5 mm diam aperture (A3). For the deposition experiments described here, the Wien filter was operated at a magnetic field of about 2000G (corresponding electric field: 130 V

for V_2^+) which gave a resolution (M/ΔM) of approximately 6-7, i.e., sufficient to

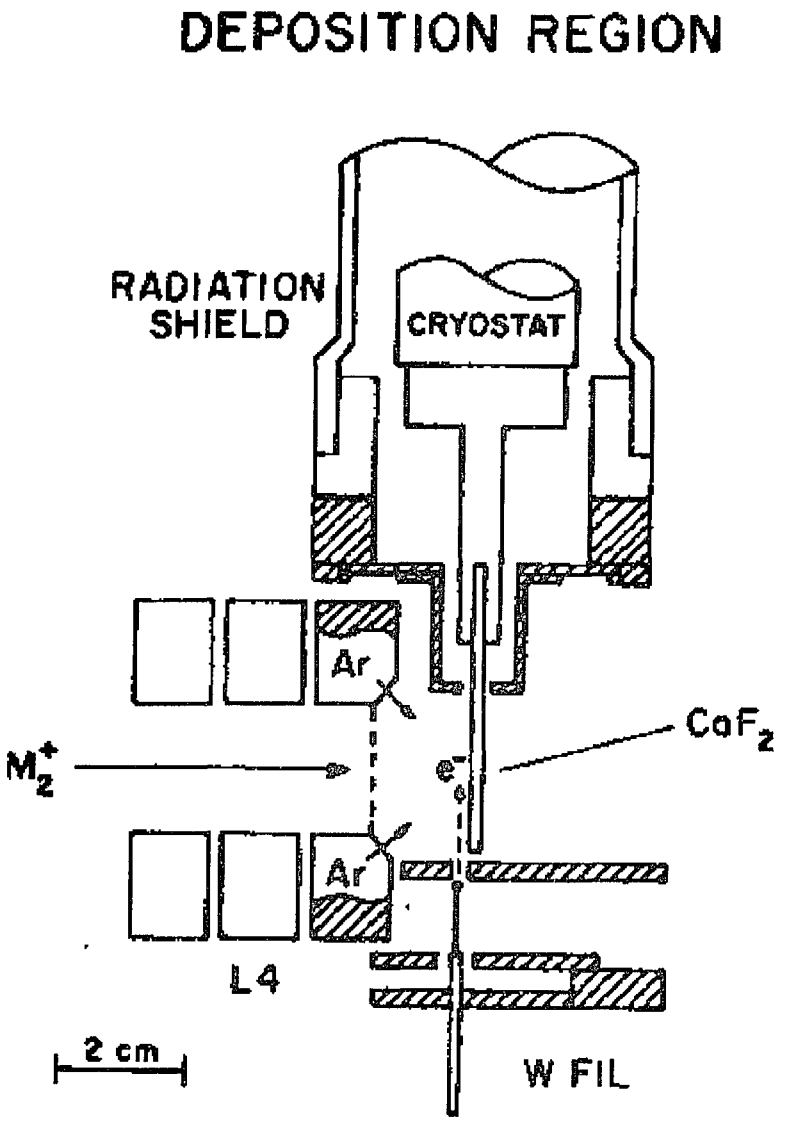

Fig.1.2. Detail of the deposition region.

separate the dimer from the atom and trimer and to ensure that oxides are not present. After mass separation, the dimer ion beam was bent by 10^0 (using

deflector plates D2, mounted in a short bellows section) and then guided to the deposition region by two einzel-like lenses L3 and L4. The deposition chamber consists of an 8 in. conflate cube, (MDC Vacuum Products) and is pumped by a second 500 l/s turbomolecular pump. The 10^0 bend separates dimer ions from neutral sputtered products, whose flux may be comparable to or greater than that of the ions. By depositing neutral silver clusters both with and without a 10^0 bend, we estimate that only about 0.1% of the neutral species are deposited in our experiments.

The deposition region is quite similar to that described elsewhere[1-17]. Vanadium dimer ions were codeposited with Ar and electrons on a 45 x 8 x 1 mm polished CaF_2 plate (Maris-Delfour, Paris) mounted (using Wood's metal and an In gasket) to a closed cycle cryostat (APD Displex, 204SL/DMX-6). The cryostat temperature was measured by a Si diode in conjunction with a Scientific Instruments model 5500 temperature controller. Deposition temperatures were typically about 20 K. The CaF_2 substrate was largely enclosed by a "Faraday cage" (denoted FC in Fig.1.1), composed of two side plates (with openings for optical measurements), the lower half of the cryostat radiation shield, the electron source, and the last lens element of L4 which was closed by a 90% transmitting Ni mesh. This same lens element also incorporates a coaxial injector ring (eight 0.5 mm diam holes) for the matrix gas (99.9995% Ar, Alphagaz). The electron source consisted of a philips electron microscope filament (0.13 mm tungsten) on a

ceramic base (Ladd Research Industries). This assembly was enclosed by a stainless steel box having an 8 x 1 mm slit positioned so that the electrons were introduced about 1-2 mm in front of the CaF_2 substrate. In order for sufficient, low-energy electrons to reach the matrix target, the filament was biased at -3 V with respect to the Faraday cage.

Ion currents could be monitored using a Faraday plate situated near the deposition window. Since the cryostat is rotatable, the Faraday plate and the substrate could easily be adjusted in order to measure ion currents, to prepare matrix samples, or to record optical spectra. Even though the matrix and CaF_2 substrate are insulators, the potential in the deposition region can (to a large extent)[1-4] be defined and so controlled by the voltage applied to the surrounding Faraday cage. The difference in voltage (V_{dep}) between the target and Faraday cage determines the dimer deposition energy (eV_{dep}), which was held at approximately 10 eV in the experiments described here. The kinetic energy distribution of the arriving ions, measured by applying a retarding potential to the Faraday plate, was centered close to $eV_{dep} = 0$ eV had a halfwidth of about 8 eV, i.e., comparable to that reported for sputtered ionic particles [1-25]. For example, typical mass-selected currents (for 700 eV ions; beam area about 1 cm^2) were: V^+ (110nA), V_2^+ (70nA), and V_3^+ (10nA). The dimer fragmentation may be estimated by comparing the intensities of atomic excitation features in a dimer deposition with those obtained from depositions of the atom under similar conditions. By this yardstick, we

estimate that 10-15% of the vanadium dimers (neutral bond energy, 2.8 eV)[1-26] are fragmented at eV_{dep} = 10 eV, a value slightly below that found for Ag_2 (neutral bond energy, 1.7 eV)[1-27] deposited in Kr matrices[1-22]. The ratio of electron current to dimer current (as measured on the Faraday plate) was generally about 3:1. Since the dimer ionization potential (6.1 eV)[1-28] is relatively large compared to the bond energy (2.8 eV)[1-26], we suppose that the neutralization step takes place on, or very near, the matrix surface.

Matrices were grown at around 6 μm/h with an Ar : metal dilution ratio of approximately 10^4 : 1, i.e., sufficient to ensure that the dimers remain well isolated both from each other and (more difficult to achieve) from any impurity species. During deposition, the partial pressure of H_2O (the dominant background gas) in the cryostat chamber was generally about 5 x 10^{-9} Torr, as measured on a residual gas analyzer (Leybold-Inficon, Quadruvac Q100). This translates into a better than 95% probability that a dimer will be surrounded by at least 12 nearest-neighbor argon atoms.

1.2.2 RAMAN SPECTROSCOPY:

Although matrix samples may be interrogated by excitation and fluorescence spectroscopy[1-17], transition metal clusters (apart from a few examples e.g. Group IB clusters and Mo_2)[1-29] show a notable lack of fluorescence. Accordingly Raman spectroscopy is a relatively sensitive probe of these species,

provided that the exciting laser is resonant with an absorption band[1-30]. As a consequence, it is first necessary to map out the cluster absorption spectrum (discussed in more detail below) and then to have available both a wide range of laser wavelengths and a correspondingly versatile detection system. A fixed wavelength monochromator and notch filter combination (for example) is not suitable. Raman spectra were recorded using both an Ar^+ laser (Spectra Physics, 164-08) and a dye laser (Coherent, 599-02), focused to an estimated 50u spot by a 240 mm focal length lens (F1 in Fig.1.1). The laser power incident on the sample was typically about 50 mW. Plasma lines were removed by predispersing the laser beam with a grating. Scattered light was collected at 90^0 using f/1 optics (lens F2) and focused onto the slits of a 1/4 m Spex " Doublemate " monochromator (1800 groove holographic grating) by a 200 mm focal length lens (F3) with a magnification of about 5. The monochromator (modified so as to have an adjustable middle slit) was driven by a Dell 386 computer using a data translation (DT 2817) digital I/O board. The Raman signal was detected by a cooled (Hamamatsu R943-02) photomutiplier tube (PMT), processed by an amplifier/discriminator (Uniphoton) and stored by the computer using a specially designed prescalar and the DT 2817 digital I/O board.

1.2.3 SCATTERING DEPLETION SPECTROSCOPY:

Absorption spectra are normally recorded by observing (as a function of wavelength) the light transmitted by or reflected through a matrix sample. An

alternative method, which we term " Scattering Depletion Spectroscopy " (SDS), involves detecting the light scattered at 90^0 to the incident. Thus, if the sample absorbs at a particular wavelength, the scattered light will be depleted at this wavelength and so (at least in principal) also contains the absorption spectrum of the sample. In general scattering depletion spectra are recorded as the ratio of a "reference intensity" to a "signal intensity". The latter corresponds to light scattered from the cluster-rich center of the sample, whereas the former pertains to that scattered near an edge. The absorption signal was recorded using the same detection system but with the PMT mounted directly on the deposition chamber. We find that the SDS technique is in fact somewhat more sensitive than conventional absorption measurements.

1.3. RESULTS AND DISCUSSIONS:

1.3.1 Vanadium dimers in argon matrices:

Figure 1.3 shows a typical Raman spectrum for divanadium in an argon matrix.

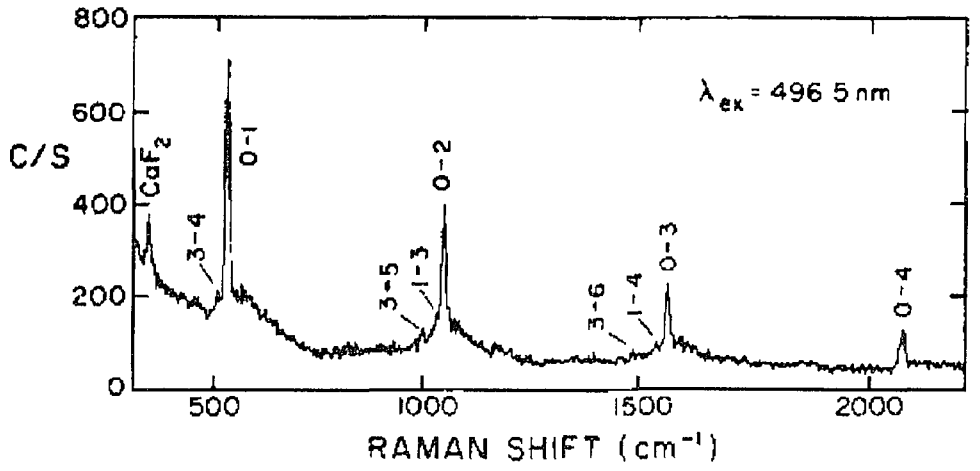

Fig.1.3 Raman spectrum of divanadium in an argon matrix at 20 K

The spectrum was acquired following a 4 hour deposition of 52 nA of V_2^+ (3 x 10^{11} dimers/sec) at a deposition energy of 10 eV. Figure 1.3 was recorded using 10 cm^{-1} resolution (200 u slits) and a "scan rate" of 2000 ms for each 3 cm^{-1} step. Raman spectra were observed throughout the blue-green region of the ion laser, as well as with dye laser scans using Rhodamine 6G. The principal features of the divanadium spectra are a progression ($\nu'' = 0 \rightarrow \nu'' > 0$) in the ground $^3\Sigma^+$ state, as previously reported by Cosse et al[1-31]. Also evident in Fig.1.3 is the Raman transition from the CaF_2 support (whose 330 cm^{-1} frequency serves as a useful fiducial mark)[1-32] and several rather weak "hot band" features which apparently arise because ground state vibrational levels other than $\nu'' = 0$ may be populated by radiative processes[1-31]. Weak features, not seen in Fig.1.3 but observed for some excitation wavelengths, probably correspond to electronic resonance Raman transitions (denoted ERR1 and ERR2 in ref.1-31) to low lying

excited electronic states in the dimer. Table 1.1 summarizes the Raman frequency data for four ion laser wavelengths. All spectra were calibrated by scanning through the corresponding ion laser line and further corrected (when possible) by comparison with the CaF_2 frequency. The Table 1 data were analyzed by standard methods to give ω_e" = 536.9 (1.1) cm^{-1} and $\omega_e\chi_e$" = 4.1 (0.1) cm^{-1} . Similar parameters were obtained using excitation wavelengths between 560 nm and 575 nm (Rhodamine 6G). These constants are in excellent agreement with those previously obtained (ω_e" = 537.5 cm^{-1} and $\omega_e\chi_e$" = 4.2 cm^{-1}) from matrices containing a distribution of cluster sizes[1-31]. Raman spectra were also obtained when vanadium dimer cations were deposited in krypton matrices, but these spectra were of poorer quality than those found for argon. The progression were less extensive, owing to a broadening of the Raman lines with increasing v", and only the fundamental transition could be measured with precision. These data give a fundamental frequency, $\Delta G_{1/2}$ = 525 (2) cm^{-1} for V_2 in Kr. It should be noted that the fundamental frequencies for both krypton and argon ($\Delta G_{1/2}$ = 528.7 (1.2) cm^{-1}) matrices are within 1% of the gas-phase value, $\Delta G_{1/2}$ = 529.5 (10)[1-15].

In conclusion, we have demonstrated the practicality of Raman measurements on matrix samples formed by depositing mass-selected cluster ions. Such experiments are currently feasible only in cases where the Raman signal is resonantly enhanced. Thus, our divanadium sample contained about 5 x 10^{15} scatterers/cm^2

Table1.1. Raman frequency shifts (cm^{-1}) for divanadium in an argon matrix.

λ_{ex} (nm)	$\nu'' = 1$	$\nu'' = 2$	$\nu'' = 3$	$\nu'' = 4$	$\nu'' = 5$	$\nu'' = 6$
496.5	526.9	1046.2	1557.2	2065.5		
488.0	528.6	1051.4	1560.6	2066.5	2566.4	
472.7			1561.2	2061.3	2557.2	
457.9			1564.6	2065.7	2562.5	3047.8
Mean(σ)	527.8	1048.8	1560.9	2064.8	2562.0	3047.8

and was excited with approximately 1 x 10^{17} photons/sec. Assuming[1-34] a normal Raman cross section of 10^{-30} cm^2 and a 1% detection efficiency, the expected Raman signal is about 5 Hz. The measured Raman intensity (Fig.1.3) is about 500 Hz, consistent with a 100-fold enhancement arising from the divanadium absorption band at 494 nm[1-35].

1.3.2 Mass-selected niobium dimers in argon matrices:

Matrix samples were interrogated in-situ using both absorption and Raman spectroscopy. The extractable ion currents which measured at 10 eV on a Faraday plate in the deposition region were: Nb^+ (60 nA), Nb_2^+ (120 nA), Nb_3^+ (30 nA) and Nb_4^+ (15 nA).

1.3.2.1 Scattering Depletion Spectroscopy:

Figure 1.4 shows a " Scattering Depletion Spectrum " (SDS) of atomic niobium in an unannealed argon matrix at 13.5K. The spectrum (recorded with a tungsten/halogen lamp) was acquired following a 2 hour deposition of 32 nA of Nb^+ (64 nA*hour) at a deposition energy of 10 eV. Fig.1.4 was recorded using 1 nm resolution and a " scan rate " of approximately 500 ms/nm. The relatively sharp features between 300 and 400 nm all arise from absorption by atomic niobium and have been reported previously[1-36]. The broad background extending from 250 - 800 nm is due to a relative small, but wavelength dependent, difference in scattering and/or collection efficiency in (see below) the reference and signal beams. The weak oscillatory structure most evident at longer wavelengths is caused by interference effects in the thin matrix sample.

The ordinate in Fig.1.4 (the "SDS signal") is the ratio of the" reference intensity " to the " signal intensity ". The latter corresponds to light scattered from a region near the center of the 8 mm wide sample, whereas the former

pertains to that scattered near an edge. Prior to recording Fig.1.4, the optical density profile of the sample was obtained by recording single beam SDS spectra as a function of

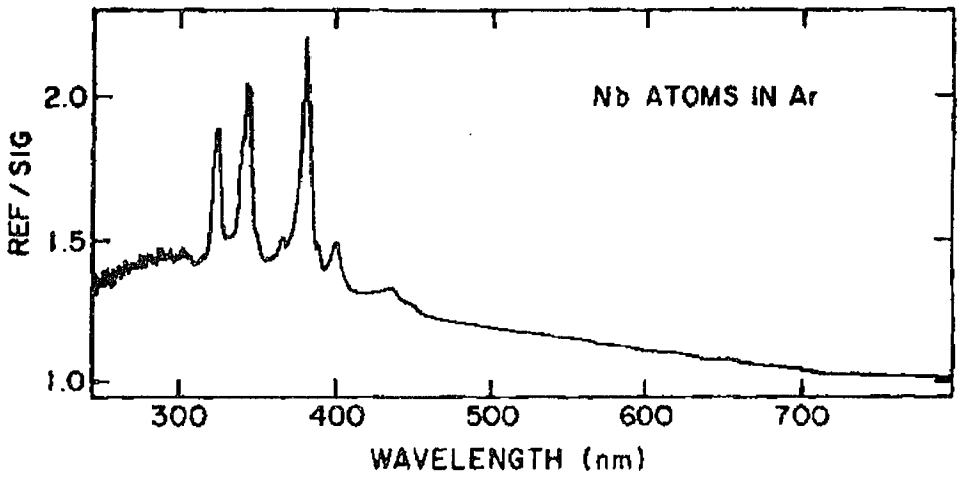

Fig.1.4 Scattering Depletion Spectrum (SDS) of atomic Nb in Ar matrix

lateral position on the sample. It is generally found that the sample is non uniform, with about twice as much absorption in the center as compared to near an edge. Thus the reference also contains absorption information but to a lesser degree than the signal. Conventional absorption spectra, using the same signal and reference positions but detecting the light transmitted through the sample, also show the same features evident in Fig.1.4. However, we find that absorption features in the scattered spectra are approximately 20 -50 % more intense than observed in transmission.

Figure 1.5 is an SDS spectrum of diniobium in an unannealed argon matrix 14K. The spectrum was obtained following the deposition of 450 nA hours of Nb_2^+ at an energy of 10 eV. The scan conditions are similar to those used in recording Fig.1.4. Since the dimer fragmentation was less than 1%, there are essentially no atomic features in this spectrum. Indeed, the presence of atomic niobium can be detected through excitation spectra which are very sensitive to atoms. Thus, although absorption spectra have been reported previously for Nb_2 clusters[1-37,38], these data were obtained from matrices containing a distribution of cluster sizes. Accordingly, all dimer features between 300 nm and about 450 nm were largely obscured by the more intense atomic transitions.

For convenience, we separate the absorption spectrum of Nb_2 into three regions. Region A covers the wavelength range 550 - 700 nm and is shown in more detail in Figure 1.6. This spectrum is of the same matrix sample but was recorded (after annealing to 28K) with a different grating in order to avoid a Wood's anomaly[1-39] which occurs near 700 nm. The feature marked " I " in both Fig.1.5 and Fig. 6 arises from a contaminant of unknown origin. Interestingly, this impurity band gives a very strong and rich resonance Raman spectrum. As shown by the stick diagram in Fig.1.6, the A region consists of two overlapping transitions: an intense, sharp feature (which we designate the A' $\leftarrow$ X transition) at

672.3 nm (14,870 cm^{-1}) and six members of a vibrational progression (denoted A ← X) which may be analyzed to give ω_0' = 426 (4) cm^{-1} with T_0 =14,720(10) cm^{-1}

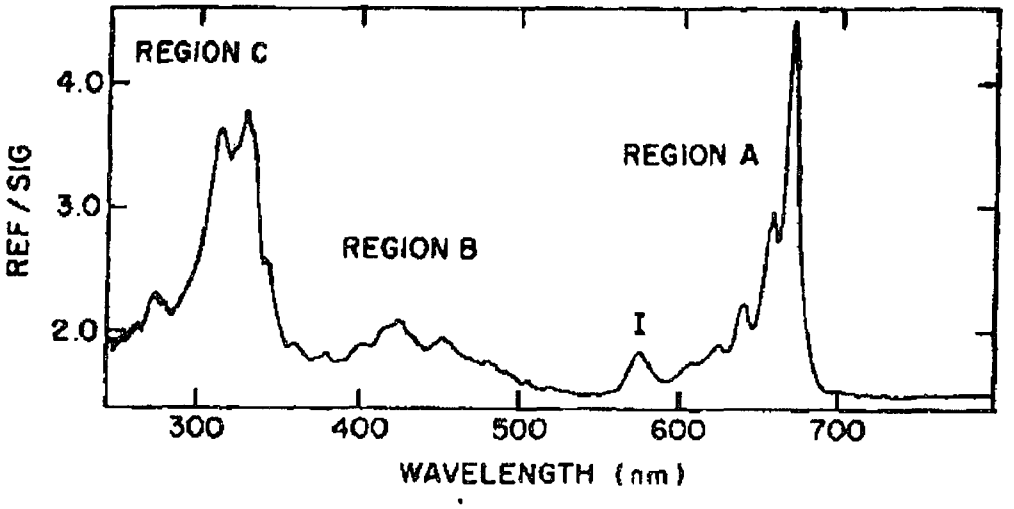

Fig.1.5 SDS of diniobium in argon, show A, B and C regions (see text)

where this latter frequency corresponds to a (nominal) origin notated v' = 0 in Fig.1.6. Diniobium transitions near 660 nm have been reported before[1-37,38], but the existence of a vibrational progression was not recognized perhaps, in the case of Kr matrices at least[1-38], due to the presence of higher mass clusters.

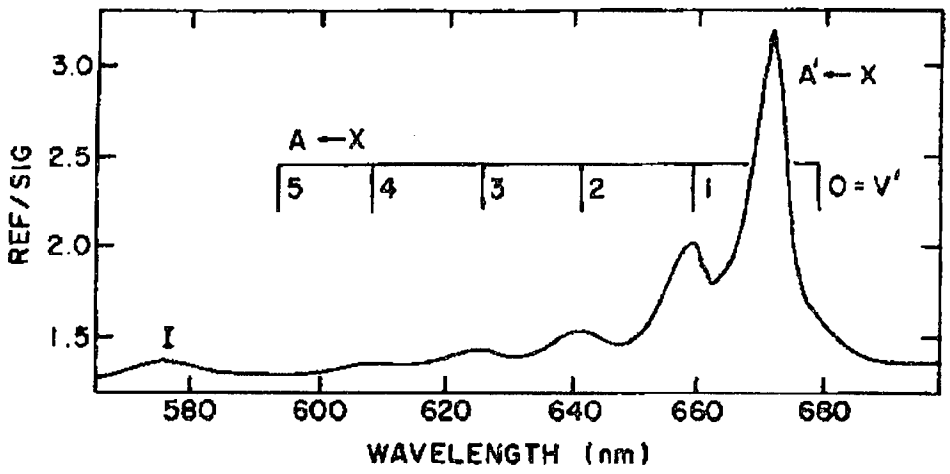

Fig.1.6 Detail of the diniobium "A region" showing two absorption bands

Region B (see Fig.1.5) extends from 550 nm to approximately 340 nm with an intensity maximum at 430 nm. Although this region of the diniobium spectrum is less easy to analyze, it appears to be somewhat structured, consisting of a series of local maxima (often doublets) spaced by around 1300 cm^{-1} . Since an energy separation of this magnitude is too large for a Nb_2 vibrational frequency, we are unable to assign this structure. Region C consists of the two intense features at 331 nm and 314 nm plus the previously reported band at 275 nm. The dividing line between Regions B and C is not clear-cut, however. Additional, but weaker, Region C transitions may be seen in absorption spectra (not shown) taken with a deuterium lamp.

1.3.2.2 Raman Spectroscopy:

Figure 1.7 shows a typical Raman spectrum for diniobium in an argon matrix. The spectrum was acquired following deposition of 200 nA hours of Nb_2^+ at an energy of 10 eV. Fig.1.7 was recorded using 10 cm^{-1} resolution (200 u slits) and a "scan rate" of 4000 ms for each 3 cm-1 step. The principal features of the diniobium spectra are a progression (v" = 0 $\rightarrow$ v" > 0) in the ground state vibrational frequency. Also evident in Fig.1.7 is the Raman transition from the CaF_2 support, whose 330 cm^{-1} frequency serves as a useful fiducial mark[1-32]. Raman spectra were observed throughout the blue-green region of the ion laser, as well as with dye laser scans using DCM. Figure 1.8 shows the observed variation in the intensity of the Raman signal with the excitation wavelength. The ordinate in this figure gives the relative intensity of the Raman fundamental (at 418 cm^{-1}) scaled by the laser power and by the fourth power of the exciting wavelength. The excitation profile bears a strong resemblance to the diniobium absorption spectrum (Fig.1.5). The peak of the excitation (near 667 nm) is slightly blue shifted (ca. 120 cm^{-1}) from the strong A' $\leftarrow$ X absorption at 672.3 nm, in approximate accord with the behavior expected for A-term resonance Raman intensities[1-40].

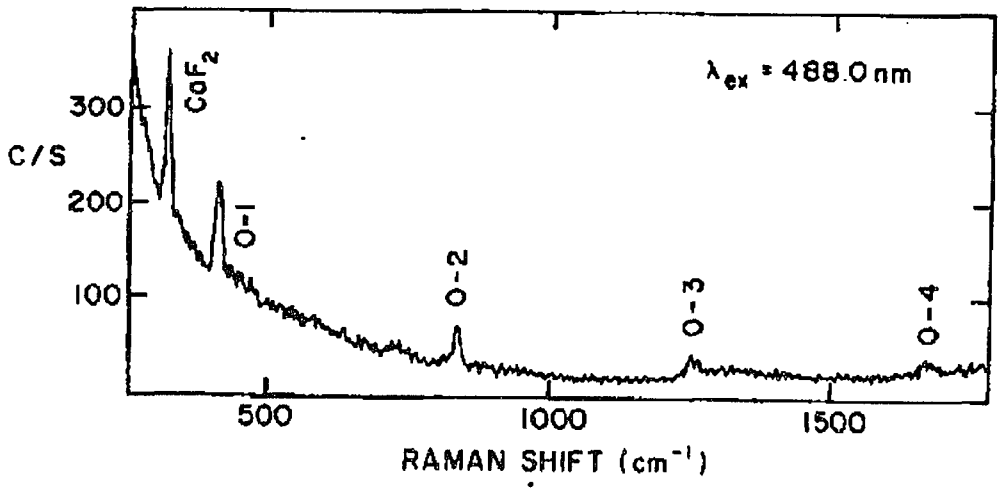

Fig.1.7 Raman spectrum of diniobium in an argon matrix at 14K

In general the diniobium Raman spectra were of poorer quality than those observed for the other Group VB dimer, V_2 and Ta_2[1-30]. Raman progressions were less extensive and the outermost transitions broadened and sometimes split, presumably due to matrix site effects. Accordingly, the diniobium vibrational constants are not as precise as those we reported for V_2[1-30]. Table 1.2 summarizes the Raman frequency data for eight laser wavelengths. All spectra were calibrated by scanning through the corresponding ion laser line and further corrected by comparison with the CaF_2 frequency. The Table 1.2 data were analyzed by standard methods to give ω_e" = 420.5 (0.5) cm^{-1} and $\omega_e \chi_e$" = 0.5 (0.3) cm^{-1}.

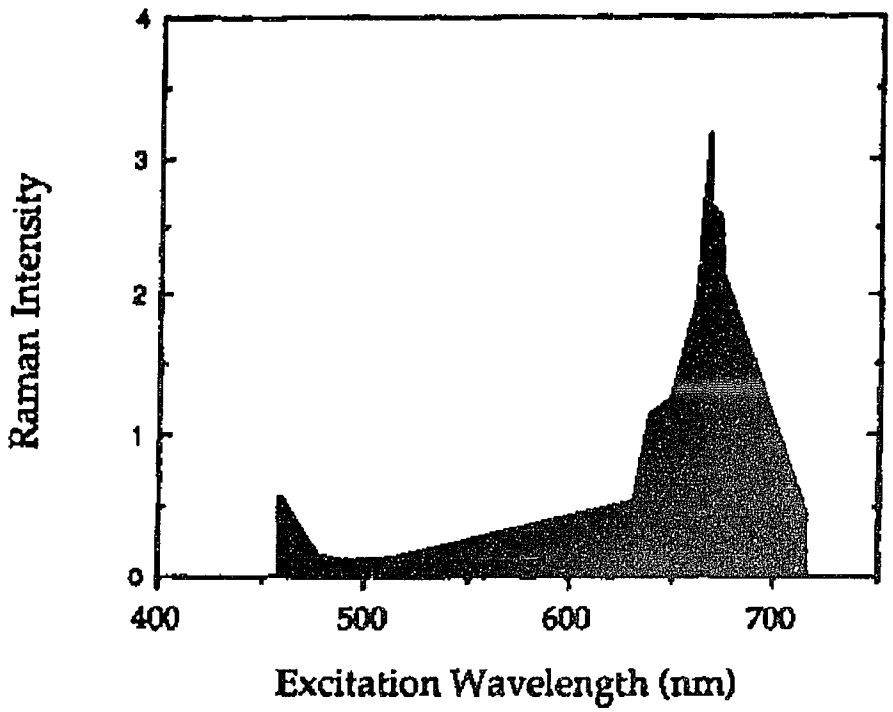

Fig.1.8 Raman fundamental excitation profile for diniobium in Ar matrix.

These constants are close to those previously obtained (ω_e" = 421 cm^{-1} and $\omega_e \chi_e$" = 1.4 cm^{-1}) for Nb_2 in a Kr matrix [1-38].

In previous work, Andrews and Ozin[1-41] noted that a common feature of many Group VB and VIB dimers was the occurrence of a structured transition in the low energy region of the dimer absorption spectrum. Based upon the results of Xα

calculations, but also making an analogy with the corresponding ligated complexes[1-42], these authors assigned the red absorption features to a $\delta \rightarrow \delta^*$ transition arising (for Group VB dimers) from a ground state configuration: $....d\sigma_g^2 d\pi_u^4 d\delta_g^2$. The observed structure had the

Table1.2. Raman Frequency Shifts (cm^{-1}) for Diniobium in an Argon Matrix.

λ_{ex} (nm)	$\nu'' = 1$	$\nu'' = 2$	$\nu'' = 3$	$\nu'' = 4$
457.9	416.0	827.0		
465.8	422.0	839.1		
472.7	419.2	837.6	1251.4	
476.5	422.1	842.2	1250.7	1674.1
488.0	421.8	842.2	1258.5	1673.8
496.5	421.1	839.7	1252.8	1667.9
501.7	418.0	839.2		
514.5	422.1	837.2	1256.6	1670.2
Mean (σ)	420.3(23)	838.1(49)	1254.0(34)	1671.5(30)

appearance of a doublet splitting which was thought to arise from a lifting of the degeneracy of the δ orbitals owing to the matrix environment. Our measurements

make this latter conclusion unlikely, at least in the case of Nb_2. Thus, the A region absorption shown in Fig.1.6 clearly consists of two different types of transitions, implying two different electronic symmetries. The sharp (A' $\leftarrow$ X) feature indicates that the upper and lower electronic states have a similar internuclear separation , whereas the long overlapping A $\leftarrow$ X progression is characteristic of a Frank-Condon envelope for a molecule in which the excited state potential curve is significantly shifted from that of the ground state. Our results do not, however, permit a definitive identification of the excited states of Nb_2, nor do they allow an assignment of the intriguing structure observed in the B region of the dimer absorption spectrum. Indeed, such a task is rather dauting for combinations of open d-shell elements. Thus, Cotton and Shim[1-43] find 75 electronic states lying within 1-2 eV of their predicted $^1\Sigma_g^+$ ground state. Walch and Bauschlicher[1-44], by contrast, find a $^3\Sigma_g^-$ ground state and low lying (< 1000 cm^{-1}) $^1\Gamma_g$ and $^3\Delta_g$ states. While the vibrational frequency calculated for $^3\Delta_g$ (501 cm^{-1}) is large compared to that measured (421 cm^{-1}), the values for $^3\Sigma_g^-$ and $^1\Gamma_g$ (488 and 427 cm^{-1} , respectively) are quite similar in magnitude. Accordingly, the Raman measurements are consistent with either a $^3\Sigma_g^-$ or a $^1\Gamma_g$ ground state for Nb_2.

In conclusion, we have demonstrate the importance of mass selection in the elucidation of the spectra of metal clusters. We have shown that "Scattering Depletion Spectroscopy" is a useful technique for absorption measurements, and have observed the first absorption spectrum of the niobium dimer which is free

from interference from atoms or higher mass clusters. Raman spectra obtained throughout the blue-green and red region are in good accord with the optical absorption data.

1.3.3 Spectroscopy of mass-selected zirconium dimers in argon:

Zirconium ions were co-deposited (at about 14K) with Ar and electrons (from a tungsten filament) on a CaF_2 plate mounted on a Displex refrigerator. Ion currents, measured at 10 eV on a Faraday plate in the deposition region, were: Zr^+ (120 nA), Zr_2^+ (110 nA) and Zr_3^+ (25 nA). Matrices were grown at 5 - 10 μm/hour with an Ar:metal dilution ratio of approximately 10^4 : 1. Fragmentation may be estimated by comparing the intensities of atomic excitation features in a dimer deposition with those obtained from deposition of the atom under similar conditions. By this yardstick, we estimate that about 1 - 2% of the zirconium dimers (neutral bond energy, $D_0 = 3.2$ eV)[1-29] were fragmented, as compared to the similarly determined parameters[1-30,45] 10 - 15% for V_2 ($D_0 = 2.8$ eV)[1-26] and 0.5% for Nb_2 ($D_0 = 5.0$ eV)[1-29]. Matrix samples were interrogated in-situ using both absorption and Raman spectroscopy. Both the Raman and the absorption measurements were made by collecting the light scattered at 90^0 to that incident as described above.

1.3.3.1 Scattering Depletion Spectroscopy:

Figure 1.9 shows a " Scattering Depletion Spectrum " (SDS) of dizirconium in an unannealed argon matrix at 14K. The spectrum (resolution 0.4 nm) was acquired following a 2 hour deposition of 125 nA of Zr_2^+ (250 nA-h)[1-46] at a deposition energy of 10 eV. The ordinate in Fig.1.9 (the " SDS signal ") is the ratio of the " reference intensity " to the " signal intensity ". The latter corresponds to light scattered from a region near the center of the 8 mm wide sample, whereas the former pertains to that scattered near an edge. Prior to recording scattering depletion spectra, the optical density profile of the sample is obtained by recording single beam spectra as a function of lateral position on the sample. It is generally found that the sample is non uniform, with about twice as much absorption in the center as compared to near an edge. Thus the reference also contains absorption information but to a lesser degree than the signal.

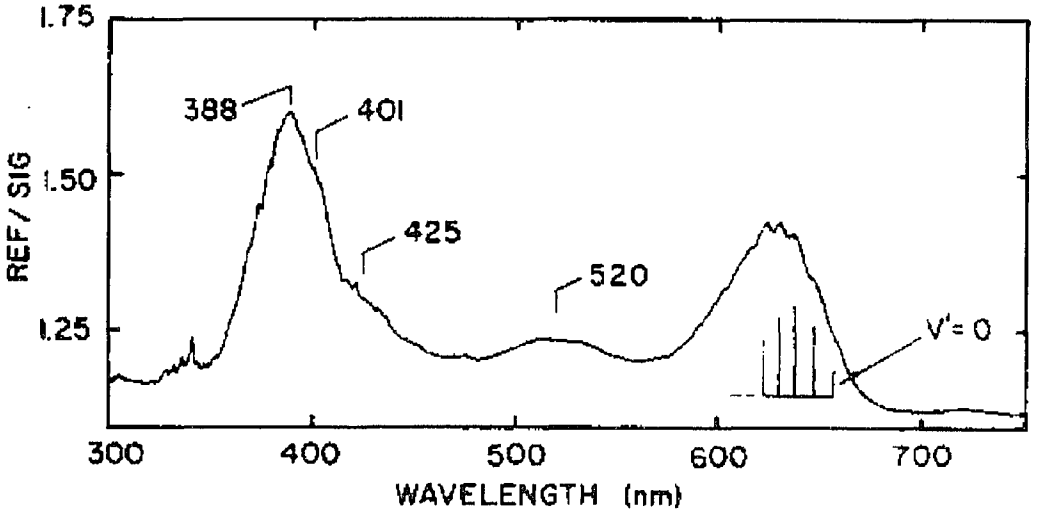

Fig.1.9 Absorption (" SDS ") spectrum of Zr_2 in Ar.

The absorption spectrum of dizirconium (Fig.1.9) consists of an intense band at 388 nm (with shoulders at 401 and 425 nm as indicated), a weaker feature near 520 nm and a structured absorption centered at about 630 nm. The relatively sharp features between 300 and 450 nm arise from absorption by atomic zirconium and have been reported previously [1-47,48]. As the dimer has no detectable fluorescence, atomic transitions are most easily identified by examining excitation spectra (not shown). Klotzbucher and Ozin identified four Zr dimer bands (390, 420, 585 and 615 nm) in matrices containing a distribution of cluster sizes[1-48]. While our spectra clearly show absorption features near 390nm and in the region 600 - 650 nm, we do not observe a strong peak at 422 nm, nor do we see a resolved feature at 585 nm as shown in Fig.1.6c of Ref.1- 48.

The 630 nm band includes a vibrational progression which ends rather abruptly after the fifth member. The SDS " signal " spectrum for this region was simulated by adjusting the positions and relative intensities of 5 overlapping Gaussian functions assumed to have the same width (250 (10) cm^{-1} FWHM). A satisfactory match (illustrated by the stick spectrum in Fig. 9) could be obtained only for a limited range of positions (10 cm^{-1}) and intensities (5%). The frequencies obtained in this manner were analyzed to give $\omega_0' = 225\ (15)\ cm^{-1}$ with $T_0 = 15{,}230(15) cm^{-1}$ where the latter frequency corresponds to the (nominal) origin notated v' = 0 in

Fig.1.9. The data fit both a harmonic and an anharmonic potential, but our analysis is not yet capable of distinguish between these two cases.

1.3.3.2 Raman spectra:

Figure 1.10 shows a typical Raman spectrum (a different sample from that of Fig. 1.9) for Zr_2 in an argon matrix. Raman spectra were recorded at eleven wavelengths in the range 600 - 625 nm and were also observed using the 454.5 and 457.9 nm argon ion laser lines, but these latter spectra were relatively weak. Because of a combination of atomic fluorescence and an increasing linewith (due in part to isotope effects) with increasing Raman shift, no more than four transitions could be assigned. The Raman data (summarized in Table 1.3) were analyzed to give (one standard deviation uncertainty in parentheses) ω_e" = 305.7 (35) cm^{-1} with $\omega_e\chi_e$" = 0.5 (7) cm^{-1}.

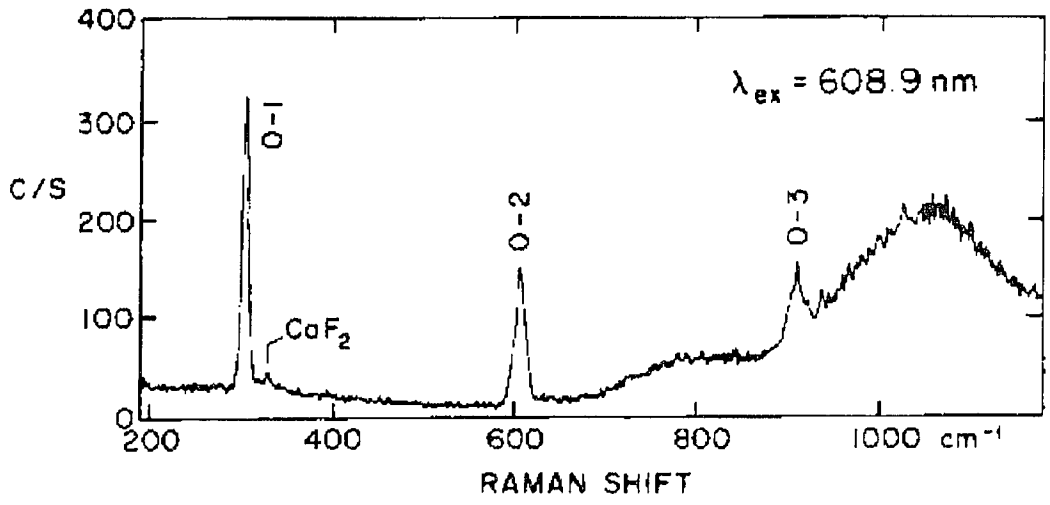

Fig.1.10 Raman spectrum (Rhodamine 6G) of Zr_2 in Ar at 14K.

Under higher resolution (not shown), the first three Stokes transitions are seen to consist of a principal band (degraded towards the Rayleigh line) plus a higher frequency "subcomponent " displaced by 3.3 (3) v" cm^{-1} . The shape of the principal band was well accounted for by simulating overlapping Gaussians corresponding to the 15 possible isotopic combinations[1-49] spaced (by ca. 1 cm-1 for v" = 2) according to their relative reduced masses[31]. No anti-Stokes Raman transitions could be observed, which implies that we are not observing "hot band" features arising from radiative process[1-31]. The relative intensity (uncertainty 0.4) of the two Raman components (also determined by simulation) was 1.7 : 1 for all three Stokes transitions. This intensity ratio was invariant (within error) to annealing, to changing temperature (15 and 25K), to the exciting wavelength and to rotating a polarizer in the path of the scattered light.

Two theoretical papers on dizirconium have recently been published[1-50,51] . As the calculations of Ref. 1-50 include both external correlation and p orbitals (important for determining transition moments), we focus on the conclusions. Four low (< 1500 cm^{-1}) lying states (ω_e in parentheses) are predicted: $^1\Sigma_g^+$ (338 cm^{-1}), $^3\Delta_g$ (305 cm^{-1}), $^3\Sigma_u^+$ (251 cm^{-1}) and $^7\Sigma_u^+$ (196 cm^{-1}). Given the estimated uncertainty (~ 30 cm^{-1}) in theoretical vibrational frequencies, our Raman measurements (ω_e" = 306 cm-1) can be said to be consistent with either a $^1\Sigma_g^+$ or a $^3\Delta_g$ ground state, but not with $^3\Sigma_u^+$ and $^7\Sigma_u^+$. Bauschlier et al. also predicted the dimer absorption spectrum, assuming a $^1\Sigma_g^+$ ground state. The three most intense dimer bands (intensities in parentheses)[1-51] are: 14,900 cm^{-1} (2.1 au), 18,800 cm^{-1} (0.6 au) and 21,900 cm^{-1} (1.2 au). While the value of 14,900 cm^{-1} is very

close to our T_0 = 15,230 cm^{-1} , the overall resemblance to the experimental spectrum (especially as regards relative intensities) is not very compelling. A prediction of the dimer absorption spectrum assuming a $^3\Delta_g$ ground state could be very instructive.

Table 1.3. Raman Frequency Shifts (cm-1) for Zr_2 in an Ar matrix.

λ_{ex} (nm)	v" = 1	v" = 2	v" = 3	v" = 4
601.9	304.0	607.2	909.0	1209.2
604.8	302.0	605.7	908.0	1213.0
606.0	302.9	605.4	911.3	1201.0
607.5	304.2	606.9	909.4	1211.5
609.6	306.0	608.0	911.7	
609.7	303.9	605.9	909.7	
610.3	303.8	608.4	909.8	
614.0	303.8	608.2	901.2	1213.5
620.4	301.8	601.7		
623.4	302.4	605.4	903.1	
625.6	304.0	605.1		
Mean (σ)	303.5(12)	606.2(19)	908.1(36)	1209.6(51)

The occurrence of "subcomponents" in a Raman spectrum (as noted above for Zr_2) can be interpreted in two ways. One possibility (as previously

invoked for V_2)[1-31] is an interaction within a single matrix site which lifts the spatial and/or spin degeneracy of the dimer. A similar argument here would exclude $^1\Sigma_g^+$ as the ground state, but we feel that other possibilities cannot be ruled out. Thus, Zr_2 might be trapped in two different matrix sites for which the dimer vibrational frequencies differ by 3 cm^{-1} (1%). For this situation, the resistance of the "subcomponent" structure to (e.g.) annealing is perhaps surprising. Finally, we note one similarity between Zr_2 and Nb_2[1-45]. Both dimers have strong absorption bands (and a vibrational progression) around 650 nm. This lowest energy (visible) transition has been interpreted in terms of a $\delta \leftarrow \delta^*$ transition[1-41,45]. While consistent with several ground state configurations for Nb_2[1-44], such an interpretation would not be possible if $^1\Sigma_g^+$ (configuration: $d\sigma_g^2 d\pi_u^4 s\sigma_g^2$) were the ground state of Zr_2.

1.4. REFERENCES:

1-1. *Thirteenth International School*, Erice, Sicily (1987). See: *Elemental and Molecular Clusters*, ed. by G. Benedek et al. (Springer-Verlag, New York).

1-2. *Fifth International Meeting on Small Particles and Metal clusters*, Konstanz, Germany, 1990. See: Zeits. Phys. D19, (1991); *Six International Meeting on Small Particles and Metal clusters*, Chicago, Illinois, 1992. See: *Zeits. Phys.* D26, (1993).

1-3. *International Symposium on the Physics and Chemistry of Small clusters*, NATO Advanced Workshop, Richmond, Virginia (1991). See: *Physics and Chemistry of Finit-Systems: From Clusters to Crystals*, edited by P. Jena and S. N. Khanna and B. K. Rao (Kluwer, Dordrecht, 1992).

1-4. *Symposium on Clusters and Cluster Assembled Materials Research Society Meeting*, Boston (1990). See: *MRS Symposium Series* 206, (1991).

1-5. *First International Conference on Nuclear and Atomic Clusters*, Turku, Finland (1991); *Second International Conference on Nuclear and Atomic Clusters*, Santorini, Greece (1993).

1-6. *Transition Metal Molecules*, W. Weltner and R. J. Van Zee, (1984) *Ann. Rev. Phys. Chem.* 35, 291.

1-7. *Clusters of Transition-Metal Atoms*, M. D. Morse, (1986) *Chem. Rev.* 86, 1049.

1-8. *Metal Clusters*, edited by M. Moskovits (Wiley, New York, 1986).

1-9. *Spectroscopy and Dynamics*, edited by M. A. Duncan, *Advances in Metal and Semiconductor Clusters* (JAI press, Greenwich CT, 1992).

1-10. T. H. Maugh, *Science,* (1983) 219, 474; 220, 592 (1983).

1-11. A. L. Robinson, *Science* 185, 772 (1974); 194, 1150 (1976).

1-12. J. H. Sinfelt, *Science*, (1977) 195, 641; *Acc. Chem. Res.* (1977) 10, 15.

1-13. J. Haggin, *Chem. & Eng. News*, page 32, Jan. 18 (1993).

1-14. J. F. Hamilton and P. C. Logel, *J. Catal.* (1973) 29, 253; *Photo. Sci. Eng.* (1974) 18, 507; *J. de Phys.* (1977) C2, 181.

1-15. G. A. Somorjai, *Acc. Chem. Res.* (1976) 9, 248.

1-16. C. Wang, S. Pollack, D. Cameron and M. M. Kappes, *J. Chem. Phys.* (1990) 93, 3787.

1-17. W. Harbich, S. Fedrigo, F. Meyer, D. M. Lindsay, J. Ligniers, J. C. Rivoal and D. Kreisle, *J. Chem. Phys.* (1990) 93, 8535.

1-18. E. C. Honea, A. Ogura, C. A. Murray, K. Raghavachari, W. O. Sprenger, M. F. Jarrold and W. L. Brown, *Nature* (1993) 366, 42.

1-19. M. E. Jacox, *J. Mol. Spectrosc.* (1985) 113, 286.

1-20. D. M. Lindsay, F. Meyer, and W. Harbrich, *Z. Phys.* (1989) D12, 15.

1-21. W. Harbich, S. Fedrigo, J. Buttet and D. M. Lindsay, *Optical Spectroscopy on Size Selected Gold Clusters Deposited in Rare Gase Solids, Z. Phys.* (1991) D19, 157.

1-22. W. Harbich, S. Fedrigo, J. Buttet and D. M. Lindsay, *Softlanding of Monodispersed Small Metal Clusters in Rare Gas Solids, Mater. Res. Soc. Symp. Ser.* (1991) 206, 369.

1-23. *R. Keller, in The Physics and Technology of Ion Sources*, edited by I. G. Brown (Wiley, New York, 1989), chap. 7.

1-24. K. Bescoke, S. Berger, W. O. Hofer and U. Littmark, *Radiat. Eff.* (1982) 66, 35.

1-25. W. Begemann, Ph. D. thesis, Universitat Bielefeld (1988).

1-26. E. M. Spain and M. D. Morse, *Int. J. Mass Spectrosc. Ion Phys.* (1990) 102, 183.

1-27. K. P. Huber and G. Herzberg, *Constants of Diatomic Molecules* (Van Nostrand, New York, 1979).

1-28. D. M. Cox, R. L. Whetten, M. R. Zakin, D. J. Trevor, K. C. Reichmann, and A. Kaldor, *Advances in Laser Science I*, edited by W. C. Stwalley and M. Lapp (Aip Conf. Proc. 146, 1986), pg. 527; *Z. Phys.* (1986) D3, 195.

1-29. M. Morse, *Chem. Rev.* (1986) 86, 1049.

1-30. Zhengdong Hu, Bo Shen, Qinwei Zhou, S. Deosaran, J. R. Lombardi, D. M. Lindsay and W. Harbich, *J. Chem. Phys.* (1991) 95, 2206.

1-31 C. Cosse, M. Fouassier, T. Mejean, M. Tranquille, D. P. DiLella and M. Moskovits, *J. Chem. Phys.* (1980) 73, 6076.

1-32. A. R. Gee, D. C. O'Shea and H. Z. Cummins, *Solid State Commun.* (1965) 4, 43.

1-33. P. R. R. Langridge-Smith, M. D. Morse, G. P. Hansen, R. E. Smalley and A. J. Merer, *J. Chem. Phys.* (1984) 80, 593.

1-34. W. Demtroder, *Laser Spectroscopy* (Springer-Verlag, Berlin, 1981).

1-35. T. A. Ford, H. Huber, W. Klotzbucher, E. P. Kunding, M. Moskovits and G. A. Ozin, *J. Chem. Phys.* (1977) 66, 524.

1-36. D. W. Green and D. M. Gruen, *J. Chem. Phys.* (1972) 57, 4462.

1-37. W. Klotzbucher and G. A. Ozin, *Inorg. Chem.* (1977) 16, 984.

1-38. M. Moskovits and W. Limm, *Ultramicroscopy,* (1986) 20, 83.

1-39. R. W. Wood, *Phil. Mag.* (1902) 4, 396.

1-40. R. J. H. Clark, *Raman, Resonance Raman and Electronic Raman Spectroscopy in Vibronic Processes in Inorganic Chemistry*, edited by C. D. Flint, NATO ASI Series (Kluwer Academic Publishers, 1989), page 301.

1-41. M. P. Andrews and G. A. Ozin, *J. Phys. Chem. Soc.* (1986) 90, 2852.

1-42. M. C. Manning and W. C. Trogler, *J. Amer. Chem. Soc.* (1983) 105, 5311.

1-43. F. A. Cotton and I, Shim, *J. Phys. Chem.* (1985) 89, 952.

1-44. S. P. Walch and C. W. Bauschlicher, *in Comparison of ab initio Quantum Chemistry with Experiment*, edited by R. J. Bartlett (Reidel, Boston, 1985).

1-45. Zhendong Hu, Bo Shen, Qinwei Zhou, S. Deosaran, J. R. Lombardi and D. M. Lindsay, *Proc. SPIE* (1992) 1599, 65.

1-46. We use units of nA-h (the product of the current times the deposition time in hours) where 1 nA-h = 2.25×10^{13} particles.

1-47. J. K. Bates and D. M. Gruen, *High Temp. Sci.* (1978) 10, 27; C. Steindruchel and D. M. Gruen, *J. Chem. Phys.* (1981) 74, 205.

1-48. W. Klotzbucher and G. A. Ozin, *Inorg. Chem*, (1980) 19, 3767.

1-49. *Handbook of Physics and Chemistry*, edited by R. C. Weast (chemical Rubber, Cleveland, 1975).

1-50. C. W. Bauschlicher, H. Partridge, S. R. Langhoff and M. Rosi, *J. Chem. Phys.* (1991) 95, 1057.

1-51. K. Balasubramanian and Ch. Ravimohan, *J. Chem. Phys.* (1990) 92, 3659.

PART 2
CHAPTER TWO
SYNTHESIS AND MODIFICATION OF PEPTIDES

2.1. INTRODUCTION:

2.1.1 Peptide synthesis:

The synthesis of peptides has been a challenge to organic chemist since the turn of the century. The early endeavors, notably those of Emil Fischer and his colleagues, were stimulated by the emerging theories of protein structure [2-1]. By the middle of the century, however, the realization that other biologically important molecules had simpler amino acid sequences increased the stimulus and reduced the dimension of peptide synthesis to attainable proportions. The isolation, structure determination and synthesis [2-2] of the lactogenic nonapeptide amide hormone oxytocin by du Vigneaud and his coworker in the early 1950s initiated a new era in both biology and chemistry. New biologically active peptides were isolated apace, requiring new and improved methods for their synthesis. Pharmacological studies required synthesis not only of the often hard-to-isolate natural peptides, but also of numerous analogues, thus permitting investigation of the relationship between chemical structure and biological activity.

The classical methods of solution peptide synthesis were hard pressed to meet this explosive increase in demand. The total number of steps in synthesis of moderately sized peptides is substantial, and many of these are consecutive even if

a segment condensation strategy is adopted in preference to stepwise elongation from the amino or carboxy terminus. Even in skillful hands, yields in peptide bond forming reaction were often only modest, giving low overall yields and contamination with side products. In short, although very substantial success was achieved using classical solution techniques, they were highly labor intensive and needed much skill and experience. This was the background for the search in the 1950s for workable accelerated procedures, of which solid phase synthesis has proved by far the most successful.

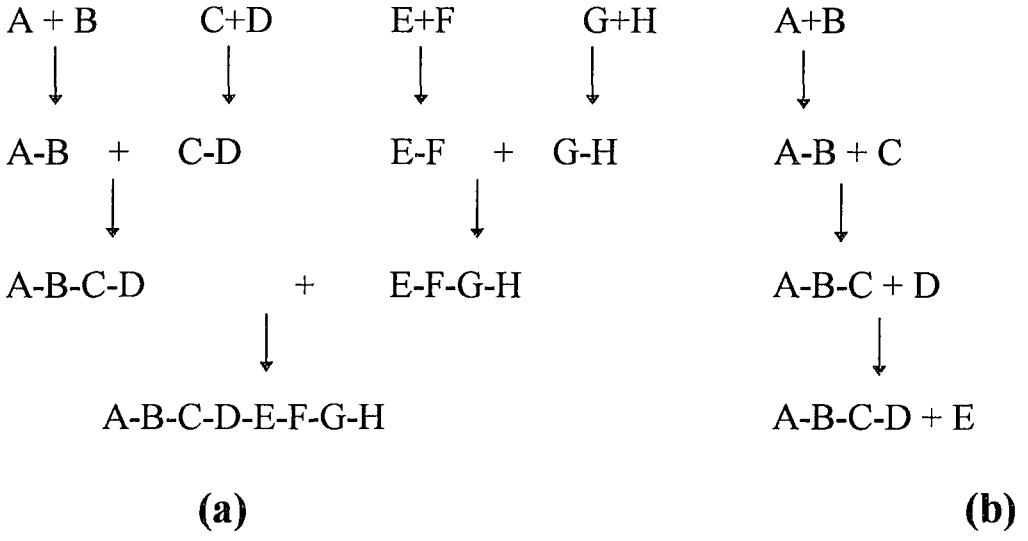

Figure 2-1 A, B, C, etc. represent individual amino acids. (a) Synthesis by regular segment condensation. (b) Stepwise synthesis by extension of the peptide chain from the amino terminus towards the carboxy terminus.

2.1.2 Protecting groups

Unambiguous formation of a peptide bond between two structurally similar amino acids requires that the amino group of one and the carboxy group of the other be prevented from participating in the coupling reaction. The protecting groups also have the important role of destroying the dipolar or zwitterionic character of amino acids and peptides and thus incease the reactivity. Early in the history of peptide synthesis it was realized that urethane derivatives were particularly suitable for amino protection. Thus from 1932 when they were first introduced by Bergmann and Zervas [2-3], benzyloxycarbonylamino acids [2-4] (Z-amino acids) have been key intermediates in solution peptide synthesis. To a large extent they satisfied the criteria given above for protecting group design. They were easily prepared and chemically stable. The urethane nitrogen atom is usually inert to the subsequent peptide synthesis reaction conditions. Most importantly, the benzyloxycarbonyl group was easily cleaved by catalytic hydrogenolysis, a very mild chemical procedure which left newly formed peptide bonds unaffected. This facile cleavage made the benzyloxycarbonyl function ideal for temporary protection. Subsequently the group was also found to be cleavable under rather strong acidic conditions, by hydrogen bromide in acetic acid and later again by liquid hydrogen fluoride. These procedures for final deprotection enabled benzyloxycarbonyl groups (and benzyl ester derivatives in general) to be used in different strategies for more permanent protection. Finally it was found that benzyloxycarbonyl amino acids posed a high degree of optical stability. Racemization of chiral centers adjacent to benzyloxycarbonylamino functions was

usually inhibited. This is now known to be a property of urethane protecting groups in general, and is an important factor favoring their widespread adoption.

The concept of temporary and permanent protecting groups requires at least two complementary types. t-Butoxycarbonylamino acids (t-Boc) have properties which are substantially complementary to those of benzyloxycarbonyl derivatives. Thus t-Boc derivatives are unaffected by catalytic hydrogenation, but are cleaved completely under relatively mild acidic conditions (for example trifluoroacetic at room temperature) where benzyloxycarbonyl groups are essentially inert. Thus selective cleavage of one in the presence of the other is usually possible. t-Boc protecting groups dominated peptide synthesis strategies for many years. Very many others have been devised but found relatively slight application in solution techniques. Of these may be mentioned a number of ring-substituted benzyl urethanes with modified acid lability; one notable base-labile urethane, the fluorenylmethoxycarbonyl group (Fmoc), which has become the most popular protecting group recently.

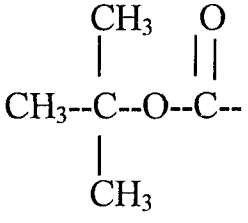

t-Boc

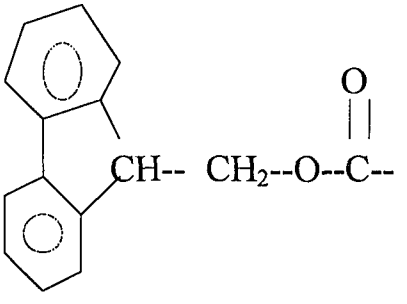

Fmoc

2.1.3 Solid Phase Peptide Synthesis (SPPS) - the Merrifield technique

SPPS was first proposed by R.B. Merrifield in 1962, with a full paper [2-5] published in 1963. In the latter, Merrifield described the preparation of the tetrapeptide Leu-Ala-Gly-Val by successive addition of benzyloxycarbonylamino acids to a polystyrene resin. To enable cleavage of the benzyloxycarbonyl protecting groups without concomitant detachment of the peptide from the resin support, the latter was nitrated, the nitrobenzyl ester linking groups being more resistant to acids. The synthesis was undoubtedly successful, but perhaps did not augur well for extended applications because the coupling and/or deprotection reaction were not brought to completion and the target tetrapeptides was contaminated with shorter peptides. Thus extention to longer sequences with increased purification problems was unpromising. Within a year , however, the situation had changed dramatically. A third paper [2-6] again by Merrifield, published in 1964, described substantial changes in technique, particularly replacement of benzyloxycarbonyl protected amino acids by the much more acid labile t-Boc derivatives. This and other changes resulted in greatly improved chemical efficiency and permitted synthesis of the naturally occurring nonapeptide bradykinin in highly purified form. This synthesis was a landmark in peptide chemistry. It took just a few days to complete single-handed (it could have taken as many weeks or months using classical techniques), and offered immediate

advantages over a solution to the fast growing demands for peptides in pharmacology and other biological science.

The principle of all solid phase synthesis is simple enough. The growing chain, peptide, oligonucleotide or other desired oligomer, is elongated while it is attached to a stable, solid particle. It usually remains attached to this particle throughout all the synthetic steps and is separated from soluble reagents and solvents by simple filtration and washing. Finally, the desired product is detached from the solid support, and purification and characterization is carried out in free solution.

There are a number of immediate consequences. The separation processes are quick and simple, and can be machine-aided. There is an enormous time and labor advantage over the corresponding operations in solution chemistry which commonly involve techniques of solvent extraction, filtration, evaporation, and crystallization. These often result in substantial losses of material, so that solid phase synthesis may be much more effective in this sense also. Retention of the resin-bound peptide in the same reaction vessel at all times also minimizes physical losses. Because soluble reagents can be so easily removed by filtration, large excesses can be used, encouraging high efficiency in the various chemical steps.

The original chemistry [2-6] of the Merrified system is illustrated for synthesis of a simple dipeptide in Figure 2-2. It may be noted that some early beliefs regarding solid phase synthesis must now be recognized as requiring modification which will be discussed later.

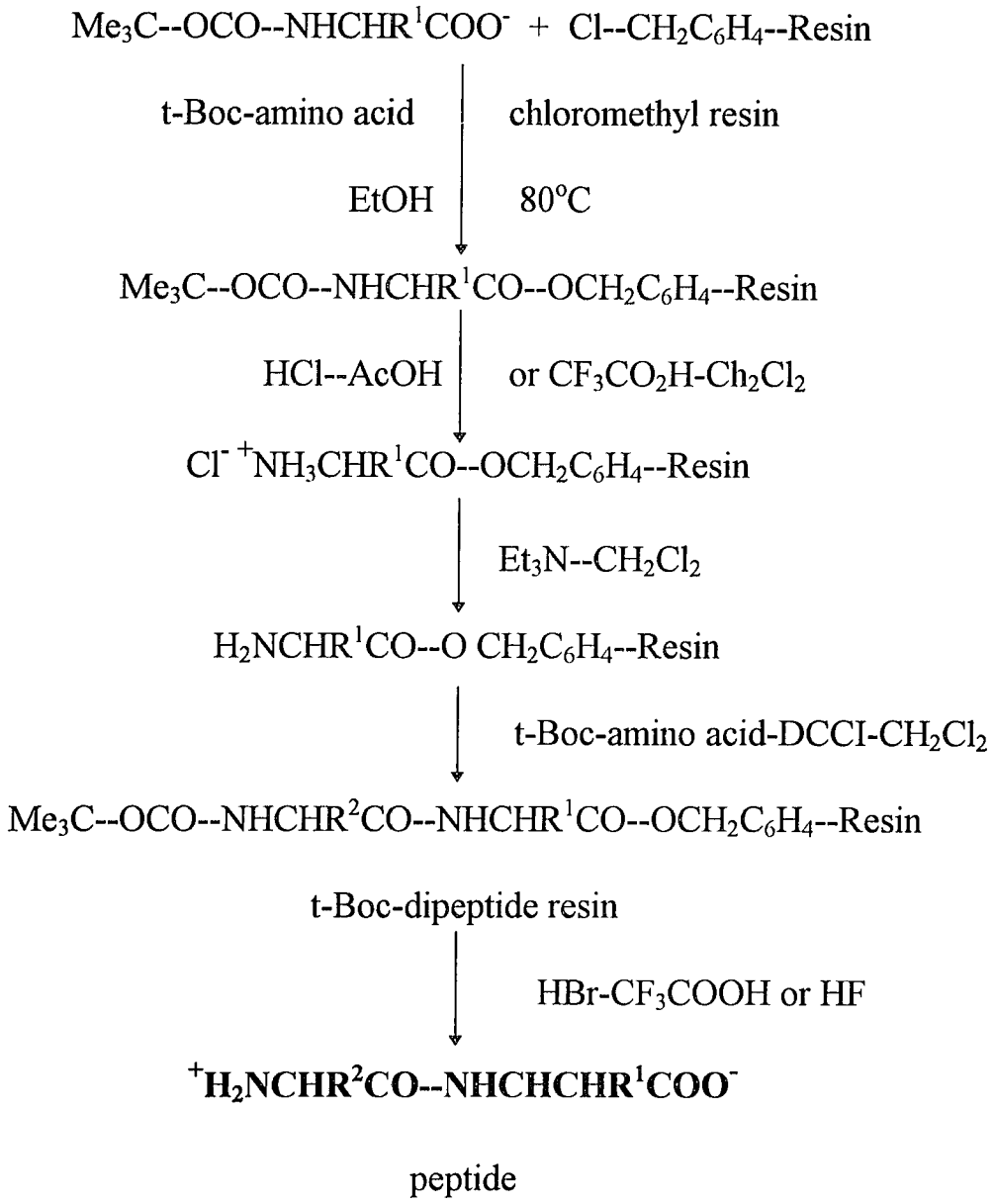

Figure 2-2. Original experimental scheme for solid phase peptide synthesis; synthesis of a dipeptide.

In solid phase synthesis, peptide chains are assembled from the carboxyl terminus one amino acid at a time working towards the amino terminus. The first (C-terminal) amino acid is covalently attached to an insoluble supporting resin. The remaining amino acids are added one by one until peptide assembly is complete. Cleavage of the peptide-resin bond then allows isolation of the product.

Amino acids contain two and sometimes three chemically reactive groups and to obtain unambiguous synthesis it is necessary to employ protecting groups. The α-amino group is temporarily protected and trifunctional amino acids require additional side chain protection to avoid participation of these reactive groups during chain assembly.

A typical solid phase peptide synthesis includes the following steps:

a) The carboxyl terminal amino acid is attached to the solid support by formation of an ester linkage (esterification) if a peptide acid is desired.

b) The temporary α-amino protecting group is removed under conditions that leave side chain protecting groups (if present) intact. This process is termed deprotection.

c) The next, protected, amino acid is "coupled" (via amide bond formation) to the support bound carboxy-terminal residue. Since coupling (acylation) does not occur spontaneously some form of activation is required. Activation can be achieved by employing active esters (available as ready-to-use crystalline

powders), symmetrical anhydrides (prepared just prior to use), or in situ activation methods.

d) once coupling is complete, the next cycle begins with deprotection of the α-amino group of the N-terminal amino acid. The process of α-amino deprotection followed by coupling is repeated for as many cycles as necessary to assemble the desired peptide chain.

e) After the peptide is assembled it must be cleaved from the support and any side chain protecting groups must be removed.

f) The peptide may be used without further isolation or may be purified prior to use.

The amino acid sequence of a peptide chain is conventionally written so that the N-terminus is to the left and the C-terminus is on the right. For example, methionine enkephalin is represented as H-YGGFM-OH or, in the three letter notation, H - Tyr - Gly - Gly - Phe - Met - OH.

2.1.4 Fmoc chemistry:

More and more laboratories started to switch from t-Boc chemistry to Fmoc chemistry recently. It is believed that more than 75% of people in this area are now using the Fmoc strategy and the number is still rising. The guiding principles governing development of the Fmoc-polyamide solid phase synthesis are straightforward. Accepting that stepwise addition of amino acids to polymer support leads to accumulation of the products of incomplete reaction and to the

products of undesired side reactions, the immediate objective must be to establish a system optimized in chemistry so that reactions proceed with maximum efficiency and yet mild enough so that undesired degradative reactions are minimized. Optimization of reaction conditions is to be achieved by careful choice of reactants and solvents. Ambiguous reactions, for example the potential two-way opening of mixed anhydrides, are to be avoided or subjected to careful evaluation before use. Likewise, differential reactivity in the selective cleavage of protecting groups is to be avoided if possible. Minimization of side reactions requires that synthesis and deprotection steps are carried out under chemically mild conditions, and that no other reactive species are present or inadvertently introduced into the system which might participate in side reactions. This last requirement underlines the need for highly purified reactants and solvents. Amongst the reactants must be considered the polymer support itself. Purity of polymers is difficult to establish. Chemical manipulation of the polymer support should therefore be minimized to reduce the risk of accumulation of unknown reactive groups prior to peptide synthesis. Flexibility should be a feature of any new solid phase system. It should, for example, be readily adaptable to the synthesis of side-chain-protected as well as free peptides and peptide amides, and if possible to the assembly of protected peptides in a solid phase fragment condensation approach to the synthesis of large peptides. Finally, opportunity should be taken wherever possible to facilitate analytical control of solid phase synthesis, particularly by real-time quantitative monitoring of both acylation and deprotection reaction.

These are all desirable principles. Inevitably some compromises have been necessary as development of the Fmoc-chemistry has proceeded.

The chemical features of the current Fmoc-polyamide peptide synthesis are summarized below.

a) Optimization of reaction conditions. The importance of solvation

Optimization of reaction conditions is a matter of organic chemistry. While unimolecular reactions are concentration-independent, bimolecular and high-order reactions proceed faster at higher concentration. Thus coupling reactions which must involve at least two reacting species are best carried out at maximum concentration when they are favored relative to unimolecular decompositions. On the other hand, high concentrations encourage aggregation. In free solution, aggregation may lead to precipitation. In the solid (gel) phase, aggregation is not necessarily prevented by the polymeric nature of the system but is manifested differently. It may cause marked hindrance of reaction. Thus solvation of the entire polymeric system may be crucial for efficient solid phase synthesis. In actual solid phase peptide synthesis, the situation is a dynamic one because of the changing nature of the peptide chain as elongation proceeds, and also because of the alternation between protected, positively charged and neutral end groups. Certainly at all times the desired situation is that both the support and the growing peptide are extended, mobile, and unhindered. Thus optimization of solid phase synthesis requires that the dispersing medium be a good solvating agent for both

the polymer support and the protected peptide. It must also, of course, continue a good reaction medium for the various chemical steps involved.

Experience from peptide synthesis in solution suggests that dipolar aprotic solvents of the dimethylformamide (DMF) type are most likely to satisfy these requirements. Long, side chain protected peptides are frequently only sparingly soluble in organic solvents, but, of those available, DMF has been by far the most widely and successfully used. Many simple acylation reactions are faster in DMF than in less polar media such as dichloromethane (DCM) or chlorroform. In a study of the reaction of benzyloxycarbonylglycine p-nitrophenyl ester with ethyl glycinate, Kemp and his colleagues [2-7, 8] found that the reaction in DMF was some 4500 times faster than in chloroform. Intermediate rates were measured for reactions in acetonitrile, dioxan, and toluene; only dimethylsulphoxide (DMSO) provide a faster reaction with enhancement by a further factor of three. Another solvent which was used frequently in Fmoc chemistry under carefully controlled conditions is N-methylpyrrolidone (NMP).

b) Mildening of reaction conditions. New protecting group combinations.

In any solid phase synthesis, the starting resin and the progressively extended synthetic chain are subjected to many treatments with chemical reagents without intermediate purification. In the cleavage of t-Boc groups, for example, the total exposure to trifluoroacetic acid (TFA) may exceed 7 hours in the synthesis of a 20-residue peptide. Total exposure to acylating conditions may exceed 20 hours. During all this time, the existing polypeptide chain as well as the

permanent protecting groups must remain unaffected. This last requirement has led to the use of very stable side chain protected derivatives which will themselves ultimately require vigorous conditions for their cleavage. They require the nasty and dangerous liquid hydrogen fluoride (HF) as a cleavage reagent.

There is thus a clear need for exceptionally mild and specific reagents to achieve repetitive α-amino protecting group cleavage, acylation, and final side-chain deprotection and detachment from the resin. A cleavage reagent safer and more experimentally convenient than liquid hydrogen fluoride was also desirable. Thus a number of base-labile protecting groups were considered for α-amino protection [2-9]. Among them, the 9-fluorenylmethoxycarbonyl (Fmoc) derivatives of Carpino and Han [2-10] proved particularly suitable. They were cleaved cleanly and rapidly by solutions of secondary bases such as piperidine in DMF, conditions which as far as could be discerned left even particularly sensitive t-butyl derivatives entirely unaffected. Thus seemingly complete selectivity between α-amino and side chain deprotection reactions was easily obtained. Use of individual peptide-resin linkage agents rather than direct linkage to the resin confers considerable advantage and flexibility to the Fmoc-polyamide technique.

c) Coupling reactions

Efficiency and freedom from side reactions are the overriding requirements in peptide bond formation. It has been proved that Fmoc amino acids are well activated by Benzotriazolyloxytetramethyluronium hexafluorophosphate (HBTU). Reaction rates can be accelerated by addition of acylation catalysts such as 1-

hydroxybenzotriazole (HOBT). Furthermore, four-fold excess of Fmoc protected amino acids to peptidyl resin are usually utilized in the coupling step in order to achieve the coupling efficiency as high as 99+%. Similar minimization of side reactions was achieved by use of previously prepared and purified activated easter derivatives. The strength of the carbon-fluorine bond and the absence of other reactive centers encouraged the belief that their use would be exceptionally free of side reactions.

The difficulty of analytical control of solid phase synthesis has been one of its major drawbacks. Most usual spectroscopic techniques are inapplicable. Techniques as diverse as electronic titration, nuclear magnetic resonance spectroscopy, binding of colored reagents to the resin and subsequent elution, among others, have been suggested from time to time for monitoring solid phase reactions quantitatively. None, however, have provided a method useful and simple enough to become a regular part of day-to-day solid phase synthesis. A possible exception is the simple qualitative color test with ninhydrin for residual unreacted amino group carried out under conditions suggested by Kaiser and Colescott [2-11]. This provides a sensitive indication of completion of the acylation reaction. The ninhydrin reaction on amino resins has also been quantitated [2-12], but usually provides only a post-synthesis measure of acylation.

Table 2-1 Comparison of Fmoc and t-Boc methods

Fmoc	t-Boc
Polar polyamide support (many kinds)	Polystyrene support
Fmoc alpha-amino protection	t-Boc alpha-amino protection
Mild base deprotection (piperidine)	Strong acid (TFA) deprotection
No neutralization step	Neutralization step required
Convenient TFA cleavage/deprotection	Dangerous HF cleavage/deprotection
Single solvent system	Multi solvents
Continuous flow or batch	Batch only
On-line monitor	No
Acid, amide and fully protected peptides	Acides and amides

2.1.5 Peptide purification and characterization by HPLC:

The earliest example of the use of chromatography to elicit a separation is credited to the highly gifted Russian botanist Michael Tswett who, in a period between 1903 and 1906, used adsorption chromatography on a calcium carbonate column to separate various plant pigments from leaf extracts. In 1931 the first of a series articles originating from laboratory of Richard Kuhn was published [2-13] which described the use of adsorption chromatography to resolve from the " lutein

" of egg yolk two different carotenes. Rapid expansion followed and in 1941 partition chromatography was described by Martin and Synge[2-14], and subsequently paper chromatography by Consden in 1944 [2-15] which revolutionized approaches to biochemical analysis. The basic principles underlying the technique of liquid chromatography were thereby established and within a short time span advances in both the theoretical and practical aspects of the science resulted in its rapid popularization as the method of choice for the separation and quantitation of the components of unknown mixtures.

The advances in column and pump technology and the introduction of microprocessor controls have allowed HPLC to become accessible as an analytical tool to individuals not specifically devoted to the technique and it is this expansion in availability which has resulted in an upsurge in the popuparity of HPLC such that it is now commonly the method of choice in chromatographic analysis.

Liquid chromatography is a separation method in which a mixture of components is resolved into its constituent parts by passage through a chromatographic column. It is carried out by passing the mobile phase, containing the mixture of the components, through the stationary phase, which consists of a column packed with solid particles. Physical and chemical forces acting between the solutes and the two phases are responsible for the retention of solutes on the chromatographic column. It is the differences in the magnitude of these forces that determine the resolution and hence separation may be considered to be determined

by the distribution of the solutes between the two phases. The elementary forces acting on the molecules are of five types:

(1) London dispersion forces or van der Waals forces operate between molecules causing momentary distortion of their electrostatic configuration.

(2) Dipole interactions arise in molecules temporarily distorted and result in electrostatic attraction between the molecules.

(3) Hydrogen bonding interactions occur between proton donors and proton acceptors.

(4) Dielectric interactions resulting from electrostatic attraction between the solute molecules and a solvent of high dielectric constant.

(5) Electrostatic or coulombic interactions.

Of all the chromatographic techniques used, reversed phase HPLC is by far the most popular with at least 60% of all analytical separations carried out in this chromatographic mode. The term reversed phase chromatography was originally coined by Haward and Martin in 1950 [2-16] who carried out liquid-liquid chromatography on a stationary phase of paraffin oil and n-octane with aqueous eluents. In such a partition system the conventional methodology, which used a polar stationary phase and a less polar mobile phase, was reversed, with the mobile phase being more polar than the stationary phase. We only use reverse phase (RP-HPLC) in this study.

2.2 INSTRUMENTS:

2.2.1 Peptide synthesizers:

Two peptide synthesizers have been utilized in this research. One is Applied Biosystem Division of Perkin Elmer model 433A peptide synthesizer and the other is MilliGen/Perceptive model 9050 plus peptide synthesizer.

2.2.1.1 Applied Biosystem Division of Perkin Elmer's synthesizer 433A.

This is the newest model in ABI family. The main feature of the 433A is a unique feedback monitoring system that allows one to create longer, more complex peptides-efficiently. It provides real-time visual assurance of synthesis progress, while using data obtained from conductivity monitoring to control difficult synthesis. The conductivity system, which uses enhanced FastMoc chemistry, monitors the deprotection reactions and automatically extends deprotection and coupling in difficult regions. For more difficult peptides, the conditional capability allows to program the synthesizer to perform more complex operations based on the monitoring data. With conditional feedback programming, we don't have to treat an entire peptide as difficult just because of a few troublesome regions. Instead, we can plan ahead for potentially difficult couplings without having to predict exactly where the problems will occur. Simply specify alternate steps to take place when a cycle fails to meet target conditions. For instance, we can program the synthesizer to extend deprotection and coupling, then follow with capping when a difficult sequence is encountered. Other choices

include double coupling, changing coupling conditions with co-solvents or additives, or stop the synthesizer. Conditional feedback programming reduces trial-and-error time and wasted reagents because it either ensures a successful synthesis or stops the synthesis as instructed. Therefore, the step yields for most routine syntheses are greater than 99.0%.

2.2.1.2 MilliGen of Perceptive model 9050 plus

The 9050 plus peptide synthesizer is a continuous flow instrument that automates the Fmoc method of solid-phase peptide synthesis. In continuous-flow solid-phase peptide synthesis, an insoluble solid support is contained in a reaction column. Chemical reactions necessary to produce a peptide occur on the support. The peptide chain is elongated by adding (coupling) amino acids one at a time in a sequential fashion. During synthesis the growing peptide chain remains immobilized on the support, and the excess reagents and by-products from the synthetic cycle are washed out of the column by the continuous flow of reagents. The efficiency of washing by continuous flow reduces the consumption of reagents and decreases the cycle time. The result is an average cycle time on the 9050 plus peptide synthesizer of approximately 60 minutes.

The 9050 plus peptide synthesizer consists of three modules:

(a) IMB PC-AT compatible computer.

(b) Synthesis Module.

(c) Amino Acid Module (AAM).

The process of peptide synthesis is executed through precise interaction of the modules' components. The computer and the Express-Peptide software program are the communication links between instruments. Under control of the CPU, reagents and solvents are sent to the reaction columns by the action of the reagent delivery system. The AAM and transferred to the delivery system. (An external source of nitrogen is required for both the Synthesis Module and the AAM).

On route to the columns, the stream of reagents passes through the online spectrophotometer (detector). The column effluent is passed through a second channel of the detector and is routed to waste or is recirculated through the columns. The data output from the detector is sent to the CPU and the computer. The current detector data is displayed on the monitor in graphic form and the data for an entire synthesis can be stored on the computer's hard disk. The detector provides real-time visualization of the synthesis progress and also tells you the coupling efficiency of each cycle.

2.2.2 High performance liquid chromatography (HPLC)

The Waters model 625 HPLC system has been involved in this study. It is a non-metallic High Performance Liquid Chromatography (HPLC) solvent delivery system for liquid chromatography applications. The system is capable of automatically selecting flow and gradient composition to blend up to four solvents. Two different detectors can be attached to it, one is Waters Non-metallic 486

Tunable UV detector and the other is Waters 996 Photodiode array detector. Waters 717 autosampler is also connected in order to auto inject samples. The whole system is fully controlled by Millennium 2010 software package.

2.3 EXPERIMENTS AND RESULTS:

2.3.1 Peptide synthesis:

Fmoc chemistry is utilized on all of the sample preparations in this study since its obvious advantages over the t-Boc chemistry. 0.1 to 0.25 mmol scale are used to give about 50 mg yield of crude tetrapeptides. Both batch and continuous methods are utilized in the synthesis. Either Fmoc-Rink MBHA amide resin or Fmoc-PEG-PS amide resin served as solid support. Piperidine is the deprotecting base reagent and HBTU/HOBT, the coupling reagent. DIPEA is the catalyst to assure greater than 99% coupling yield being achieved during the coupling step. NMP was used as wash solvent for ABI batch synthesizer while DMF was used as wash solvent for Milligen continuous synthesizer. Final peptidyl resins were washed by DCM and ethyl ether. At this point, the peptidyl resins are dry and ready for the next step of the procedure which is cleavage. The following is a schematic of the Solid Phase Peptide Synthesis. Three chemical reactions are repeated for each amino acid that is added to the peptide chain: deprotection, activation, and coupling. In Fmoc chemistry, the α -amino acid protecting group is Fmoc.

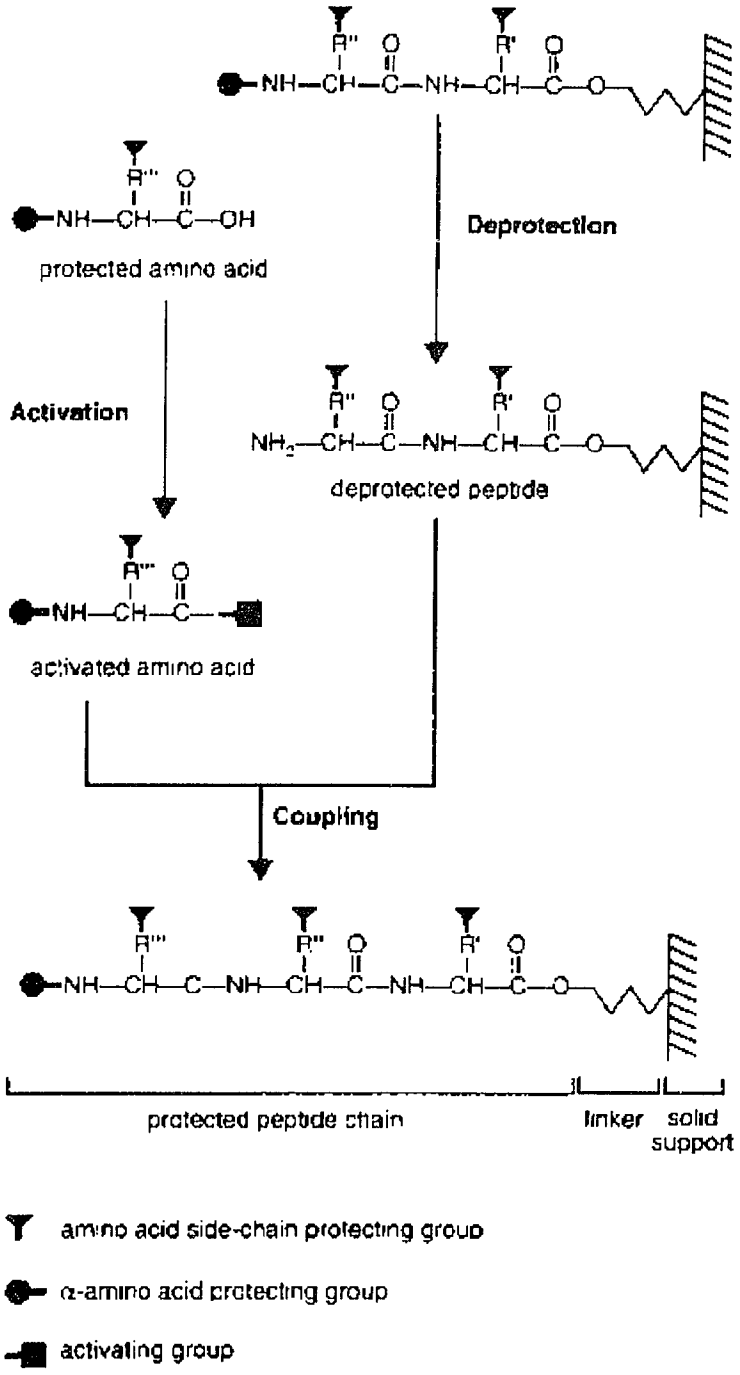

Solid-phase Peptide Synthesis

Fig. 2-3 Pathway of Solid-Phase Peptide Synthesis.

The amino acid side-chain protecting groups that we are using are as follows:

Table 2-2 Side-chain protecting groups of the twenty amino acids

Amino Acids	*Side-chain protecting group*
Ala	None
Arg	Pmc
Asn	Trt
Asp	OtBu
Cys	Trt
Gln	Trt
Glu	OtBu
Gly	None
His	Trt
Ile	None
Leu	None
Lys	Boc
Met	None
Phe	None
Pro	None
Ser	tBu
Thr	tBu
Trp	Boc
Tyr	tBu
Val	None

These are the only twenty common L-amino acids found in nature used by all organisms. " None " means that no side-chain protecting group is needed for that particular amino acid to proceed Solid Phase Peptide Synthesis. Next page is

an example of a trimer (Cys-Pro-Cys) peptide synthesis sheet. The synthesis detector tracer for this trimer which refers to the deprotection efficiency and coupling yield is showed in the following page. There are three cycles which are Cys, Pro, and Cys. Four peaks in the beginning of each cycle represents to the deprotection of Fmoc-resin, Fmoc-Cys-resin, Fmoc-Pro-Cys-resin, and Fmoc-Cys-Pro-Cys-resin. Three oscillating lines stand for the coupling of three residues.

2.3.2. Cleavage and extraction:

The dried resin bonded peptide needs to be cleaved off the resin and all the side-chain protecting groups also need to be deblocked. For a batch size of 500 mg peptidyl resin, 5 ml of total cleavage solution is used. The compositions of cleavage solution are mainly Trifluoacetic acid (TFA) with a small amount of scavengers which prevent the peptide from the further reaction of the side-chain protecting groups. The ingredients include: 4.5 ml TFA + 0.25 ml Thioanisole + 0.15 ml 1,2-ethanedithiol + 0.1 ml Anisole. Briefly, add 4.5 ml TFA to a glass test tube and allow it to cool in an ice bath, add scavengers to the TFA and mix well. After cooling the 50 ml Falcon tube containing the peptidyl resin for 20 minutes, add the TFA and scavenger mixture drop by drop to the peptidyl resin and let it react at room temperature for 3 hours. After reaction, the mixture are added to precooled anhydrous ether. Since the peptide is usually not soluble in ether, a white precipitate will form during this procedure. The mixture is vortexed and centrifuged for 10 minutes and then decanted. The mixture will be washed six

times before transfer to funnel filter. The peptide is now ready to be extracted and lyophilized.

Peptide Synthesis Calculation Sheet:

Mode is "User Cycles".

Notebook name is "cpc".
Notebook file is "CPC.NBK".

Target Peptide: length = 3. MW = 320.434

NH2-END-Cys-Pro-Cys-SPC-CONH2

Support substitution = 0.210 meq/g
Support quantity = 0.510 g
Excess amino acid = 4.000 x

Peptide Quantity = 0.107 mMoles
Theoretical Yield = 0.034 g

Starting Support: Peptide-Amide

Cycle	AA	Proto	Time	Derivative	Grams	mL	Vial
5)	SPC	0	00:07:50	System Preparation	0.000		1
4)	Cys	Bd	01:18:10	Fmoc-L-Cys(Trt)-OH	0.251	1.7	2
3)	Pro	Bd	01:18:10	Fmoc-L-Pro-OH	0.145	1.6	3
2)	Cys	Bd	01:18:10	Fmoc-L-Cys(Trt)-OH	0.251	1.7	4
1)	END	F	00:20:15	Final Cycle	0.000		5

Minimum loop size = 5 mL
Installed loop size = 10 mL

Estimated time required for synthesis completion: 04:22:35

Estimated Reagent consumption and requirements for synthesis completion:

	consumption	required
Main Wash	355 mL	455 mL
Deblock	93 mL	193 mL
Wash 2	43 mL	143 mL
Aux Wash	13 mL	113 mL
Syringe 2	6 mL	18 mL
Syringe 3	5 mL	17 mL
AAM Wash	56 mL	156 mL
Synth Waste	420 mL	
SP1 Waste	10 mL	
AAM Waste	141 mL	

Quantity	Chemistry	Vial #
2 Cys	Fmoc-L-Cys(Trt)-OH	2 4
1 Pro	Fmoc-L-Pro-OH	3
1 SPC	System Preparation	1
1 END	Final Cycle	5

Figure 2-4 Synthesis sheet of tripeptide Cys-Pro-Cys.

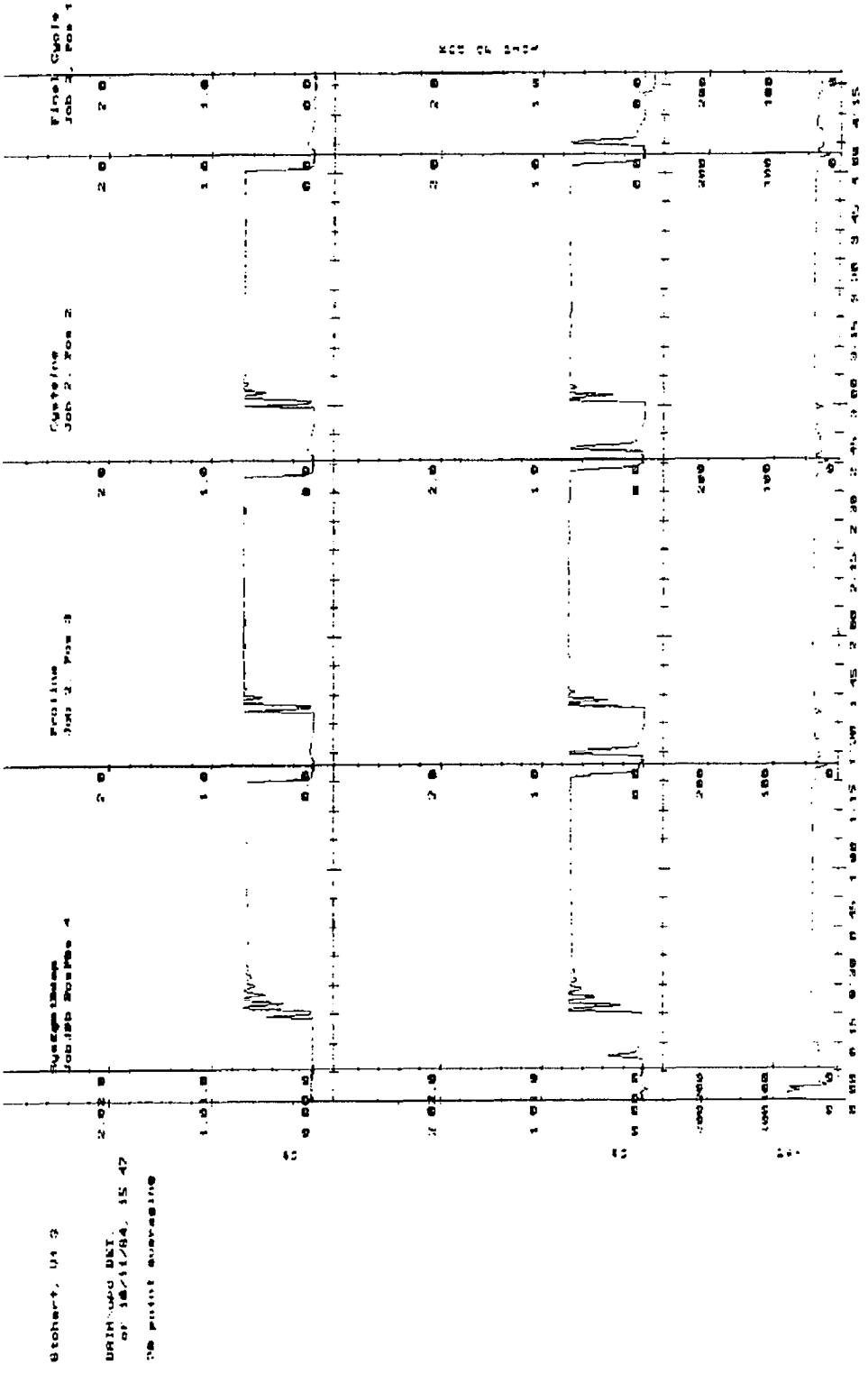

Figure 2-5 Detector printout of tripeptide Cys-Pro-Cys.

2.3.3. Cyclization of peptide:

The model peptides with two Cys at C-terminal and N-terminal could be cyclized through S-S disulfide bond linkage which is formed from the free -SH on the side-chain of Cys. Disulfide bonds comprise the major covalent cross-linkage in proteins and may be intra- or inter-chain in nature. Intra-chain disulfide bonds serve to confer conformational stability on the folded polypeptide chain. Additionally, by limiting or directing this folding these bonds may contribute to the correct orientation of the amino acid residues that form the active sites of enzymes, antibodies and other biologically active proteins. Inter-chain disulfide bonds are functional in maintaining the quaternary structure of multi-chain proteins, serving as the only linkage between subunits or providing covalent stability to structures otherwise maintained by non-covalent forces [2-17]. Thus, the studies of polypeptide involved disulfide bonds are very important.

The method that we are currently utilizing is oxidation of the peptide by hydroperoxide at low temperature [2-18]. Here, to a dilute peptide solution (0.5 mg/ml) in degassed water and H_2O_2 is added dropwise to a final concentration of 0.2%. The mixture is left at 4 ^{0}C overnight; and checked by analytical HPLC for completeness of cyclization. After completion of the cyclization, the cyclized peptide solution is frozen and lyophilized. The cyclized peptide will be further purified using preparative HPLC depending upon the requirement of the peptide purity. The octapetide discussed later in this part is cyclized by other method since

there is a Trp residue in the peptide. Briefly, a 0.2 mg/ml peptide solution is prepared and adjusted to PH = 7.4 by adding $(NH_4)_2 CO_3$. The solution is stirred at room temperature for 48 to 72 hours depending on the completion of the cyclization which is checked by HPLC.

Here are the sample HPLC profiles of octamer peptide with and without cyclization. The bottom one is uncyclized while the top one is cyclized. Both peptides have a purity of more than 95% from HPLC method. The condition of HPLC at these runs are: solvent A, 0.05% TFA in water; solvent B, 0.05% TFA in acetonitrile; C18 column at room temperature; flow rate 2 ml/min and gradient from 95% solvent A 5% solvent B to 24% solvent A 76% solvent B in 40 minutes.

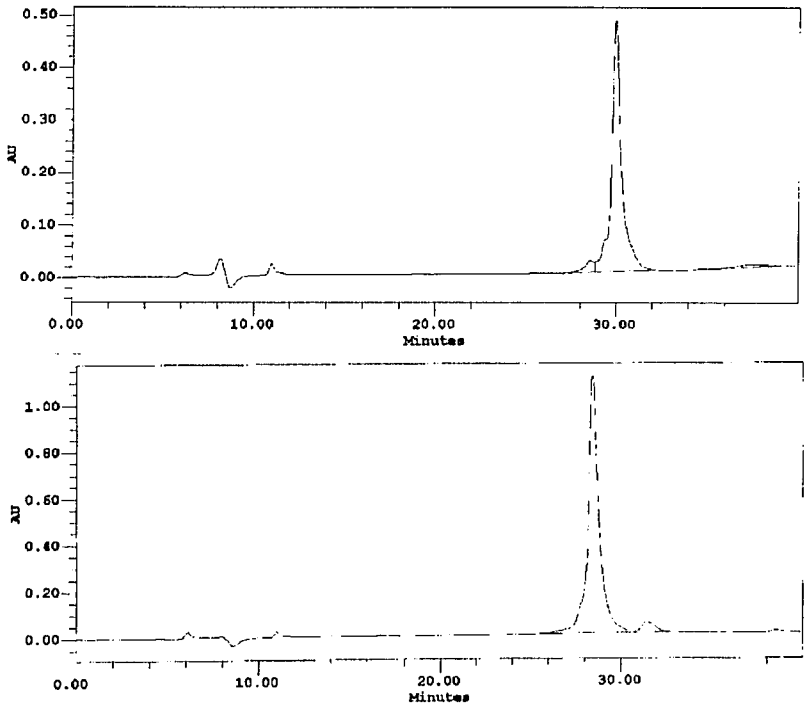

Fig. 2-6 HPLC graphics of cyclized and uncyclized octamer peptide (H-Phe-Cys-Phe-Trp-Lys-Thr-Cys-Thr-NH_2).

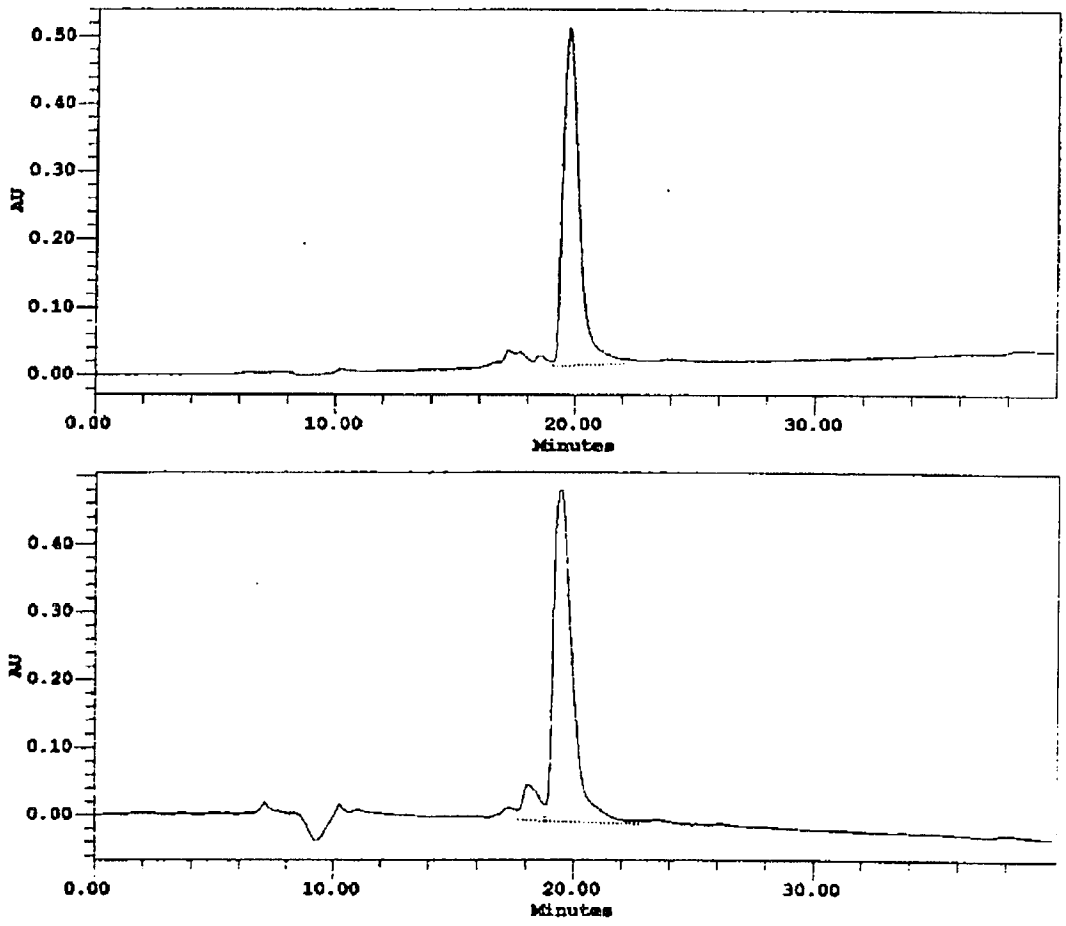

Fig. 2-7 Reverse Phase HPLC profiles of linear peptide of CP(dF)C. Upper one is purified and the lower one is crude.

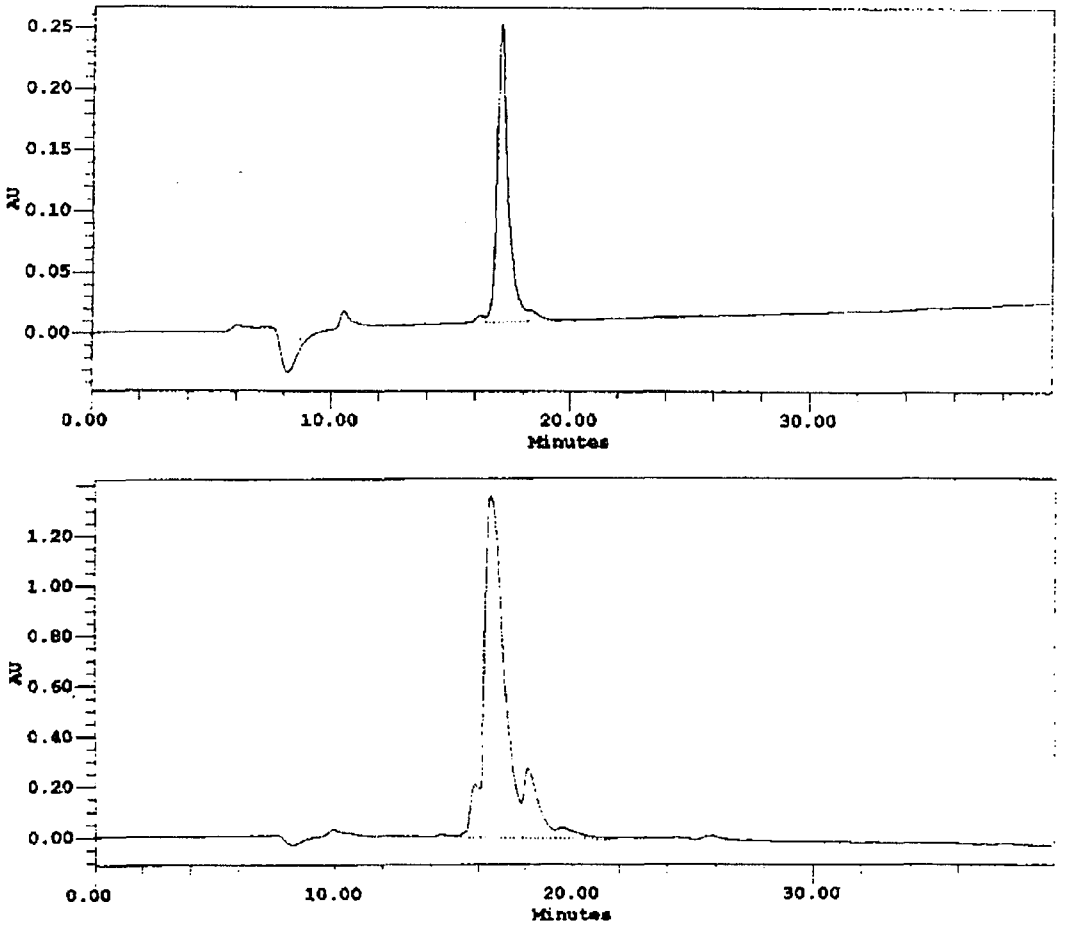

Fig. 2-8 Reversed Phase HPLC profiles of the linear peptide of CPFC. The top one is purified and the bottom one is crude.

2.4 CONCLUSIONS:

2.4.1. Linear peptides:

H-Cys-Pro-Gly-Cys-NH_2 , H-Cys-Pro-Phe-Cys-NH_2 , H-Cys-Pro-(d-Phe)-Cys-NH_2 , H-Cys-Ala-Cys-NH_2 , H-Cys-Pro-Cys-NH_2 , H-Cys-Pro-Lys-Cys-NH_2 , H-Cys-Pro-Asp-Cys-NH_2 , CH_3CO-Cys-Pro-Gly-Cys-NH_2 , and H-Phe-Cys-Phe-Trp-Lys-Thr-Cys-Thr-NH_2 have been successfully synthesized according to the methods we discussed above. Several peptides are also purified by HPLC when they are necessary for the later experiments. Figure 2-7, 8 show the HPLC profiles of both crude and purified peptides CPFC and CP(dF)C. The peptide purity can be estimated above 85% for crudes and 95% for purified peptides by HPLC.

2.4.2. Cyclized peptides:

c(Cys-Pro-Gly-Cys), c(Cys-Pro-Phe-Cys), c(Cys-Pro-(d-Phe)-Cys), c(Cys-Ala-Cys), c(Cys-Pro-Cys), c(Ac-Cys-Pro-Gly-Cys), c(Phe-Cys-Phe-Trp-Lys-Thr-Cys-Thr) have been successfully synthesized, cyclized and purified according to the above methods. The HPLC graphics of cyclized octapeptide is shown in Figure 2-6. The figure indicated that more than 95% of purity of the peptide has been achieved.

2.5 REFERENCES:

2-1 For a review of the early history of peptide synthesis, see Fruton, J.S. (1987) in *Peptides 1986*, Theodoropoulous, D. (ed.), Walter de Gruyte, Berlin, p. 25.

2-2 du Vigenaud, V., Ressler, C., Swann, J.M., Roberts, C.W. and Katsoyannis, P.G. (1954) *J. Amer. Chem. Soc.*, 76, 3115.

2-3 Bergmann, M. and Zervas, L. (1932) *Chem. Berichte*, 65, 1192.

2-4 Goddard, P., McMurray, J. S., Sheppard, R. C. and Emson, P. (1988) *J.Chem. Soc. Chem. Commun.*, 1025.

2-5 Merrifield, R. B. (1963) *J. Amer. Chem. Soc.*, 85, 2149.

2-6 Merrifield, R. B. (1964) *Biochemistry*, 3, 1385.

2-7 Kemp, D. S. (1973) in *Peptides 1971*. Nesvadba, H. (ed), North Holland, Amsterdam, p. 1.

2-8 Kemp, D. S., Choong, S. L. H. and Pekaar, L. (1974) *J.Chem. Soc.*, 4097.

2-9 Atherton, E., Logan, C. J. and Sheppard, R. C. (1981) *J. Chem. Soc., Perkin Trans.* 1, 538.

2-10 Carpino, L. A. and Han, G. Y. (1972) *J. Org. Chem.*, 37, 3404.

2-11 Kaiser, E., Colescott, R. L., Bossinger, C. D. and Cook, P. I. (1970) *Analyt. Biochem.*, 34, 595.

2-12 Sarin, V. K., Kent, S.B.H., Tam, J.P. and Merrifield, R.B. (1981) *Analyst. Biochem.*, 117. 147.

2-13 Kuhn, R., Winterstein, A. and Lederer, E. (1931) *Hoppe-Seyler's Z. Physiol. Chem.*, 197, 141.

2-14 Martin, A.J.P. and Synge, R.L.M. (1941) *Biochem. J.*, 35, 1358.

2-15 Consden, R., Gordon, A.H. and Martin, A.J.P. (1944) *Biochem. J.*,38, 224.

2-16 Howard, G.A. and Martin, A.J.P. (1950) *Biochem. J.*, 46, 532.

2-17 Hruby, V.J. (1993) *Proceedings of the Thirteenth American Peptide Symposium*, p. 3.

2-18 Norbert P.N. (1972) *Methods in Enzymology*, 25-6.

CHAPTER THREE
OPTICAL ACTIVITY OF MOLECULES AND VIBRATIONAL CIRCULAR DICHROISM

Optical rotatory dispersion and circular dichroism have been known for more than 100 years.[3-1, 2, 3] In the early 1950s, revolutionary progress in the study of optically active molecules was brought about through the introduction of new instruments to measure optical rotatory dispersion routinely. Until the 1960's, most applications in chemistry only utilized the optical rotation at some transparent wavelength. The last two decades have seen the use of ORD diminished and really all O.A. method are performed.

Vibrational Circular Dichroism (VCD) was first reported nearly two decades ago in 1974, [3-4] progress in the field has been slow, and observation of VCD in the mid-infrared region (5 to 10 nm , or 2000 to 1000 cm^{-1}) from aqueous solution has not been possible until the mid 1980's. Most unfortunately, the number of research groups involved in this area has remained constant, at best, or even decreased somewhat, due to the difficulties in constructing the necessary equipment, which is not yet commercially available.

In the past, VCD was observed by one of two experimental approaches, dispersive or Fourier Transform instrumentation. For biological samples, there are normally no enantiomeric samples available to check for the accuracy of the measurement, dispersive instruments have been used dominantly.

3.1 OPTICAL ACTIVITY OF MOLECULES

Optical activity is a property exhibited by enantiomerically pure, chiral molecules. Chirality, or handedness, describes the relationship between two molecules that are related to each other like a left hand is left to a right hand, namely, by being mirror images of each other. A molecule is said to be chiral when it is nonsuperimposable on its mirror image.

With the exception of glycine, the alpha carbon atom in amino acids is tetrahedrally attached to four different atoms or groups of atoms. Such a carbon is called chiral (from the Greek "cheiros", meaning "hand") or asymmetric. Because of this arrangement, amino acids can exist in different stereoisomeric configurations, distinguished from each other by the spatial orientation of the groups attached to the alpha carbon. For each asymmetric carbon there are two different configurations. The two stereoisomers are called L and D configurations, representing two nonsuperimposable mirror image structures called enantiomers.

One of the essential differences between the chemistry of living and nonliving systems is the greater structural complexity of biological macromolecules. That implies the shape of a molecule is an important feature for peptides or proteins. Most of their bioactivities attribute the folding of a peptide or protein into a certain tertiary structure.

Twenty amino acids except Glycine discussed above are all asymmetric chromophores. The dissymmetric chromophore is one where the symmetry of the isolated chromophore is sufficiently high to preclude optical activity. Optical activity is observed only in cases of chiral interaction of these symmetric chromophores. As such, the signed magnitudes of the associated rotational strength provide information as to the chemical nature of the molecular environment and its disposition relative to the symmetry planes of the chromophore, whereas inherently symmetric chromophores exhibit rotational strengths that are generally significantly less in magnitude. Mostly, this second

case is a major application which would deal with molecular conformation rather than configuration. Whereas the configuration around an asymmetric carbon atom is fixed and can only be altered by the breaking a chemical bond, molecular conformation is less well defined and can change as rotation about single bonds occurs. Molecular conformation may be monitored in optical activity via the coupling of transitions in groups which are arranged in a dissymmetric fashion. One such example as of coupling of transition is the "Coupled Oscillator". In this case, Circular Dichroism (CD) consists of positive and negative contributions for the coupled transitions. The coupling lifts the degeneracy; thus, produces an absorption spectrum consisting of two overlapping peaks. From the relative magnitudes of the positive and negative CD peaks, the dihedral angle between the groups, on which the transitions are localized, can be deduced.

This last mechanism is mostly responsible for the large CD features of well-ordered polymers, such as peptide α-helices, in which the peptide moieties are arranged in such a manner that their transitions occur in well-predictable geometric patterns. Upon conformational changes of the ordered polymer, for example during denaturation, significant changes in the CD spectra observed since the geometric order is destroyed or altered.

3.1.1 QUANTUM MECHANICS OF OPTICAL ACTIVITY

Moffitt, Moscowitz and Djerassi and co-workers[3-5] classified optically active chromophores into terms of two limiting types:

(a) the inherently dissymmetric chromophore (asymmetric, C1 point group)

(b) the inherently symmetric, but dissymmetrically perturbed chromophore (dissymmetric, Cn and/or Dn point group, n = odd number).

In general, there are two theories that can be followed, based respectively on the theory of oscillators, and the principles of quantum mechanics. Here we only quote some results from the quantum mechanics. The first application of the quantum theory to optical activity was made by Rosenfeld[3-2], and elaborated upon by Condon.[3-3] Moffitt and Moscowitz[3-4] also revised and extended these calculations.

A molecule represented in a system which is not subjected to the action of an external field can presented by the wave function Ψ. The mean value of a variable connected with this system is then given by

$$\langle f \rangle = \int \Psi^* F \Psi d\tau \tag{3.1}$$

where Ψ^* is the complex conjugate of Ψ and F is the operator connected with the variable under consideration.

A well-known quantum mechanical operator is the energy operator H, called the Hamiltonian. The energy of the system is then:

$$E = \int \Psi^* \mathrm{H} \cdot \Psi d\tau \tag{3.2}$$

The total absorption of the molecule in electric field:

$$A_{0\to 1} = \frac{1}{2\pi h^2 \nu^2} \left| \left\langle \Psi_1(q,Q) \left| \sum_j \frac{e_j}{m_j} e^{i\bar{k}\cdot\bar{r}_j} \cdot \bar{\varepsilon}_U \cdot \bar{p}_j \right| \Psi_0(q,Q) \right\rangle \right|^2 \tag{3.3}$$

Here, e_j and m_j are the electric charge and mass on the jth particle, respectively. $\bar{K}$ is the light wave vector, $\bar{K} = (2\pi\nu/c)\bar{\varepsilon}_k$. $\bar{\varepsilon}_K$ *and* $\bar{\varepsilon}_U$ are the unit vectors in the

propagation direction and the polarization direction of light respectively, and $\bar{p}_j$ is the linear momentum of the jth particle.

The operator $e^{i\bar{K}\cdot\bar{r}_j}$ can be expanded into a converging Taylor series since $\bar{K}\cdot\bar{r}_j << 1$.

$$e^{i\bar{K}\cdot\bar{r}_j} = 1 + i\bar{K}\cdot\bar{r}_j - 0.5(\bar{K}\cdot\bar{r}_j)^2 + \cdots \tag{3.4}$$

The first terms in Eq.(3.4) produces the electric dipole transition moment, $\boldsymbol{\mu}$

$$\mu_{e(0\to 1)} = \langle \Psi_1 | \bar{\mu} | \Psi_0 \rangle \tag{3.5}$$

$$\bar{\mu} = \sum_j e_j \bar{r}_j \tag{3.6}$$

where the second term is:

$$\left\langle \Psi_1(q,Q) \left| \sum_j \frac{e_j}{m_j} (i\bar{K}\cdot\bar{r}_j)(\bar{\varepsilon}_U \cdot \bar{p}_j) \right| \Psi_0(q,Q) \right\rangle \tag{3.7}$$

Since $\bar{K} = (2\pi\nu/c)\bar{\varepsilon}_K$, equation (3.7) becomes:

$$2\pi i\nu \left\langle \Psi_1(q,Q) \left| \sum_j \frac{e_j}{m_j} (\bar{r}_j)_K (\bar{p}_j)_U \cdot \right| \Psi_0(q,Q) \right\rangle \tag{3.8}$$

This integrand actually contains two terms: the magnetic dipole moment, ***m***:

$$\begin{aligned} m_{(0\to 1)} &= \langle \Psi_1 | \bar{m} | \Psi_0 \rangle \\ \bar{m} &= 0.5 \sum_j (\bar{r}_j \times \bar{p}_j) K x U^* \end{aligned} \tag{3.9}$$

and electric quadrupole transition moment, Θ:

$$\Theta_{0\to 1} = \langle \Psi_1 | \bar{q} | \Psi_0 \rangle \tag{3.10}$$

$$\bar{q} = 0.5 \sum_j \left[\left(\bar{r}_j \bar{p}_j \right)_{KU\cdot} + \left(\bar{r}_j \bar{p}_j \right)_{U\cdot K} \right] \tag{3.11}$$

In regular absorption, Θ is small and can be ignored. Therefore, the total absorption of the molecule is:

$$A_{0\to 1} = \frac{4\pi^2 \nu}{\eta c} n \sum_f G_f(\bar{\nu}) \left| \bar{\varepsilon}_{U\cdot} \cdot \mu_{e(0\to 1)} + (\bar{\varepsilon}_K x \bar{\varepsilon}_{U\cdot}) \cdot \mu_{m(0\to 1)} \right|^2 \tag{3.12}$$

Here, $G_f(\nu)$ is a band shape function; n is the number of molecules per cm^3, n= CN/1000. N is Avogadro's number.

When the square (dot product) in the equation (3.12) is evaluated, it is composed of three significant terms. If unpolarized light passes through an isotropic solution, the total absorption will involve the first term in (3.12) only, which is due to the electric dipole transition moment. This is called the dipole strength:

$$D = \left| \mu_{e(0\to 1)} \right|^2 = \mathrm{Re} \langle \Psi_0 | \bar{\mu} | \Psi_1 \rangle \cdot \langle \Psi_1 | \bar{\mu} | \Psi_0 \rangle \tag{3.13}$$

If circularly polarized light passes through an isotropic sample, the total absorption of molecules will involve all three terms in (3.12). They actually are composed of two part: a real and an imaginary part. The latter gives the information about optical activities of both molecules and light beam present. In regular cases, the second component of imaginary part is small and can be ignored.

The first imaginary component is the cross term between $\mu_{e(0\to1)}$ and $\mu_{m(0\to1)}$, that gives rise to the molecular optical activity called rotatory strength R:

$$R_i = \mathrm{Im}\left[\left\langle \Psi_0 \middle| \mu_i \middle| \Psi_1 \right\rangle \cdot \left\langle \Psi_1 \middle| m_i \middle| \Psi_0 \right\rangle\right] \tag{3.14}$$

From quantum chemistry, one can derive the following relationship:

Dipole strength:

$$D = \left|\mu_{e(0\to1)}\right|^2 = \mathrm{Re}\left\langle \Psi_0 \middle| \bar{\mu} \middle| \Psi_1 \right\rangle \cdot \left\langle \Psi_1 \middle| \bar{\mu} \middle| \Psi_0 \right\rangle = \frac{2.303x3hc}{8N\pi^3} \int \frac{\varepsilon(\bar{\nu})}{\bar{\nu}} d\bar{\nu} \tag{3.15}$$

The second part of this equation can be derived from statistical thermodynamics. The integration represents the area under an absorption peak corresponding to one electronic transition.

The rotatic nal strength, R, is a unique quantity observed in CD, that accounts for the interaction between the electronic transition and the magnetic transition.

$$\begin{aligned} R_i &= \mathrm{Im}\left[\left\langle \Psi_0 \middle| \mu_i \middle| \Psi_1 \right\rangle \cdot \left\langle \Psi_1 \middle| m_i \middle| \Psi_0 \right\rangle\right] \\ &= \frac{2.303x3hc}{32N\pi^3} \int_{band} \frac{\varepsilon_L(\bar{\nu}) - \varepsilon_R(\bar{\nu})}{\bar{\nu}} d\bar{\nu} \\ &= 2.297X10^{-39} \int_{band} \frac{\varepsilon_L(\bar{\nu}) - \varepsilon_R(\bar{\nu})}{\bar{\nu}} d\bar{\nu} \end{aligned} \tag{3.16}$$

Here, $\varepsilon_L(\bar{\nu}), \varepsilon_R(\bar{\nu})$ are the molar absorptivity due to the left and right circular polarized light (CPL) respectively. Thus circular dichroism measures the absorption difference between left and right CPL of molecules. The optical

activity of molecules can be characterized by a dissymmetric factor, or anisotropy (g), which is defined by:

$$g = \frac{\Delta\varepsilon(\bar{\nu})}{\varepsilon(\bar{\nu})} = \frac{\varepsilon_L(\bar{\nu}) - \varepsilon_R(\bar{\nu})}{0.5\left[\varepsilon_L(\bar{\nu}) + \varepsilon_R(\bar{\nu})\right]} = \frac{4R}{D} \qquad (3.17)$$

g is a dimensionless quantity. To be more detailed, $\Delta\varepsilon(\nu)$ and $\varepsilon(\nu)$ should be the areas under the respective absorption bands. The latter part of the equation is easily obtained, from equations (3.15) and (3.16). The anisotropy, g, is a characteristic constant which is used to identify a compound and its optical activity.

3.2 VIBRATIONAL CIRCULAR DICHROISM (VCD)

VCD is conceptually a straightforward experiment [3-6, 7] in which the differential absorption of left and right circularly polarized infrared radiation by a vibrational transition of a chiral molecule is observed. As such, it is a direct extension of the principles of electronic CD toward a different spectral range, namely, that involving vibrational transitions [3-8, 9].

3.2.1 Phenomenological Description and Basic Equations

VCD can be viewed as an extension of the principles of electronic circular dichroism (CD), normally observed in the ultraviolet spectral region, into the domain of vibrational transitions in the infrared spectral region. In infrared VCD,

the experimental result is the differential absorption between left and right circularly polarized infrared radiation, defined as

$$\Delta A = A_L - A_R \qquad (3.18)$$

Here, capital subscripts R and L are used to denote right and left circularly polarized radiation. For a given transition, the differential absorption ΔA can be related to the quantum mechanical observable known as the rotatory strength R_{01} by converting from ΔA units to $\Delta\varepsilon$ units, using the Lambert - Beer law and integrating over the VCD peak:

$$R_{01} = \int (\Delta\varepsilon / \nu)\, d\nu \qquad (3.19)$$

Similarly, the dipole strength D_{01} is obtained by converting from absorbance units A to units of ε and integrating:

$$D_{01} = \int (\varepsilon / \nu)\, d\nu \qquad (3.20)$$

The ratio of the integrated VCD and absorption peaks can be defined as

$$\Delta A / A = 4\, R_{01} / D_{01} \qquad (3.21)$$

and is typically on the order of 5×10^{-4} to 5×10^{-5}.

The rotatory strength is given in terms of the molecular transition moments by

$$R_{01} = \mathrm{Im}\, [\, \langle 0 | \mu | 1 \rangle \bullet \langle 1 | m | 0 \rangle\,] \qquad (3.22)$$

in analogy to the dipole strength of a transition

$$D_{01} = \langle 0 | \mu | 1 \rangle^2 \qquad (3.23)$$

In these last equations, $|0\rangle$ and $|1\rangle$ denote vibrational ground and excited state wavefunctions, and $\boldsymbol{\mu}$ and $\mathbf{m}$ are the electric and magnetic dipole operators, respectively.

As in all manifestations of natural optical activity, the desired observables (ΔA or R_{01}) arise through the interference of electric and magnetic dipole transition moments. The sensitivity of chiroptical techniques toward the handedness of the molecule results directly from the form of the magnetic moment operator: it contains the vector product of momentum and position vectors, the result of which is another vector. The sign of this vector is determined by the handedness of the coordinate system, and it is well known that a vector product will change sign upon converting from a left- to a right-handed coordinate system. By changing the configuration of the molecule from one to the other enantiomer, the sign of the magnetic transition moment changes. Similarly, by keeping the configuration of the molecule fixed and changing from left to right circularly polarized light, we reserve the sign of the magnetic transition moment. Since VCD is a very small effect, its observation was and still is rather difficult. However, through the diligent efforts of a few research groups in the field, VCD has now become a generally applicable spectroscopic technique.

3.2.2. Principles of Vibrational Circular Dichroism

For VCD measurement, the actual differential signal, at constant circular dichroism of the sample, will vary with the light level transmitted at a given wavelength. Denoting the signal at modulator frequency as I_{AC} (ν), and the overall transmission of the instrument and the sample as I_{DC} (ν), it can be shown from an analysis of the radiant energy at the detector, the electronic output of the detector is proportional to the time averaged intensity. The intensity is:

$$I = 0.5E_0^2\left\{\left[1+\sin\alpha\right]10^{-A_+(\nu)} + \left[1-\sin\alpha\right]10^{-A_-(\nu)}\right\} \tag{3.24}$$

$$I = I_{DC}(\nu) + I_{AC}(\nu) \tag{3.25}$$

Only the ratio of I_{AC} (ν) over I_{DC} (ν) is of importance to a dichroism measurement.

$$I_{AC}(\nu)/I_{DC}(\nu) = \tanh(1.15\Delta A)\sin\alpha \tag{3.26}$$

Here, α denotes the retardation between two linearly polarized components of light used for the production of circularly polarized light, and equation (3.26) demonstrates that the ratio $I_{AC}(\nu)/I_{DC}(\nu)$ is proportional to ΔA. When using a PEM, sin(α) itself varies sinusoidal with time, and the retardation α may be rewritten as

$$\alpha = \alpha_0 \sin(\omega_M t) = \alpha_0 \sin(2\pi f_M t) \tag{3.27}$$

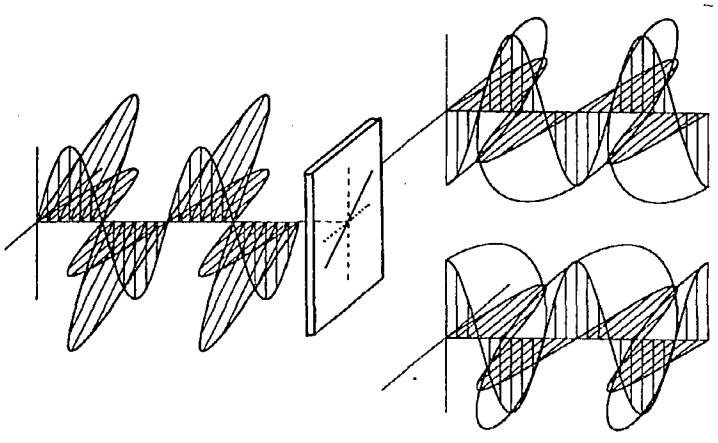

Figure 3-1. Left: linear polarized light; top right: right circular polarized light; bottom right: left circular polarized light.

Here, ω_M is the oscillation frequency of the modulator. The sine of a sine function may be expressed in terms of the Bessel function, $J_1(\alpha)$. Thus,

$$I_{AC}(\nu)/I_{DC}(\nu) = \tanh(1.15\Delta A(\nu))J_1(\alpha_0)\sin(2\pi f_M t) \tag{3.28}$$

where $J_1(\alpha_0)$ is the first order Bessel function. Obviously, α_0 is chosen to have the maximum $J_1(\alpha_0)$ for a maximum observable signal; therefore, α_0 =1.84. Equation (3.28) becomes,

$$\begin{aligned} I_{AC}(\nu)/I_{DC}(\nu) &= 2(1.15\Delta A(\nu))J_1(1.84) \\ &= 2 \times 0.5819 \times 1.152\ \Delta A(\nu) \\ &= 1.340\ \Delta A(\nu) \end{aligned} \tag{3.29}$$

The term $\sin(2\pi f_M t)$ disappears because the output of the lock-in amplifier, tuned to f_M, is a direct current (DC) signal proportional to the amplitude of the sine ($2\pi f_M t$) term. Thus, by taking the ratio of $I_{AC}(\nu) / I_{DC}(\nu)$, the VCD spectrum, $\Delta A(\nu)$, is acquired rather simply. This ratio-taking process is called normalization of $I_{AC}(\nu)$. Inspection of equation (3.29) yields that for the observation of ΔA, a signal in phase with ω_M must be monitored via a lock-in amplifier and continuously divided by the DC signal. Here, the $I_{DC}(\nu)$ should be due to an absorption of the functional group which contributed to $I_{AC}(\nu)$ rather than the total absorbency.

3.2.3. Dispersive Vibrational Circular Dichroism

The schematic of the electronic system in dispersive VCD is shown in Figure 3-2. The signal from the detector is first amplified via a preamplifier. Subsequently, the

signal is split into two paths. One of them leads into a digital lock-in amplifier which monitors the total signal at 79.5 Hz (I_{DC}). This amplifier features computer-controlled variable input gains of 1, 10, 100, followed by a voltage-to-frequency converter and fast, synchronous pulse counting. The other signal path is used to measure I_{AC} . Here, the signal is first demodulated at the PEM frequency (31.2 kHz) by a lock-in amplifier operating in a bandpass mode with Q of 100, a high-dynamic reserve, and a time constant of 1ms at 12 dB oct. (Figure 3-2) The output of signal from this lock-in amplifier actually are I_{AC} signals at frequency of 79.5 Hz. Further demodulation of this signal on another lock-in amplifier tuned to 79.5 Hz yield I_{AC}.

Compared to regular dispersive IR, the major difference between IR absorption and VCD is the additional PEM and a polarizer, to produce CPL. The optimized design of VCD considers two goals. One is the highest light throughput and the best possible resolution. These two requirements are, of course, mutually exclusive. Thus, one attempts to optimize throughput and resolution by carefully matching light source size, optical aperture, expected bandpass, slit width, and grating groove density.[3-10, 11, 12.]

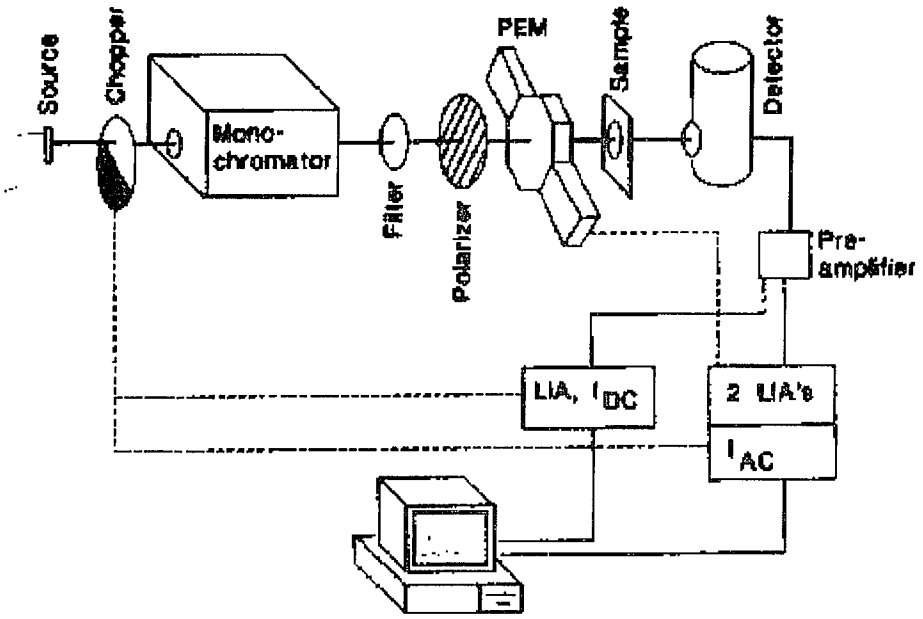

Fig. 3-2. Schematic of a dispersive VCD instrument. PEM, photoelastic modulator. LIA, lock-in amplifier.

3.2.4 Photoelastic Modulator (PEM) and Circular Polarized Light (CPL)

The heart of all chiroptical instruments is the device that produces alternating left and right circular polarized light. In VCD we use a device called photoelastic modulator (PEM). It is based on the phenomenon of stress birefringence to introduce a phase difference between two orthogonally polarized components of light incident on the modulator. The PEM crystal consists of a uniaxial piece of material which is transparent in the spectral region of interest and is aligned with its unique axis (the Z axis) along the propagation direction of the light.

Under the influence of the mechanical or electrical stress or strain, applied perpendicularly to the propagation direction of the light and along the crystal X or

Y axes; the refractive indices along the axes, n_x and n_y become unequal, causing light waves polarized along the X and Y directions to travel with different velocities through the crystal. At the exit face of the crystal circularly polarized light is produced if the retardation between the two orthogonal components of light is $\lambda / 4$ ($\pi/2$).

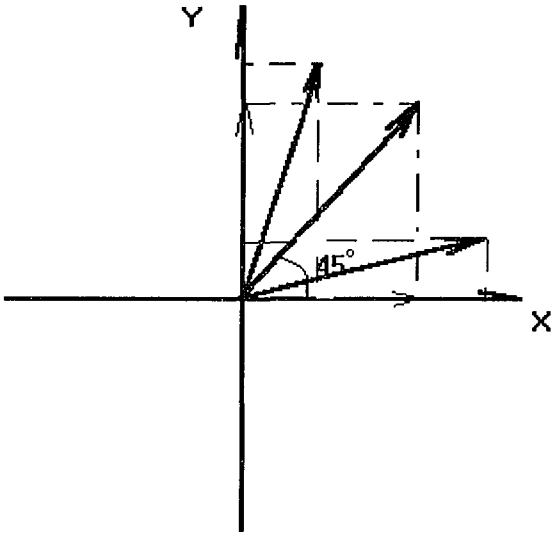

Figure 3-3. Linear polarized light can be decomposed into two components of linear polarized light (LPL) along in x and y axes. Under the strain/stress of PEM, the LPL along with either X axis or Y axis is retarded.

The polarizer axis is set at 45° with respect to the optical axis of the PEM (X axis). As the light reaches the PEM, it is considered a superposition of two linearly polarized waves, one parallel to the X axis, and the other parallel to the Y-axis of the PEM axis (Figure 3-3).

The alternating strain / stress is produced by squeezing the modulator crystal between two piezoelectric drivers. An AC voltage is applied to the

piezoelectric crystals, and the amplitude of this voltage determines the stress/strain and therewith, the retardation. Commercial modulators are available for the infrared region, using CaF_2 above 1200 cm^{-1}, and ZnSe down to about 600 cm^{-1} as stress optical materials. The retardation varies sinusoidal at the modulator frequency ω_M, which is determined by the crystal material, and its size. Since the modulation frequency is fixed, the retardation for each individual wavelength depends on the voltage applied to the piezoelectric drivers (Figure 3-1).

3.2.5 Double Modulation and Phase Sensitive Detector

As mentioned before, the difficulty for VCD is that the differential absorption ΔA is very small. A special electronic techniques, double modulation and phase-sensitive detection via lock-in amplifiers, is employed to extract the small signal out of noise level that is much larger.

The intensity of polarization components is described in Figure 3-4. The PEM works at 31.2 kHz with λ /4 retardation time. The shape of modulation voltage is a regular sine function. Ahead of the PEM, a polarizer is set up to produce linear PL oriented at 45° with modulator axis. The linear polarized light consist of two components (X and Y). During the first half period (0-180°) of modulation, the positive voltage is applied to the crystal. Right CPL is produced and reaches a maximum when the voltage is maximum. During the second half period (180°-360°) of modulation, a negative voltage is applied to the crystal. Left CPL is produced and a maximum left CPL is reached at minimum of modulation voltage. The retardation of the crystal is controlled by adjusting the amplitude of voltage applied to crystal. The right and left CPL have same intensity and the phase difference between them is 180° . When the applied voltage is zero, the light is still linear polarized. At this point the total light intensity is constant

and is equal to $I_{DC}(\nu)$; $I_{AC}(\nu)$ is equal to zero. It is shown at (a) in Figure 3-4. Because the absorption coefficients of a chiral sample toward right CPL and left CPL are different, the intensities of right and left CPL become different after sample. The total intensity of light, I_{DC} (ν),

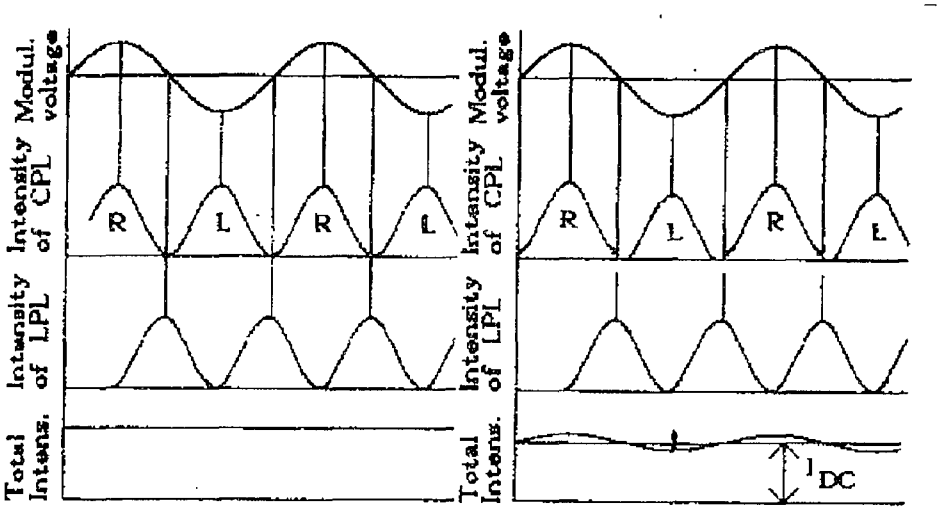

Before Sample After sample

Figure 3-4. Intensity of R, L and linear polarized light components during cycle before and after sample.

depends on the absorption of sample. At that time, the difference between the right and left CPL $I_{AC}(\nu)$ is not zero any more and depends on the difference between the intensity of right and left CPL and has same frequency as that of modulation voltage.

3.3. COMPUTATIONAL METHOD: COUPLED OSCILLATOR MODEL

To predict the conformation of a molecule in solution, one needs to compare the experimentally observed IR and VCD spectra to calculated ones, which are based on certain theoretical models. There are several methods that have been applied to compute the CD and VCD spectrum of biopolymer. Here we like to introduce the simplest method to calculate a VCD spectrum, called " coupled oscillator model". The pioneers of this work are Moffiit and Tinoco, who started it in the 1950's.[3- 13, 14, 15, 16, 17, 18.]

In a biopolymer (protein or DNA), the polar transitions of certain functional group, such as C=O stretching vibration, are arranged by the geometry of the fixed secondary structure of a biopolymer. For example, the C=O amid I transitions aligned almost parallel to the axis of α-helix in peptide. If one vibrational quantum is absorbed by these degenerate oscillators, the resulting vibrationally excited state is best described by sum over all possible one-quantum excitations. This implies that the excitation is no longer localized on one of the oscillators, but is delocalized over the entire array of identical oscillators. This delocalized excitation is referred to as an " exciton"[3-2]. The dipolar coupling between the transitions lift their degeneracy; consequently, one observes as many discrete exciton energy levels as there are interacting dipoles.

The coupled oscillator model considers the interaction among identical or near identical dipoles. When they are radiated by an appropriate wavelength, the dipoles can oscillate in correlated manner as if they saw each other instead of independently. For example, the absorption intensity of a dimer is equal to twice the monomer absorption plus a small correction caused by the interaction of the monomers. However, the rotation of a dimer is all due to the monomer

interaction, if the monomers are chosen to have no optical rotation. The dimer will also have new energy levels which will affect both the absorption and the rotation. The magnitudes and wavenumbers of the couplet depend on the geometry of the dipoles (direction of dipole and distance between dipoles). However, the coupling is not limited to two dipoles, and can be extended to any number of dipoles (called n-mer) until infinity (polymer).

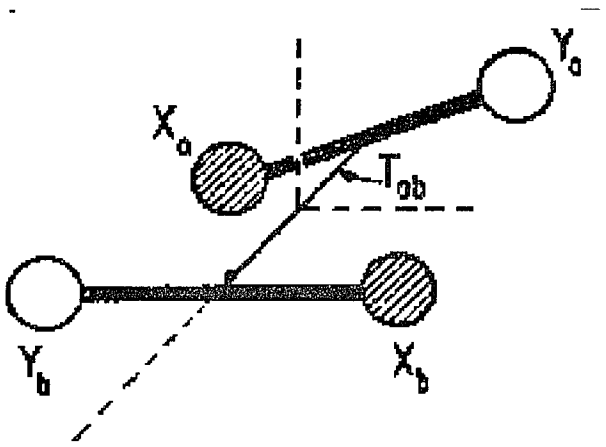

Figure 3-5. An optically active dimer consisting of two identical diatomic molecules X and Y. The vector tab connects the center of mass of monomer A to the center of mass of molecule B.

For simplicity, consider a hypothetical, optically active dimer composed of two diatomic, polar molecules, 1 and 2. The distance vector, T_{12}, links the centers of mass of the each dipole. The properties of such a dimer provide useful insight into the behavior of real molecules. Let us consider the ground state and first excited states of monomer 1 $\psi_g^1(q,Q)$ and $\psi_f^1(q,Q)$, with similar function for monomer 2, where q and Q symbolizes electronic and nuclear coordinates respectively. The total wavefunction of the dimer for ground state is:

$$\Psi_g = \psi_g^1(q,Q)\psi_g^2(q,Q) \tag{3.30}$$

Because of degeneracy between the function $\psi_f^1\psi_g^2$ and $\psi_g^1\psi_f^2$, the zero order vibrational excited states of the dimer will consist of symmetrically and antisymmetrically coupled monomer functions. Designating these by Ψ^+ and Ψ^-, one has

$$\Psi^{\pm} = (\psi_f^1\psi_g^2 \pm \psi_g^1\psi_f^2)/\sqrt{2} \tag{3.31}$$

The energies corresponding to the functions Ψ^+ and Ψ^- will generally differ because of coupling between the monomers; this may be viewed as a form of Fermi resonance.

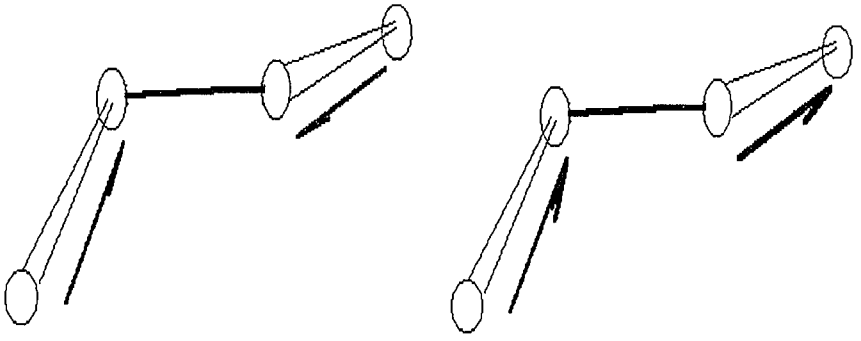

Symmetric Oscillation Antisymmetric Oscillation

Figure 3-6. Oscillation Model of Chromophomers

As mentioned above, the infrared optical activity of dimer, i.e. its circular dichroism and vibrationally induced optical rotation, are most succinctly characterized by the rotational strengths R of the vibrational transitions. The rotational strength R of a transition from state g to state f is given by

$R = \mathrm{Im}(\mu_{gf} \bullet m_{fg})$ where μ_{gf} is electric transition dipole moment for the transition g to f and m_{fg} is the magnetic transition dipole moment for transition f to g. Thus, in order to evaluate the rotational strength R_+ and R_- for the transitions $\Psi^0 \rightarrow \Psi^+$ and $\Psi^0 \rightarrow \Psi^-$, we need to evaluate the electric and magnetic dipole moments of these transitions.

For the dimer or two coupling dipoles,

$$D_{\pm} = \mu^2 \pm \bar{\mu}_1 \cdot \bar{\mu}_2 \tag{3.32}$$

$$\begin{aligned} R_{\pm} &= \pm(\pi \bar{\nu}_0 / 2c)(\bar{\bar{T}}_{1,2} \cdot \bar{\mu}_1 x \bar{\mu}_2) \\ &= \pm(\pi \bar{\nu}_0 / 2c) R\ \mu^2 \sin\phi_1 \cos\theta_2 \end{aligned} \tag{3.33}$$

θ, ϕ give the orientation of μ in spherical coordinate system. Notice that:

$$\nu_{\pm} = \nu_0 \pm V_{1,2} \tag{3.34}$$

$$V_{1,2} = \frac{\bar{\mu}_1 \cdot \bar{\mu}_2}{\left|\bar{\bar{T}}_{12}\right|^3} - \frac{3(\bar{\mu}_1 \cdot \bar{\bar{T}}_{12})(\bar{\mu}_2 \cdot \bar{\bar{T}}_{12})}{\left|\bar{\bar{T}}_{12}\right|^5} \tag{3.35}$$

$$D_+ + D_- = 2D = 2\mu^2 \tag{3.36}$$

$$R_+ + R_- = 0 \tag{3.37}$$

$$\nu_+ + \nu_- = 2\nu_0 \tag{3.38}$$

Also the values of D, R, and V_{12} are all proportional to μ^2, the monomer absorption. The rotational strengths $R_{\pm}$ have the worrisome property of becoming large as the distance between monomers increases. However, the actual rotation at any wavelength will approach zero as the distance increases, because ν_+ approaches ν_- rapidly.

Therefore, from those equation, the optical activity of the dimer strongly depends on the orientation of transition moments in the dimer. For example, if one branch is absent, however (this corresponds to parallel moments), then $R\pm = 0$. Also, of course, coplanarity leads to $R\pm = 0$, and colinearity with R_{12} leads to $R\pm = 0$. The latter two conformations have planes of symmetry which preclude optical activity. A special case is the dimer with perpendicular transition moments. Then $R_{\pm} \neq 0$, but there is no splitting ($\nu_+ = \nu_-$), and therefore no rotation.

For a system of n coupled dipoles, the kth resultant exciton transition is given by:

$$R_k = -(\pi \nu_0 / c) \sum_{i=1}^{n} \sum_{j>i}^{n} c_{ik} c_{jk} \left[T_{ij} \cdot \mu_i \times \mu_j \right] \tag{3.39}$$

where c is velocity of light, and the c_{ij} are the eigenvector components of the (dipole-dipole) interaction matrix:

$$V_{i,j} = \frac{\overline{\mu}_i \cdot \overline{\mu}_j}{\left|\overline{T}_{ij}\right|^3} - \frac{3(\overline{\mu}_i \cdot \overline{T}_{ij})(\overline{\mu}_j \cdot \overline{T}_{ij})}{\left|\overline{T}_{ij}\right|^5} \tag{3.40}$$

here, T_{ij} is the distance vector between dipoles μ_i and μ_j. ν_0 is the center frequency of the unperturbed transition, and the subscript k refers to the k'th

exciton component (1< k<n). The infrared absorption intensities can be obtained from the dipole strengths D, defined by:

$$D_k = \sum_{i=1}^{n} c_{ik}^2 \mu_i^2 + \sum_{i=1}^{n} \sum_{j<i}^{n} c_{ik} c_{jk} (\mu_i \cdot \mu_j) \tag{3.41}$$

For near-degenerate vibrational transition, such as certain C=O and amide I stretching vibrations in peptide, equation (3.39) needs to be modified as follows:

$$R_k = -(\pi_0 / c) \sum_{i=1}^{n} \sum_{j>i}^{n} c_{ik} c_{jk} \left[(\bar{\nu}_j X_j - \bar{\nu}_i X_i) \cdot \mu_i \times \mu_j \right] \tag{3.42}$$

In this " nondegenerate extended coupled oscillator (NECO)" equation, the X are the coordinates of the center of mass of an oscillator. If $\nu_i = \nu_j$, Eq. (3.42) simplifies to the DECO expression presented in Eq. (3.39).

The computations of dipole and rotational strengths for the polymers are carried out using cartesian coordinates of the C and O atoms of the various carbonyl groups on the peptide linkages. Furthermore, the transition frequency ν_0 of an unperturded carbonyl transition is needed, and its monomeric dipole strength D, which is proportional to μ^2. For the conversion between rotational (or dipole) strengths (in esu cm)^2 and the extinction coefficients (in L mol^{-1} cm^{-1}) the approximations

$$D \approx 9.2\mathrm{D} \approx 9.2\times 10^{-39}\, \pi \varepsilon_{max} W / \nu_0 \tag{3.43}$$

and

$$\mathrm{R} \approx 2.3\times 10^{-39}\, \pi \Delta\varepsilon_{max} W / \nu_0 \tag{3.44}$$

were used. Here w denotes the width of the observed VCD or absorption band. Equations (3.43) and (3.44) hold for Lorenzian shapes; for Gaussian bands, the factor π needs to be replaced by $\sqrt{\pi}$.

Once the geometry of the dipole transition moments is defined, the interaction energies of all dipoles with each other is calculated according to equation (3.40) , and the interaction matrix is diagonalized numerically. The eigenvalues of V_{ij} are the frequency displacements for each of the exciton components from ν_0 and the eigenvector components are used, according to equations (3.40) and (3.41), to compute the rotational and dipole strengths of the exciton components.

Atomic coordinates of the carbonyl groups can be derived from crystallographic data, or from any of a number of molecular graphics program, such as Hyper Chem. To predict the conformation of a molecule in solution, one needs to compare the experientially observed IR and VCD spectra to the calculated ones, and to find a reasonable fit with the observed one. Several results were reported by Diem group[3-19]. In following chapters we will in detail discuss results from such computation in examples of small peptides.

3.4. REFERENCES:

3-1 Kuhn, W. (1958) *Ann. Rev. Phys Chem.* 9, 417.

3-2 L.Rosenfeld, (1929), *Z. Physik*, 52,161

3-3 E. U. Condon, (1937), *Rev. mod. Physics* 9, 432.

3-4 G. Holzwearth (1974) *J. Am. Chem. Soc.* 96, 252.

3-5 W. Moffitt and A. Moscowitz, (1959), *J. Chem. Physics* 30, 648

3-6 M. Diem, (1993), *Introduction to Modern Vibrational Spectroscopy*

3-7 L. A. Nafie (1976), *J. Am. Chem. Soc.* 98 2715.

3-8 L.A. Nafie and M. Diem (1979), *Accts. Chem. Res.* 12, 296.

3-9 L. A. Nafie and M. Diem (1979) *J. Am. Chem. Soc.* 101, 496.

3-10 M. Diem,. (1988), *Appl. Spectr.* 42, (1) 20-27.

3-11 O. Lee and M. Diem, (1992) *Analy. Instr.* 20(1) 23-43.

3-12 M. Diem, (1992), *SPIE Proceedings* 1681, 67-78.

3-13 Moffit, W., (1956) *J. Chem. Phys.*, 25, 467- 78.

3-14 C. W. Duetsche, (1969) *Ann. Rev. Phys. Chem.* 20 407-448.

3-15 Tinoco, I. (1963), *Radiation Research*, 20, 133-39.

3-16 Holzwarth, G. and Chabay, I. (1972), *J. Chem. Phys.* 57, 1632-1635.

3-17 T. R. Fraulkner (1977) *J. Chem. Chem. Soc.* 99, 8160-8168.

3-18 C. Marcott (1977) *J. Am. Chem. Soc.* 99, 8169-8175.

3-19 Birke, S. S. and Diem, M. (1992) *Biochemstry* 31, 450-455.

CHAPTER FOUR

CONFORMATIONAL STUDIES OF β-TURNS IN CYCLIC PEPTIDES BY VIBRATIONAL CD

In this chapter we report the infrared absorption and Vibrational Circular Dichroism (VCD) spectral features of peptide β-turns observed in small cyclic peptides dissolved in non-aqueous solvents. The molecules studied, *cyclo*-(Cys-Pro-Xxx-Cys), with Xxx = Gly, Phe, D-Phe, all form 14-member rings closed by a -S-S- linkage. The VCD spectra of these molecules vary enormously when the polarity and H-bonding ability of the solvent is varied. Furthermore, type I and type II β-turns can be formed, depending on the chirality of the residue Xxx in the 3-position. VCD intensity calculations, based on standard type I and type II geometries, were carried out and found to agree well with the observed VCD spectra.

4.1. INTRODUCTION

Turns are common structural motifs in proteins, comprising on average about 25% of the residues.[4-1] A survey of 29 proteins[4-2] showed that the frequency for turns is 32%, compared to 38% for helices and 20% for β-sheets. Specific turns, linking strands of anti-parallel β-sheet structures, were first recognized over 20 years ago by Venkatachalam,[4-3] and are referred to as β-turns.

Thus it is clear that turns in general, and β-turns in particular, are an essential and fundamental class of polypeptide structures.

In globular proteins, the secondary structures are organized in specific ways to bring together functional groups form different regions of the protein sequence to create the active site. The turn structures between structurally rigid peptide sections allow the polypeptide chains to adopt the appropriate globular structures. Turns have also been portrayed as nucleation sites for the protein folding process,[4-4, 5] and it has been suggested that turns function as recognition sites in complex immunologic, metabolic, genomic and endocrinologic regulatory mechanisms because of the location of turns on the surface of proteins, and because of the predominance of reactive functional groups in the side chains of amino acids involved in turns.

The general definition of a β-turn is the area where a polypeptide chain reverses its overall direction. In β-turns, this area comprises four amino acid residues, whereas γ-turns involve three residues. Turns may or may not be stabilized by an intramolecular hydrogen bond. Compared to other peptide conformations, such as α-helices or β-sheets, the geometry of β-turns is less unique, and several different β-turns, categorized as Type I, II, III (as well as Type I', II', III'), are found in proteins, *cf.* Table 4-1. The most common β-turns in proteins are the Type I , II and III structures. The standard geometry for each type of turn, based on X-ray crystallographic data of proteins, is defined by the ϕ and ψ angles of residues at the i+1 and i+2 positions. However, due to the

variations in amino acid residues in a β-turn region, the angles may vary by as much as ±30°. These large variations make the Type III and Type I turns indistinguishable in extreme cases, and also imply that the geometry of β-turns is less well defined than that of other secondary structures. The conformational angles in a turn depend on the environment involved, the sequence of amino acids in the β-turn, and the secondary structures connected by the β-turn: two single, β-sheet strands may be connected by a tight, U shaped β-turn that consists of four residues. On the other hand, the turn between two bulky secondary structures, such as α-helices, would exhibit a different shape and resemble an open helical structure (it is referred to as an "open turn" in the literature). This kind of turn might have a left or right handed chirality depending exclusively on the side chains. In these structures, it is not necessary to have a $1 \rightarrow 4$ intramolecular hydrogen bond.

Since β-turns consists of only a few residues, the spectroscopic signatures of these turns are hard to detect in larger proteins. In addition, the large degree of variation in the conformational angles of turns, as compared to other secondary structures, makes the conformational analysis much more complicated. Therefore, the structures of turns in peptides in solution is less well understood, and novel spectroscopic results can enormously enhance our present understanding of these structures.

We present the results of conformational studies of β-turns using VCD, which is a relative new technique for the study of peptide conformation. Therefore,

this paper is aimed at establishing whether or not there are characteristic VCD patterns for β-turns, and whether or not different types of turns can be distinguished from each other by VCD. Recent VCD results shows that VCD is a particularly sensitive probe for the conformation of small peptides containing turn motifs.[4-6,7,8] It combines and enormously enhances the sensitivities of CD and FTIR spectroscopies, and overcomes some disadvantages of both techniques.

Table 4-1 Dihedral Angles for Hydrogen-Bonded β–turns

	i+1		i+2	
Turn	ϕ	φ	ϕ	φ
Type I	-60	-30	-90	0
Type I'	60	30	90	0
Type II	-60	120	80	0
Type II'	60	-120	-80	0
Type III	-60	-30	-60	-30
Type III'	60	30	60	30
Type VIa (cis)	-60	120	-90	0
Type Vib(cis)	-120	120	-60	0

We find from the VCD results that small, cyclic peptides incorporating β-turns exhibit large conformational differences when the chemical environment is changed, although they are conformationally restricted. This change in environment was accomplished by varying the solvent polarity and hydrogen bonding ability. In spite of the perceived rigidness of the peptides reported here, we find that polar and hydrogen bonding solvents interfere with the internal hydrogen bonds between the peptide linkages, cause the polar group of the β-turn to be solvent exposed, and therewith induce conformational changes. In inert solvents, peptides tend to form intramolecular hydrogen-bonded structures and to be conformationally more restricted.

Finally, in order to understand the relationship between the observed VCD spectra and the conformations of peptides, we carried out VCD intensity simulations using the Non-degenerate Extended Coupled Oscillator (NECO) model.[4-9] The patterns of calculated VCD spectra for standard Type I and II β-turns, based on literature conformational data, agree well with experimental data. We conclude that the NECO model is useful for interpreting VCD data in peptides of the size reported here. The coupling between carbonyl group of the peptide linkages, which is considered the major mechanism for generating VCD intensity within the NECO model, will be different in single β-turns and in fused turns in larger peptides. We find that even these differences can be interpreted through the calculated VCD spectra.

4.2. PREVIOUS STRUCTURAL STUDIES ON β-TURNS

4.2.1. Previous Spectroscopic Methods

Because of the complicated properties of β-turn, a variety of techniques have been employed to study the conformation of β-turns. The first systematic study of β-turns was carried out by Venkatachalam[4-3] using conformational computations. In the 1970's, the most accurate structural information available for turns was obtained by crystallographic techniques.[4-10,11] In recent years the NMR, CD, and FT-IR spectroscopies have become the most popular techniques to study β-turns,[4-12-16] because these techniques are sensitive to conformation and conformational changes of peptides and proteins in solution.

CD is very useful technique for conformational determination, especially for biomolecules. Because of its fast time scale, population-weighted average conformations will be measured, from which individual populations can be extracted. Thus, all existing conformer populations are observed simultaneously. For β-turns, four classes of CD spectra were established computationally by Woody[4-17,18] for the different subtypes. However, their direct observation proved to be difficult,[4-14] because the CD features of the turns are generally weak, and because there will be a population distribution of different turn subtypes. Furthermore, in model peptides and proteins, the signatures of the turn was found to be overlapped by the strong CD spectrum of other conformations or side-chain and disulfide bond contributions.

Several techniques in NMR can be used to determine conformation of β-turn, such as J-J coupling, ROSEY and chemical shift temperature dependence.[4-10,11,15] A common and powerful method to distinguish between Type II and other

types of β-turns is NOE spectroscopy. β-turns exhibit a number of NOEs, but the most significant one is the interaction of the α-proton on carbon atom C_{i+1} with the amide proton on N_{i+2} in the Type II β-turn. In general, NOEs are observable when two protons are less than 3Å apart. In a standard Type II turn, the distance between the two protons, henceforth referred to as $C_{\alpha i+1}H$ and HN_{i+2}, is typically 2.1 Å, and strong NOE is observed. However, since there is a large variation of the conformational angles ϕ and ψ, the distance between $C_{\alpha i+1}H$ and HN_{i+2} can vary to such an extent that no NOE's are observable. In addition, the intensity of NOE is proportional to the population of each type of turn that may co-exists; therefore, interproton distances generated by NMR experiments may not fit a unique structure. Furthermore, the slow time scale of NMR, which is generally longer than the time scale of conformational interconversions, will further reduce the intensity of NOE's, particularly in small peptide system.[4-15] Many of the peptides studied via NMR techniques were linear and cyclic tetrapeptide, which were found to exhibit different conformations in various environments. In addition, they were found to be more flexible than the turns in large peptides or proteins, in which the conformation of the turn is limited by the entire protein environment .

IR absorption spectroscopy has been used quite extensively to investigate turn structures, particular in recent efforts. The assignment of absorption bands to given conformational angles, however, is not a unique one, particularly since infrared absorption peaks are broad and solvent dependent. We found in some previous studies on γ-turns, and in the present study, that the changes in infrared absorption spectra are relatively small and insignificant compared to the changes in VCD features.[4-6,8] However, the amide I stretching frequency of a proline containing peptide linkage is quite different from that containing other amino acid residue: In a Gly-Pro peptide linkage, where the nitrogen is a tertiary amine, the $C{=}O_{(Gly)}$ stretching frequency is observed around 1640-1655 cm^{-1}, whereas in

Pro-Gly where nitrogen is a secondary amide, the $C=O_{(Pro)}$ frequency is observed at 1670-1685 cm^{-1}. Thus, these frequency shift caused by changes in the chemical environment of peptide linkages can interfere with the frequency shift generally associated with changes in secondary structure, causing the results of vibrational work to be inaccurate.[4-6] In this study, we use the different frequencies of the secondary and tertiary amide groups to our advantage, since they allow us to differentiate between the various possible interactions of the carbonyl groups.

4.2.2. β-turn Structural Considerations

Type I and Type II β-turns are composed of four residues. In the case of a tight β-turn, the $C=O_i$ can form an intramolecular hydrogen with HN_{i+3}. The $C=O_{i+1}$ is approximately perpendicular to the plane of the ring, pointing either down (Type I) or up (Type II), *cf.* Figure 4-1. It is able to interact with solvent molecules and exhibits large conformational flexibility. Thus, the geometry of β-turn is determined by the arrangement of the three carbonyl groups $C=O_{i,}$, $C=O_{i+1}$ and $C=O_{i+2}$. The advantage of VCD as a structural tool is that it monitors the orientation of these three probe groups.

The peptides reported in this study are cyclic tetrapeptides closed by a disulfide bond, and a cyclic pentapeptide. The cyclization reduces the flexibility of the peptides, and the disulfide bond will constrain the distance between $C_{\alpha i}$ and $C_{\alpha i+3}$. This latter factor may determine whether the particular peptide sequence will prefer a Type I or Type II turn. The peptides all have proline residue at the i+1 position, because proline is well known to play a key role in β-turn conformations of proteins.[4-2] On the basis of x-ray crystallographic data in proteins, proline is the most frequently occurring residue in the i+1 position of β-turn. In addition, the sequence Pro-Y, in position i+1 and i+2, with Y= Ser, Asp, Asn or Glu, is found almost exclusively in type I or III turns, whereas the Pro-Gly sequence may occur

both in type I(III) and type II turns. The limitations on conformational freedom is due to the constraint of the ϕ angle of proline.

In this study, we concentrate on solution conformations derived from the amide I' vibration of the peptide linkage. This vibration, which can be describes mostly as the carbonyl stretching motion of the amide moiety, occurs between 1630 and 1700 cm^{-1}, and has a dipole transition moment of 0.29D. The VCD spectra reflect the dipolar coupling among the different C=O groups of neighboring peptide linkages which depends on the distance between C=O groups and their dihedral angles. Since the turn geometry is directly related to the orientation of the carbonyl groups, the VCD results in this spectral region is particularly sensitive to the peptide conformation.

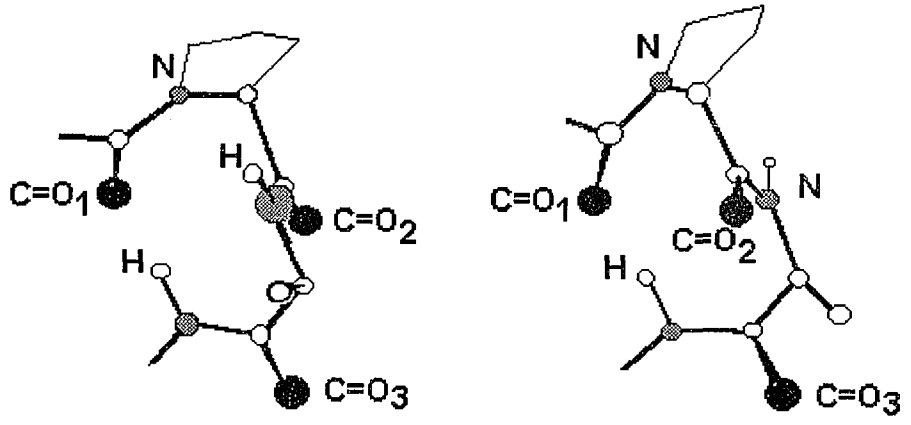

Figure 4-1. The schematic structure of Type I (left) and Type II (right) β- turn.

4.3. MATERIALS AND METHODS

All data presented in the following publication were collected on the broadband (800-1800 cm^{-1} spectral range), dispersive VCD spectrometer at Hunter College described previously.[4-19] Several improvements were implemented since the earlier description of the instrument. Mostly, these improvements deal with further lowering the artifact levels. Thus, VCD spectra with amplitudes of about $3 \cdot 10^{-7}$ ΔA units can now be measured reliably. Details of the modifications will be reported at a later date.

Sample handling in VCD is entirely analogous to that in infrared spectroscopy. Samples are contained between CaF_2 plates, separated by Teflon spacers of appropriate thickness, typically 25 μm. Sample volumes of 10 - 20 μL, at peptide concentrations of 5 - 20 mg/mL, were utilized. These peptide concentrations result in peak absorbances of about 0.15 at the pathlength indicated. To check for association effects, VCD data of some peptides at lower concentration were collected as well. At present, the lowest absorbance levels at which VCD can be collected reliably is about 0.06 absorbance units. At these lower concentrations, no change in the VCD spectra were observed in the cyclic peptides, although the linear precursors did show concentration dependent VCD features.

The cyclic peptides *cyclo*-(-Cys-Pro-Gly-Cys-) [*c*(GPGC)], *cyclo*-(-Cys-Pro-Phe-Cys-) [*c*(GPFC)] and *cyclo*-(-Cys-Pro-D-Phe-Cys-) [*c*(GPdFC)], were prepared by standard F-Moc solid phase synthetic methods as described previously.[4-8] The cyclic molecules were obtained from the linear precursors by oxidative ring closure in the presence of H_2O_2. *Cyclo*-(-Gly-Pro-Gly-D-Ala-Pro-) [*c*(GPGdAP)] was provided by H. Wyssbrod.[4-7] All peptides were lyophilized from D_2O prior to dissolving them in the solvents discussed for each experiment. Thus,

all reported C=O stretching vibrational frequencies will be for the deuteriated peptide linkage, referred to as the amide I' vibration.

Molecular modeling, the calculation of atomic coordinates and the generation of structures shown, were carried out using program HyperChem running on a personal computer equipped with a 90 MHz Intel Pentium processor. The simulated VCD and infrared absorption spectra were obtained using exciton-type calculations allowing for non-degenerate frequencies of prolyl and glycyl carbonyl groups.[4-8,9]

4.4. RESULTS

The observed IR and VCD spectra of three cyclic peptide, *c*(GPGC), *c*(GPFC) and *c*(GPdFC) in three different solvent systems are shown in Figures 4-2 to 4. The solvent systems, DMSO/$CDBr_3$ (1:1, v:v), DMSO and DMSO/D_2O (1:2, v:v) were selected to represent different polarity and hydrogen bonding ability. In principle, the pure solvents $CDBr_3$, DMSO and D_2O would have been preferable since polarity and dielectric constants may be reproduced more accurately, but low solubilities prevented us from using the pure solvents. Figure 4-5 shows the observed VCD and infrared absorption spectra of the pentapeptide *c*GPGdAP in bromoform.

4.4.1. Absorption Spectra

The changes in the absorption spectra in Figures 4-2, 3 and 4 are relatively small. The general band shapes are very similar for the three peptides in the three different solvents, even if the amino acid at the 3-position is changed. However, the choice of solvent influences the frequency of the absorption maximum: there is

a trend toward lower wavenumber of the peak absorbance between DMSO, DMSO/$CDBr_3$ and DMSO/D_2O. The solvent may affect the absorption spectra in two ways: either by a direct interaction between the carbonyl groups and the solvent, or by inducing a conformational change. The direct interaction usually lowers the vibrational frequency, whereas the second effect can result in a frequency shift in either direction, accompanied by a variation of intensity in the amide I' band.

Even though the peptides are cyclic and conformationally restricted, the solvent can cause conformational changes. The most common way is by breaking the intramolecular hydrogen bond, and forming hydrogen bonds with the solvent. We believe that the shifts toward low frequency of the spectra in DMSO/D_2O are directly attributable to solvent hydrogen bonding of all four carbonyl groups, with a concomitant breaking of the intramolecular hydrogen bond.

Between solution in DMSO/$CDBr_3$ and DMSO, all C=O vibrations (except for $C=O_4$ in *c*CPGC, *cf.* Table 4-2) shift up. We believe that these frequency changes are due to conformational changes induced by breaking the $1\rightarrow 4$ intramolecular hydrogen bond. In a low polarity solvent, such as bromoform, peptides prefer to form an intramolecular hydrogen bond which is manifested by a shift of the tertiary amide I' vibration by at least 6 cm^{-1}, compared to their value in DMSO (Table 4-2). Upon increasing the DMSO concentration, this hydrogen bond is broken by stronger solvent interactions, and a slight conformational change seems to occur. This change shifts the carbonyl peak to higher frequencies. Since the observed VCD spectra of the peptides in different solvents vary significantly, but the absorption spectra exhibit only minor changes only, we conclude that the conformation changes of the β-turns cannot be detected reliably by monitoring absorption spectra alone.

4.4.2. VCD Spectra

The VCD spectra of the peptides *c*(GPGC), *c*(GPFC) and *c*(GPdFC) show much larger variations when the solvent is varied than the corresponding absorption spectra. A comparison between the VCD spectra of the three peptides in the same solvent reveals that the peptides actually exhibit quite similar VCD spectra. This coarse observation will lead us to believe that the changes in solution conformation caused by the solvent interaction are more severe than those caused by variation of the peptide sequence.

In *c*(GPGC), a VCD spectrum with a positive/positive/negative pattern is observed in DMSO/$CDBr_3$. This pattern is similar to that observed for *c*(GPGC) in pure DMSO. In DMSO/D_2O, a spectral pattern is observed which is devoid of the tertiary amide (low frequency) VCD intensity, and resembles the VCD of a cyclic peptide, *cyclo*-(Cys-Ala-Cys), which may include a γ-turn.[4-8] The peptides with a larger side group in the 3-position, *c*(GPFC) and *c*(GPdFC), exhibit more significant changes in the VCD spectra as the solvent polarity is varied. They both exhibit large, all-negative VCD patterns in DMSO/D_2O, which we are unable to interpret at the present time. In this solvent, which is the most polar of the solvents studied, the interactions of the peptide with the solvent dominate and influence the conformation profoundly. The changes in the VCD spectra as a function of solvent polarity could correspond to changes in conformation, or a change in equilibrium populations in a mixture of different conformations. This possibility is

very likely since the energies for Type I and Type II turns are very similar for *c*(GPGC).

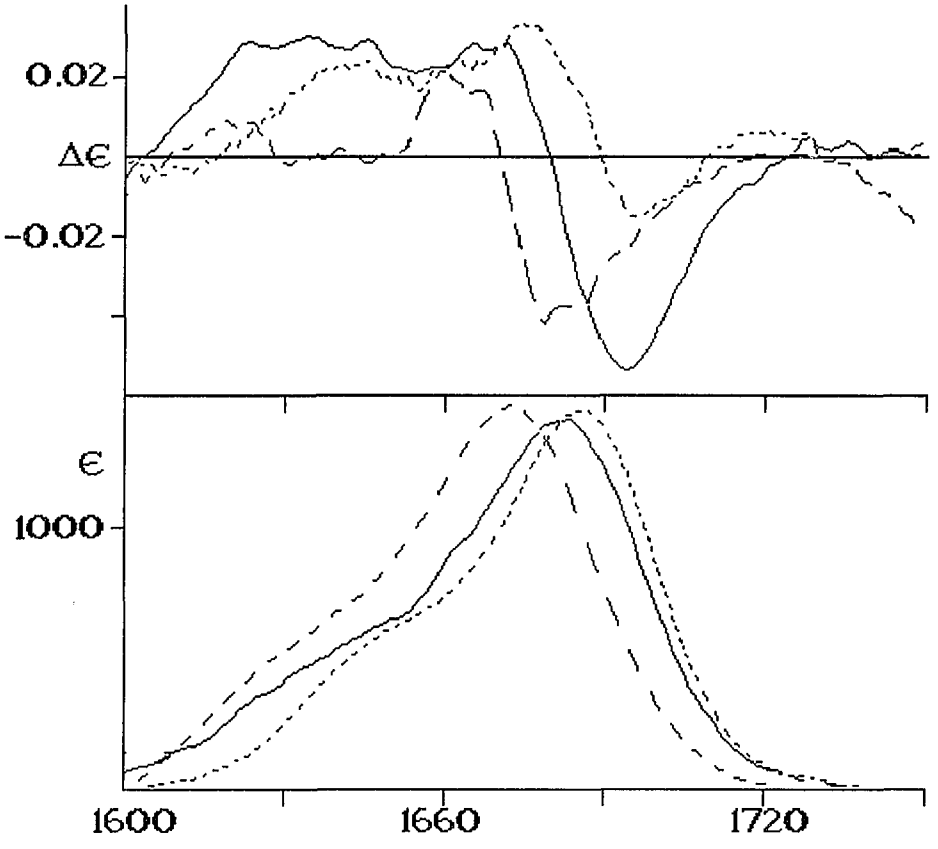

Figure 4-2. Infrared VCD (top) and absorption (bottom) spectra of *cyclo*- (Cys- Pro- Gly -Cys) in DMSO/ $CDBr_3$ (solid trace), DMSO (dotted trace) and DMSO/ D_2O (broken trace)

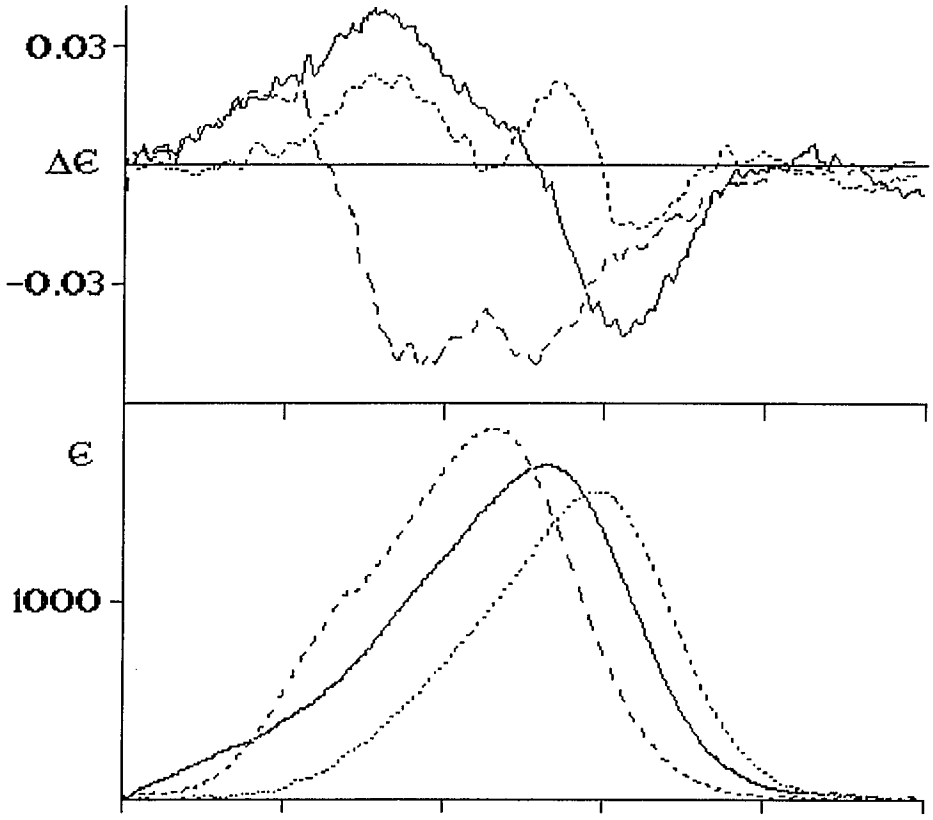

Figure 4-3. Infrared VCD (top) and absorption (bottom) spectra of *cyclo-* (Cys- Pro- Phe -Cys) in DMSO/ $CDBr_3$ (solid trace), DMSO (dotted trace) and DMSO/ D_2O (broken trace)

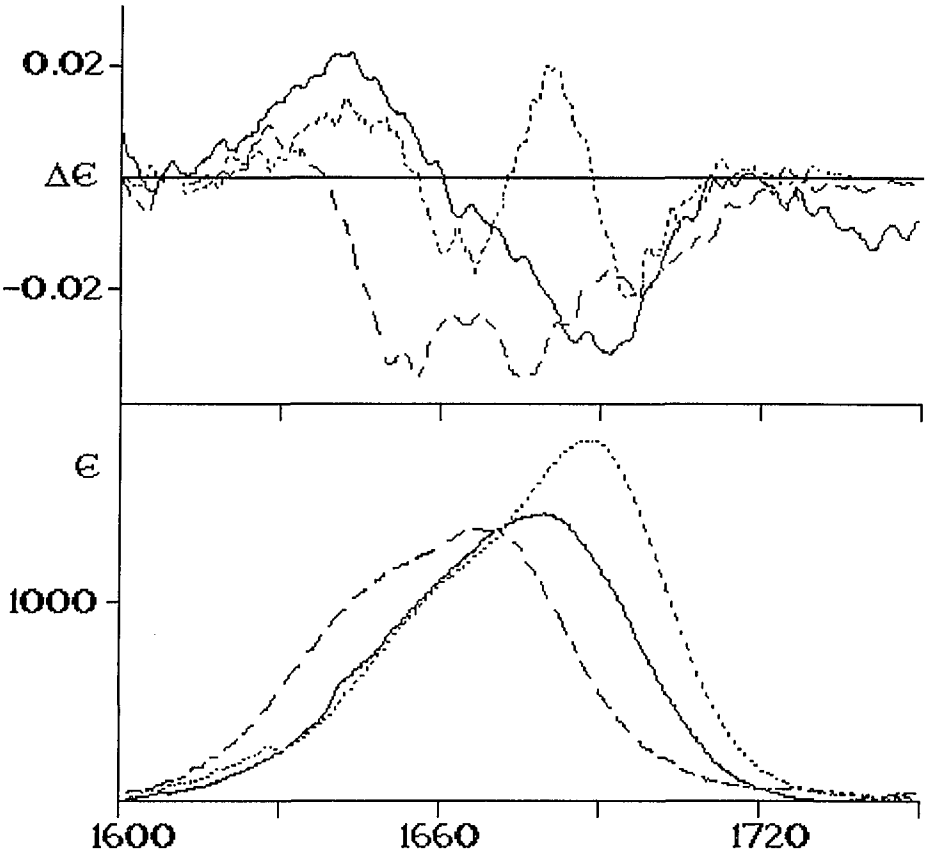

Figure 4-4. Infrared VCD (top) and absorption (bottom) spectra of *cyclo*- (Cys- Pro- DPhe -Cys) in DMSO/ $CDBr_3$ (solid trace), DMSO (dotted trace) and DMSO/ D_2O (broken trace).

Table 4-2 Frequencies [cm^{-1}] of Tertiary and Secondary Amide I' Vibrations

	tert. amide I'	sec. amide I'	$C=O_{i+3}$ amide I'	solvent
cCPGC	1655	1684	1697	DMSO
cCPFC	1664	1688	1703	DMSO
cCPdFC	1661	1687	1700	DMSO
cCPGC	1648	1681	1697	DMSO/$CDBr_3$
cCPFC	1650	1679	1695	DMSO/$CDBr_3$
cCPdFC	1655	1678	1694	DMSO/$CDBr_3$

4.5. DISCUSSION

Because of steric requirements of the individual amino acids in the turns, the Type I β-turns is generally preferred for two L-amino acids in the i+1 and i+2 positions,[4-20] whereas Type II turns are preferred for L-D sequences. A glycyl residue can be accommodated in either a Type I or II turn. Among the molecules studied here, *c*CPFC should prefer a Type I geometry, whereas *c*CPdFC should exist in a Type II β-turn geometry. *c*CPGC can assume either Type I or Type II structures, and most likely exists as an equilibrium mixture of both forms. Previous NMR studied have confirmed these conformational tendencies.[4-21]

Since VCD is a technique which monitors short distance interaction, its conformational sensitivity is particularly pronounced and useful in the studies of small peptides. One of the major advantages of vibrational optical activity is its sensitivity to subtle structural differences of β-turns in slightly different solvent

systems. Furthermore, the carbonyl groups of the tetrapeptides introduced above exhibit different amide I' frequencies that are readily distinguishable in infrared absorption and VCD spectroscopies. These different amide I' frequencies are due to the carbonyl group $C=O_i$, adjacent to the tertiary (prolyl) amine, observed at 1655 cm^{-1}, the two carbonyl groups $C=O_{i+1}$ and $C=O_{i+2}$ in the turn which are adjacent to secondary amines (1685 cm^{-1}), and the carboxylic acid $C=O_{i+3}$ group with a frequency of 1697 cm^{-1}. In DMSO/$CDBr_3$, these four peaks could be identified by band decomposition.

The aim of the following discussion is an attempt to interpret the conformational changes observed for the tetrapeptides between pure DMSO and DMSO/$CDBr_3$, since these spectral changes are far less drastic then the ones observed for DMSO/D_2O. Furthermore, we wish to establish whether or not any of the observed spectra represent Type I and Type II β-turn VCD signatures. We shall attempt to determine the effects of the conformational changes induced by the different solvents on the VCD spectra by assuming that the VCD spectra in the amide I' region are determined mostly by the coupling among the carbonyl groups within a given geometry. In the cyclic tetrapeptides that were used to model β-turns, there are only three carbonyls groups involved in the turn itself, while $C=O_{i+3}$ which is outside the ring, is expected to be in an undefined geometry. As pointed out before, one of the remaining three carbonyl groups has a low frequency ($C=O_i$), and two of them have a relatively high frequencies (*cf.* Table 4-2), and it is easily to assign their VCD features based on their frequencies.

We start this attempt to interpret the observed VCD data by presenting, in Figures 4-5 and 4-6, the calculated VCD and absorption spectra for standard Type I and Type II β-turn geometries. These calculations were carried out using the carbonyl coordinates extracted from structural data of the two turns, a constant carbonyl transition moment of 0.29 D, and 1645 and 1685 cm^{-1} transition

frequencies for the tertiary ($C=O_1$) and secondary ($C=O_2$ and $C=O_3$) amide frequencies, respectively. Plotted along with the calculated VCD spectra are the observed VCD spectra of *c*(GPFC) in DMSO (Figure 4-5) and *c*CPdFC in DMSO/$CDBr_3$ (Figure 4-6). Similar cyclic dipeptides were found previously to exist in these solvents in Type I and Type II β-turn conformations. [4-21,22]

Next, we shall attempt to quantify the origin of the spectral patterns observed and calculated. Two kinds of VCD patterns were observed and calculated for these model peptides. One pattern (Figure 4-5) consists of a couplet at relatively high frequency that covers a narrow frequency range, and a low frequency positive VCD. The couplet is attributed to interactions between two high frequency carbonyl groups, $C=O_{i+1}$ and $C=O_{i+2}$ and exhibits a positive/negative pattern with a zero crossing point located at the maximum absorption of the secondary amide I' band. This $C=O_{i+1}$ / $C=O_{i+2}$ interaction indicates a favorable distance/geometry between these groups. The VCD of the $C=O_i$ group is monosignate, and at lower frequency.

The calculated and observed VCD couplet shown in Figure 4-6 is located at lower frequency, and covers a wider frequency range. Therefore, we believe it is due to the interaction of a low frequency and a high frequency carbonyl group, either $C=O_i$ with $C=O_{i+1}$, or $C=O_i$ with $C=O_{i+2}$, or both. Since it involves the coupling between a high and a low frequency carbonyl vibration, the zero crossing of the VCD spectrum is located between the absorption of the secondary and tertiary amide I'. It, too, has a positive/ negative pattern, but the spectrum is much broader. Here, either the $C=O_i$ / $C=O_{i+1}$ or the $C=O_i$ / $C=O_{i+2}$ groups must be in a good coupling geometry.

The dipolar coupling energies V_{ij} between interacting C=O groups, listed in Tables III and IV, may provide a handle to the origin of the observed VCD. The V_{ij} elements depend on the distance and the orientation between the interacting

carbonyl groups. To a first approximation, we may assume that a small conformational change in a cyclic molecule will alter the orientation much more than the distance; thus, the coupling energies may provide another sensitive clue to conformation.

According the exciton formalism, large rotational strengths are created for perpendicular geometry between the interacting groups. Such a geometry, however, produces the smallest coupling energy and splitting of the exciton components. On the other hand, a parallel or antiparallel geometry between the interacting groups will produce maximum splitting, but minimal rotational strengths. Thus, one may conclude that large VCD intensities are associated with intermediate values of V_{ij} if the distance between the carbonyl groups does not change much between the conformers.

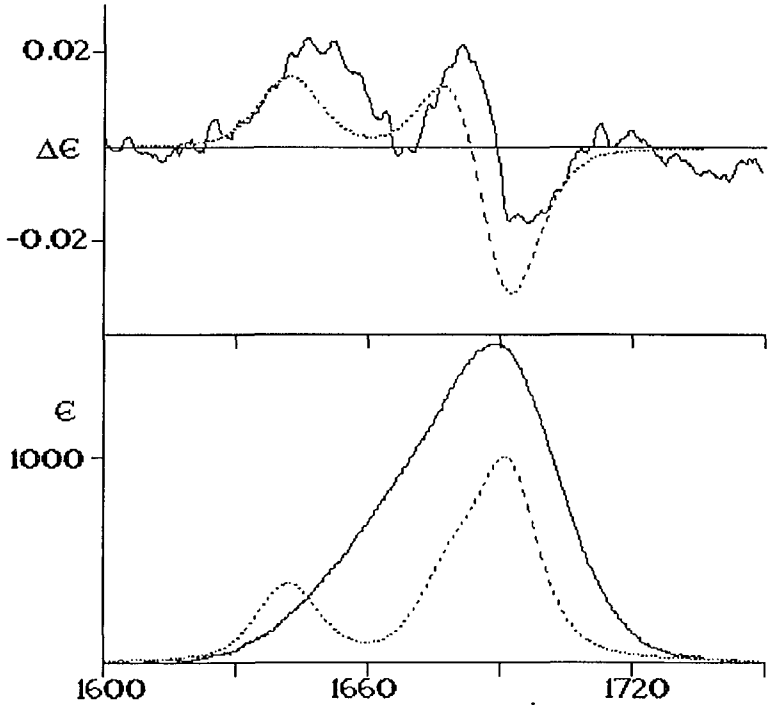

Figure 4-5. Infrared VCD (top) and absorption (bottom) spectra of *cyclo-* (Cys- Pro- Phe- Cys) in DMSO (solid trace), and calculated spectrum Type I β-turn(dotted traces).

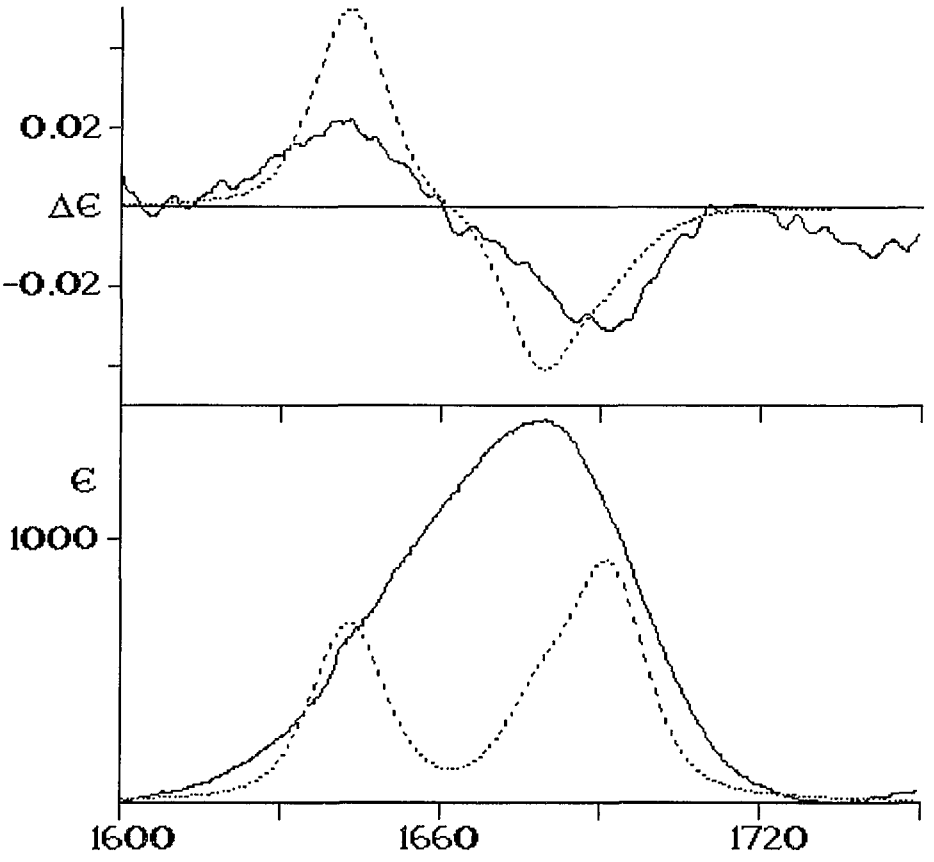

Figure 4-6. Infrared VCD (top) and absorption (bottom) spectra of *cyclo-* (Cys- Pro- D-Phe- Cys) in DMSO /$CDBr_3$ (solid trace), and calculated spectrum Type II β-turn (dotted traces).

For the Type I β-turn, (*cf.* Tables 4-3) V_{23} is responsible for the mixing of the $C{=}O_2$ / $C{=}O_3$ coordinates, whereas the large and small coupling energies V_{12} and V_{13}, may prevent the formation of a couplet as discussed above: a large term because of near parallel geometry, and a small term for lack of coupling. In the Type II turn, V_{12}, V_{13} and V_{23} all are similar in magnitude and contribute to the mixing of $C{=}O_i$ / $C{=}O_{i+1}$ and the $C{=}O_i$ / $C{=}O_{i+2}$. Inspection of Figure

4-1 reveals that in the standard Type I geometry, $C=O_i$ and $C=O_{i+1}$ are close to each other, and both point below the plane of the ring. This near parallel geometry will produce a large coupling energy, but little optical activity. $C=O_{i+1}$ and $C=O_{i+2}$ interact with an energy of about 6 cm^{-1}, which appears the optimum value for generating VCD couplets.

Based on these arguments, the observed VCD spectra of the three tetrapeptides can be categorized by a combination of $C=O_i$ / $C=O_{i+1}$ and $C=O_i$ / $C=O_{i+1}$ interactions (low frequency couplet) and a $C=O_{i+1}$ / $C=O_{i+2}$ interaction (high frequency couplet). *c*(GPFC) in DMSO exists mostly in the Type I conformation (Figure 4-3, short dashes). In the less polar solvent DMSO/$CDBr_3$, the spectrum resembles that of the Type II conformation, but still contains some positive intensity just below the zero crossing frequency. We interpret this to be due to a mixture of Type I and Type II conformation.

In contrast, *c*(GPdFC) exhibits nearly pure Type II conformation in the low polarity solvent DMSO/$CDBr_3$ and a mixture of Type I and Type II structures in pure DMSO. Based on these facts, we conclude that the higher polarity solvent will expose the carbonyl groups to the solvent, so that the $C=O_2$ prefers to stay in position similar to that found in the Type I turn, and secondly, that the disulfide bond certainly makes some contribution to the β-turn conformation. It can either limit the formation of intramolecular hydrogen bond or constrain the distance between C_i and C_{i+3}. Similar results of interconversion between turn conformations were found using other techniques in cyclic peptides containing Aib at the i+2 position [4-21].

We expect the VCD spectrum of *c*(CPGC) in DMSO/$CDBr_3$ (*cf.* Figure 4-2) to be a mixture of both Type I (or III) and Type II turns, with the former dominating. With increasing solvent polarity, the fraction of Type I conformation

becomes more pronounces which is manifested by an increase in the $C{=}O_{i+1}$ / $C{=}O_{i+2}$ couplet.

Another example of a β-turn that was studied by VCD is *c*(GPGdAP) in bromoform. The observed VCD and absorption spectra are shown in Figure 4-7. The absorption spectrum consists of two major peaks with frequencies of 1640 and 1690 cm^{-1}. The VCD spectrum shows two couplets, a strong negative couplet at low frequency (1630-1650 cm^{-1}), and a positive couplet at high frequency (1685-1700 cm^{-1}). NMR[4-23] and X-ray[4-24] studies indicated that this pentapeptide forms a Type II β-turn stabilized by a hydrogen bond between $C{=}O_{Gly(1)}$ and $HN_{D\text{-}Ala}$, and a γ-turn between $C{=}O_{D\text{-}Ala}$ and $HN_{Gly(1)}$. The carbonyls involved in the two turns are both tertiary amide I' groups that form intramolecular hydrogen bonds and are consequently observed at low frequency. Furthermore, the two tertiary C=O groups of *c*(GPGdAP) are located below the ring of the peptide and are very close each other. The three secondary C=O groups are above the peptide ring, but only $C{=}O_{Pro(2)}$ and $C{=}O_{Gly(3)}$ are relatively close to each other, and $C{=}O_{Pro(5)}$ is far away from any other carbonyl group. Thus, one would expected two separate couplets: a low frequency couplet between the tertiary amide vibrations, and a high frequency couplet for the secondary amides. The observed VCD spectrum exhibits this pattern.

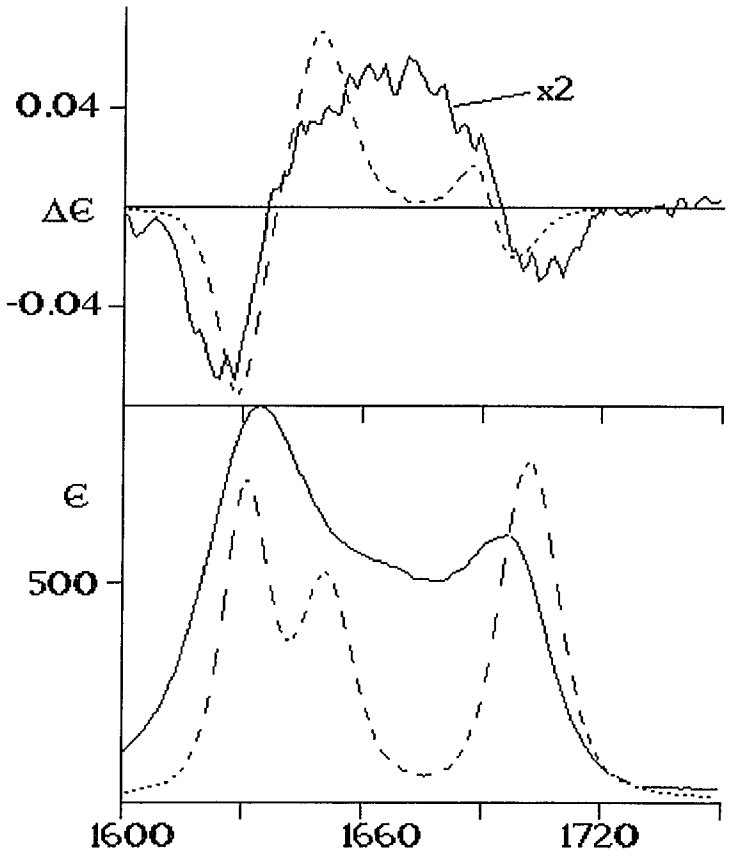

Figure 4-7. Infrared VCD (top) and absorption (bottom) spectra of *cyclo*- (Gly- Pro- Gly- d-Ala- Pro) in $CDCl_3$ (solid trace), and calculated spectrum from NMR structural data (dotted traces).

Table 4-3 Dipole-dipole Coupling Energies (cm^{-1}) for Type I β-turn (between $C=O_i$, $C=O_{i+1}$ and $C=O_{i+2}$)

V_{ij}	i =i	i =i+1	i =i+2
j =1	-	9.26	0.24
j =2		-	6.4
j =3			-

Table 4-4 Dipole-dipole Coupling Energies (cm^{-1}) for Type II β-turn (between $C=O_i$, $C=O_{i+1}$ and $C=O_{i+2}$)

V_{ij}	i =i	i =i+1	i = i+2
j =1	-	-5.60	-6.40
j =2		-	5.5
j =3			-

Table 4-5 Distribution of Conformations in the Cyclic Tetrapeptides

	DMSO	DMSO/$CDBr_3$
c(CPGC)	II, I (III)*	II & I (III)
c(CPFC)	I (III)	II & I (III)
c(CPdFC)	II & I(III)	II

This coupling pattern can be confirmed by NECO computations. Large values of V_{ij} are found to occur between the tertiary amide I' vibrations of $C=O_1$ and $C=O_4$, and the secondary amide I' vibrations $C=O_2$ and $C=O_3$. The weakest coupling occurs with $C=O_5$. Computed VCD spectra, based on the NMR solution structure, are shown in Figure 4-7. The frequency and shapes of the calculated VCD patterns agree reasonably well with the observed VCD results: the couplet at low frequency corresponds to the two tertiary carbonyls of the fused turns, and the positive couplet at higher frequency represents a partial spectrum characteristic of β-turns. The computed VCD spectrum based on the X-ray data shows less agreement with the observed VCD spectrum. This is understandable in terms of a conformational change the of peptide experiences due to the forces in the crystal. Our data demonstrate how sensitive VCD is to conformational changes of peptides, even if this change is relatively minor. The above results can also be used to draw same direct conclusion about the structure of the peptide, namely the large distance and unfavorable coupling geometry of $C=O_5$. Furthermore, since the VCD pattern of *c*(GPGdAP) is determined by fused β- and γ-turns, and we

cannot use it for the interpretation of individual or single β-turn. Finally, the interpretation of the VCD results of *c*(GPGdAP) suggests that the NECO model is a adequate method for the qualitative interpretation of the observed VCD spectra.

4.6 CONCLUSION:

After the discussion in the previous section, the question arises of whether or not a VCD pattern for "prototypical turn structures" exists, and what VCD spectrum can be expected for each of the β-turn conformations. Although we have published the VCD spectrum of *c*(GPGdAP) before and had hoped that it may exhibit a "typical" β-turn VCD, we conclude after this more detailed study that *c*(GPGdAP) gives the VCD pattern for fused turn structures only, and not that of a single β-turn. However, it appears that the VCD spectra of *c*(CPFC) in DMSO and that of *c*(CPdFC) in DMSO/$CDBr_3$ represent the VCD patterns of standard Type I and Type II β-turn structures, respectively. We arrive at this conclusion by a comparison of previously derived structures and observed VCD results, and a comparison of the observed VCD patterns with those calculated for standard β-turn geometries. These calculations are based on the ϕ and φ angles of residues i+1 and i+2 in standard Type I (-60, -30; -90, 0) and Type II (-60, 120; 80, 0) β-turns). These four angles determine uniquely the geometry of the three carbonyl groups involved in β-turns.

Experimentally and computationally, we obtain a positive couplets for both Type I and Type II turns. For the Type I turn, an additional positive VCD signal is observed at about 1635 cm^{-1}, followed by the couplet at about 1675/1690 cm^{-1}. For the Type II turn, a broad couplet between 1635/1690 cm^{-1} is observed.

REFERENCES:

4-1. Kabsch, W. and Sander, C., (1983) *Biopolymers*, 22, 2577-2637

4-2. Chou, P. Y. and Fasman, G.D., (1977) *J. Mol. Biol.*, 115, 135-175

4-3. Venkatachalam, C. M., (1968) *Biopolymers*, 6, 1425-1436

4-4. Lewis, P. N., Momany, F. A. and Scheraga, H.A., (1971) *Proc.Natl.Acad.Sci.USA*, 68, 2293-2297

4-5. Zimmerman, S. S. and Scheraga, H.A., (1977) *Proc. Natl. Acad. Sci.USA*, 74, 4126-4129

4-6. Xie, P. and Diem, M., (1995) *J.Amer.Chem. Soc.*, 117, 429-437

4-7. Wyssbrod, H. and Diem, M., (1992) *Biopolymers*, 31, 1237 - 1242

4-8. Xie, P., Zhou, Q. and Diem, M., (1994) *Faraday Discussions.*, 99, in press

4-9. Xiang, T., Goss, D.J. and Diem, M., (1993) *Biophysical Journal*, 65, 1255-1261

4-10. Venkatachalapathi, Y.V. and Balaram, P., (1979) *Nature*, 281, 83-84.

4-11. Nair, C.M.K., Vijayan, M., Venkatachalapathi, Y.V. and Balaram, P., (1979) *J. Chem. Soc Chem.Commun.*, 1183-1184.

4-12. Venkatachalapathi, Y.V., Prasad, B.V.V and P. Balaram, (1982) *Biochemistry*, 21, 5502-5509

4-13. Hollosi, M., Kawai, M. K., Fasman, (1985) *Biopolymers*, 24, 211-242

4-14. Perczel, A., Hollosi, M., Foxman, B. M. and Fasman, G. D., (1991) *J.Amer.Chem.Soc.*, 113, 9772-9784

4-15. Hollosi, M., Majer,Z., Ronal, A.Z., Magyar, A., Medzihradsky, K., Holly, S. and Fasman, G.D., (1994) *Biopolymers*, 34, 177-185

4-16. Rose, G.D., Gierasch, L.M. and Smith, J.A., in Adv. Protein Chemistry, Anfinson, C.B., Edsall, J.T. and Richards, F.M., Eds., (1985), Academic Press, NY

4-17. Woody, R.W., in *Peptides, Polypeptides and Proteins,* E.R.Blout, F.A.Bovey, N.Lotan and M.Goodman, Eds., Wiley, New York, (1974) pp 338-350

4-18. Woody, R.W., in "*The Peptides: Analysis, Synthesis , Biology*", V.J. Hruby, Ed., Academic Press, New York, (1985) 15-113

4-19. Diem, M., Roberts, G.M., Barlow, A. and Lee, O., (1988) *Applied Spectrosc.*, 42, 20-28

4-20. Chandrasekaran, R., Lakshminarayana, A.V., Pandya, U.V. and Ramachadran, G.N.,
(1973). *Biochim. Biophys. Acta,* 303, 14-27

4-21. Rao, B.N.N., Kumar, A., Balaram, H., Ravi, A. and Balaram, P., (1983) *J.Am.Chem.Soc.*, 105, 7423-7428.

4-22. Imperiali, B. ,Fisher, S.L. Moats, R.I. and Prins, T. J., (1992). *J.Amer.Chem.Soc.* 114, 3182-3188.

4-23. Pease, L.G. and Watson, C., (1978), *J. Amer.Chem.Soc.*, 100, 1279-1286

4-24. Karle, I., (1978) *J. Amer.Chem.Soc.*, 100, 1286-1289

CHAPTER FIVE

A CONFORMATIONAL STUDY OF LINEAR PEPTIDES BY VCD

In this chapter, observed and calculated VCD spectra of three linear tetrapeptides and one octapeptide are reported. Based on analysis of these spectra, we find that the linear peptide can exist in stable conformations under the same condition as do the cyclic analogs, but their conformations do not resemble those of their cyclic analogs. Furthermore, the linear peptides exhibit less defined conformational structure. We conclude that the $\alpha C_{(i)}$ -$\alpha C_{(i+3)}$ distance is a primary factor in forming a β-turn, particularly, in forming a standard type I or type II turns. We also find that VCD spectrum of the linear octapeptide in TFE show a strong α-helix pattern which confirmed by NECO calculation.

5.1. INTRODUCTION

Small peptides, particular tetrapeptides, prefer to form β-turn structure in proteins, when proline is at the second position of this peptide. The type of turns depends on the residue after proline.[5-1a,b,c.] In general, β-turns can be defined as a site at which a polypeptide chain changes direction. There are a number of characteristics that can be used to examine β-turn structures in proteins. Based on the X-ray data, the $\alpha C_{(i)}$ - $\alpha C_{(i+3)}$ distances of all 4651 tetrapeptides in proteins were computed.[5-2, 3a,b,c.] Those whose distances were below 7Å and not in a helical region were considered as β-turn. Helical regions in proteins are easily

recognizable, since at least 3 consecutive tetrapeptides all have $\alpha C_{(i)}$ - $\alpha C_{(i+3)}$ distances below 6 Å. Hence, after omission of consecutive helical tetrapeptides, it is easy to locate the isolated tetrapeptides having $\alpha C_{(i)}$ - $\alpha C_{(i+3))}$ distances below 7 Å as candidates of β-turns.

The second characteristic for recognition of a β-turn is the dihedral angles, ϕ and φ, of the backbone polypeptide chain. The ϕ, φ angles of β-turns are mainly characterized by the angles of the middle 2 residues (i+1 and i+2) of which of 3 types, I, II, III and their conformational mirror images I', II' and III', were descried by Venkatachalam. The angles of each turn are listed on Table 4-1. One turn in right-handed α-helix will be presented by 4 consecutive residues having approximate ϕ, φ angles (-57.4° and -47.5°) for each residue.

By contrast, the φ and ϕ angles in various turn structures are much diverse. Several research groups have studied the conformation of β-turns by using small, linear peptides as model peptide.[5-4,5,6.] These model peptides being used have the same properties, which can form either an extra intra-molecular-hydrogen bond beside the 1 → 4 hydrogen bond or a linkage between head and tail of β-turn core . It does seem to provide a same effect as a disulfide bond between $\alpha C_{(1)}$ and $\alpha C_{(4)}$. The basic idea in those studies of model peptide is to limit the distance between $\alpha C_{(1)}$ and $\alpha C_{(4)}$ in a peptide and to force a turn structure. Under such a constraint, the influence of residues at position i+1 and i+2 of turn becomes a primary factor, which decides what kind of turns can be formed.

Attempts have been made previously to identify β-turns in cyclic peptides, because they may be considered to have a rigid conformation. Actually, the conformations of such cyclic peptides can be varied by the nature of the chemical environment. As a follow up study of the conformations of cyclic model peptide, we report here the VCD data of linear tetrapeptides with sequences identical with the cyclic ones, and under the same condition used in the case of cyclic peptides.

The goal of this study was trying to determine the key characteristics which contribute to the formation and stabilization of turn, and the behavior of peptide sequence in forming turns. Since the VCD spectrum detects a short range interaction between carbonyls of peptide, we can focus on a locally coupled interaction among three carbonyls (i, i+1 and i+2) in β-turns.

5.2. MATERIALS AND METHODS

All data presented in this section were collected on the dispersive VCD spectrometer at Hunter college. The details of instrumentation and preparation of samples are given in the previous chapter. The concentration dependence of conformation was tested by diluting the concentration of peptide to 10mM. At this concentration, no conformational change in those peptides were observed.

5.3. RESULTS

The observed IR and VCD spectra of three linear tetrapeptides, *l*(CPGC), *l*(CPFC) and *l*(CPdFC) in different solvents, are shown in Figures 5-1, 2, 3 and 4. The solvents were DMSO:$CDBr_3$ (1:2); DMSO; DMSO/D_2O (1:2) and TFE, which represent different polarities and have various hydrogen bonding ability. In general, a less polar solvent promotes intra-molecular-hydrogen bonds in peptide and a polar solvent that is a hydrogen bond donor or acceptor destroys intra-molecular-hydrogen bonds and release constraints on the peptide chain. The linear octapeptide *l*(FVFWKTCT) was synthesized and purified according to chapter two. Both the observed and calculated IR and VCD spectra of this octamer in different solvents are shown in Figures 5-9, 10, 11, 12.

5.3.1. Absorption spectra and VCD of tetramers

The IR spectra show a broad peak with a low frequency shoulder in the amide I' region. These features indicate that two amide I' absorptions, tertiary and secondary ones are involved. The tertiary amide I' is located at a lower frequency region compared with the secondary one. Shifts in IR spectra with changes of solvents can be interpreted in that such a change on frequency and intensity reflects either variation on intra-molecular-hydrogen bonds or a change of peptide conformation in peptides, such as polar groups in the peptide being exposed to the solvent. The three tetrapeptides exhibit very similar IR spectra in each solvent. A summary of the spectral data is listed in Table 5-1.

Table 5-1. Frequency (cm-1) of amide I' vibration of linear tetrapeptides

Solvent	Tertiary Amide I' cm^{-1}	Secondary Amide I' cm^{-1}
Bromoform:DMSO (2 : 1)	1660	1680
DMSO	1665	1685
D2O : DMSO (2 : 1)	1645	1670
TFE	1655	1670

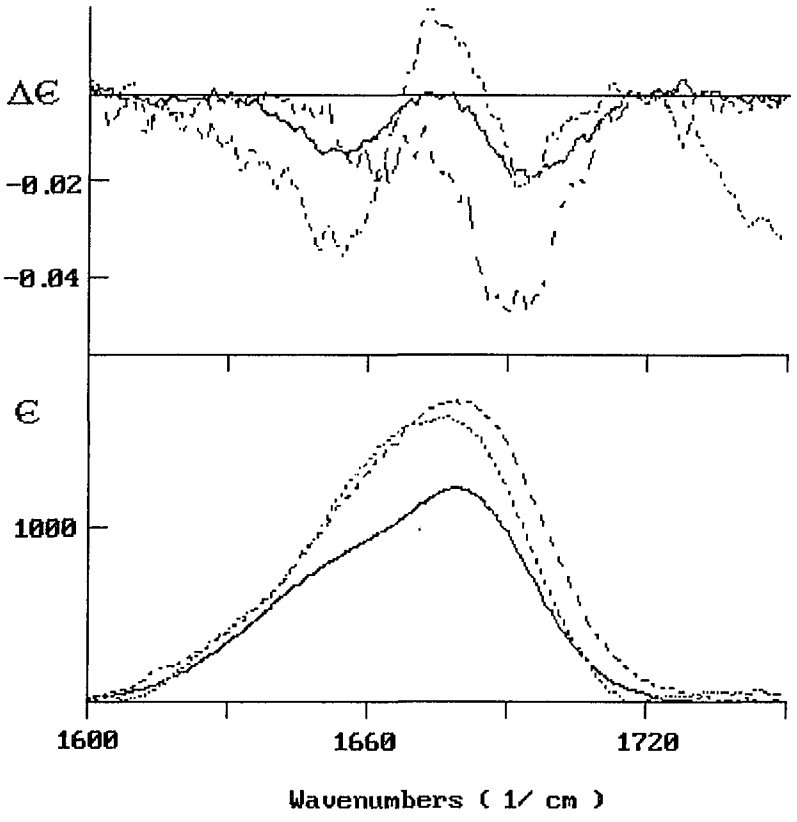

Figure 5-1 Infrared absorption (bottom) and VCD spectra (top) of *l*(CPGC) (solid line); *l*(CPFC) (dotted line) and *l*(CPdFC) (broken line) in DMSO: Bromoform (1:2 by volume).

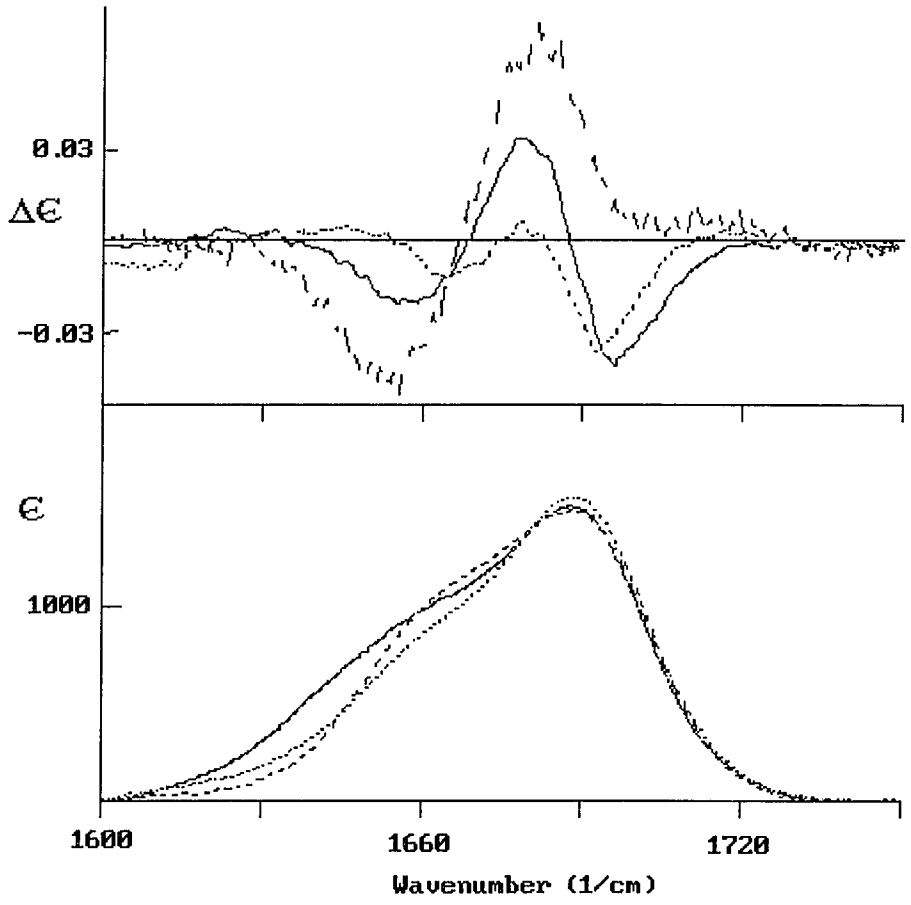

Figure 5-2 The Infrared absorption (bottom) and VCD spectra (top) of *l*(CPGC) (solid line); *l*(CPFC) (dotted line) and *l*(CPdFC) (broken line) in DMSO.

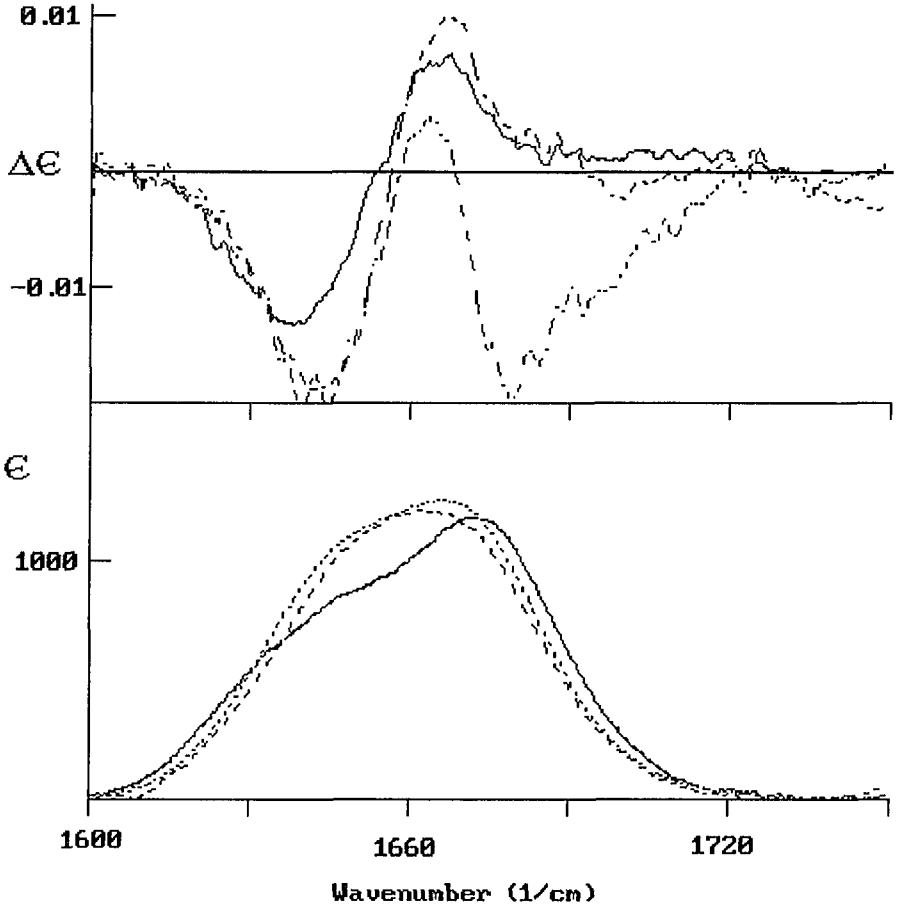

Figure 5-3 The Infrared absorption (bottom) and VCD spectra (top) of *l*(CPGC) (solid line); *l*(CPFC) (dotted line) and *l*(CPdFC) (broken line) in DMSO:D_2O (1:2by volume).

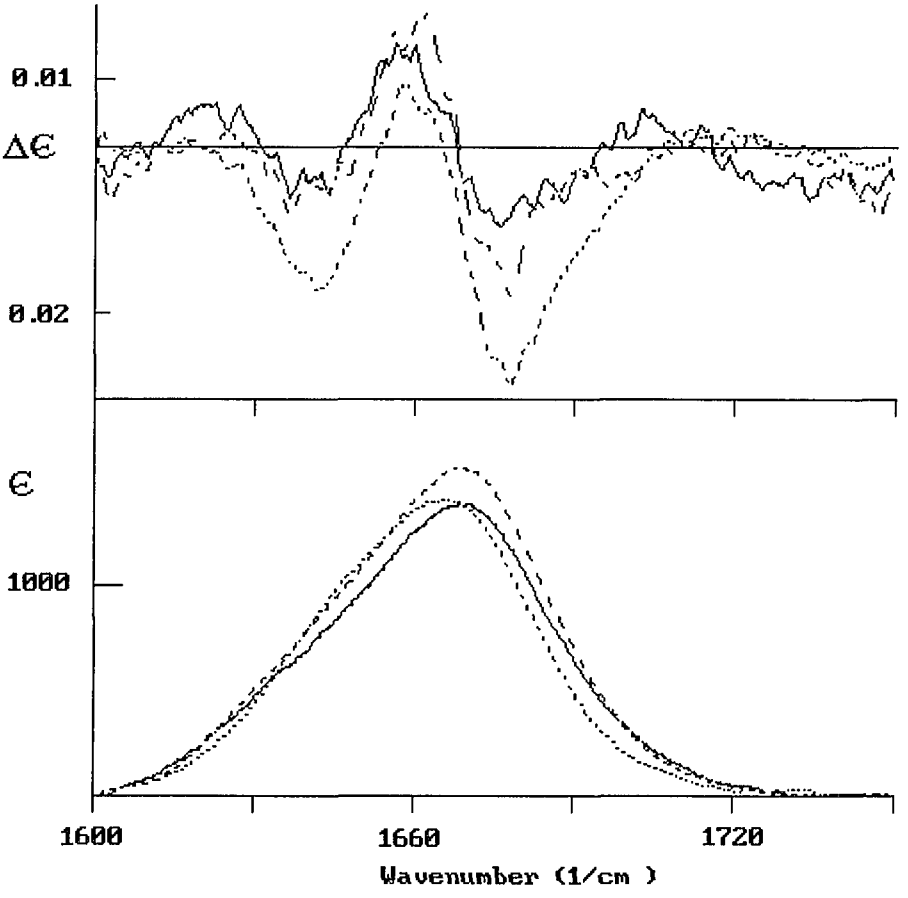

Figure 5-4 The Infrared absorption (bottom) and VCD spectra (top) of *l*(CPGC) (solid line); *l*(CPFC) (dotted line) and *l*(CPdFC) (broken line) in TFE.

In a low polarity solvent, bromoform, the IR spectra of the three peptides exhibit a broad, asymmetric peak. The absorbance of the tertiary amide I', $C=O_{(i)}$, of the three peptide occurs at 1655-1660 cm^{-1} reflecting the formation of a hydrogen bond between $C=O_{(i)}$ and $NH_{(i+3)}$. The higher frequency peak in absorption spectra is composed of two kinds of carbonyls: $C=O_{(i+1)}$ and $C=O_{(i+2)}$. Both are secondary amide I' and non-hydrogen bonded carbonyl groups with maximum at 1675-1680 cm^{-1}. Their geometry would be fixed in certain conformations of the peptides. Therefore, they might couple with each other , if their orientation is suitable. $C=O_{(i+3)}$ is conformationally the least restricted (far away from others). It has an amide I' peak in about 1690 cm^{-1}.

The polar, hydrogen bond acceptor solvent, DMSO, broadens the IR peaks and shifts them up by about 5-10 cm^{-1}. In principle, DMSO should break intra-molecular-hydrogen bonds of $NH_{(i+3)}$, since S=O group of the DMSO forms hydrogen bonds with NH in the peptide. This effect, however, can not explain why all peaks become broad and shift to higher wavenumber. An alternative interpretation of the DMSO effect is: it is due to the high dielectric constant of DMSO.

TFE which is known as a α-helix promoter is a hydrogen bond donor. It shifts the frequency of amide I' to lower wavenumber region, and the IR spectra in TFE become more symmetric. Water can form hydrogen bonds with C=O and NH groups. The frequency of all C=O are down shifted, and the peak shape of IR spectra become symmetric. TFE and D_2O seem to cause a similar conformational changes in these peptides.

In general, the kind of β-turns that can be formed depends on the residues at the third position in a turn, where proline is at the second position. Review of these IR spectra of the three peptides with various residues in the third position

does not show a pattern that can distinguish the conformational differences of three peptides, even though there is some solvent dependence observed. Structural differences in these peptides have been confirmed by other techniques. [5-4,5]

The correspondence between spectra and structure is best understood for proteins in D_2O.[5-6] For example, bands centered between 1650-1658 cm^{-1} are associated with α-helical segments, whereas the random coil segments are associated with an IR band around 1640-1648 cm^{-1}. The IR bands between 1620-1640 cm^{-1} have been assigned by many authors to β-pleated sheets. The amide I vibration at higher frequencies is considered to β-turn conformation. However, these frequency region for amide I vibration, which may relate to the structure of protein, actually should be shifted, when the protein is in a different solvent or chemical environment, even though their conformation may not change at all. Consequently, the examination of polypeptide conformation, through the analysis of their IR spectra, is somehow limited by the lack of correlation between specific backbone conformations and individual component bands.[5-7] Furthermore, because of the diversity of turn conformation and broad band shapes in the IR spectra from proteins, the interpretation of the conformation of β-turns in protein is curiously difficult by the analysis of their IR spectra alone.

The observed VCD spectra of the peptides produce entirely different features as the solvent is varied. VCD spectra of *l*(CPFC) in pure DMSO and a DMSO /D_2O are similar with negetive / positive pattern. A minor difference occurs in that the ratio between the negative part and the positive part of VCD spectra (Figure 5-5). That implies that a polarity change from pure DMSO to DMSO/D_2O does not alter conformation of *l*(CPFC).

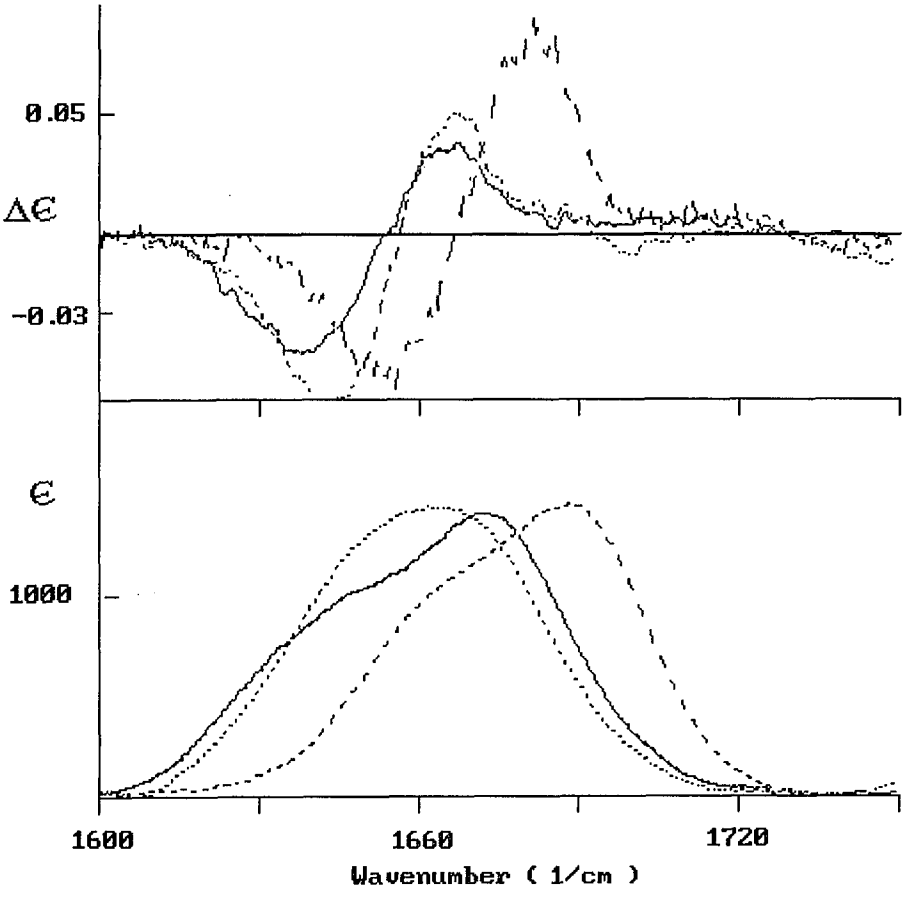

Figure 5-5. The infrared absorptions (bottom) and VCD spectra of *l*(CPGC) in D_2O/DMSO(solid line); and *l*(CPFC) in D_2O/DMSO (dotted line) as well as DMSO (Broken line), which exhibit same patterns, respectively.

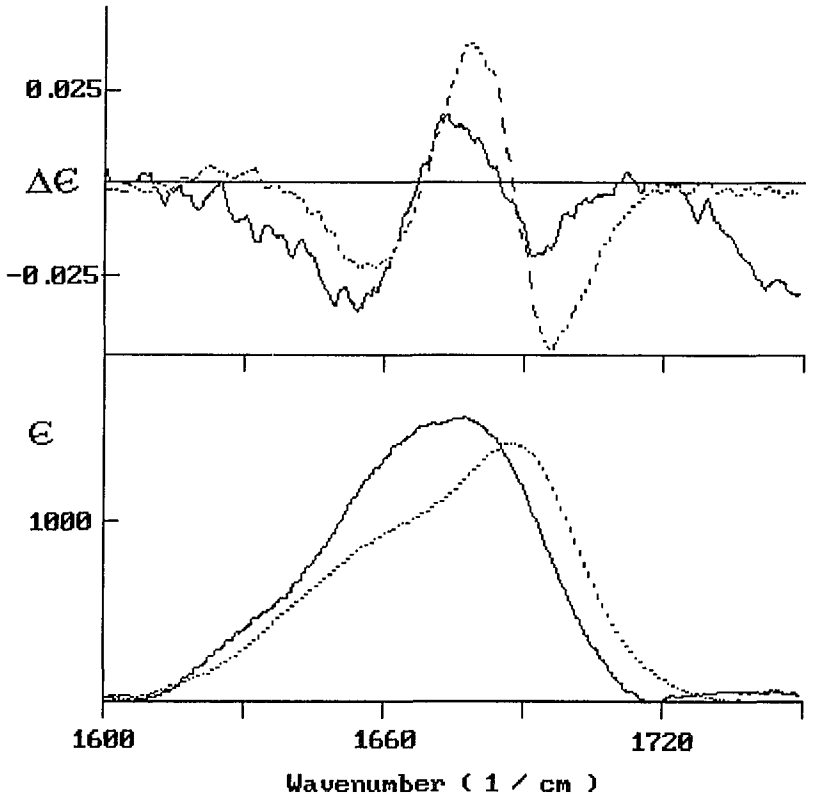

Figure 5-6. The infrared absorption (bottom) and VCD spectra (top) of *l*(CPFC) in DMSO/Bromoform (solid line) and *l*(CPGC) in DMSO (dotted line), respectively.

In *l*(CPGC), the spectrum from DMSO / D_2O has an identical pattern as that of *l*(CPFC) in the same solvent. But in pure DMSO, the pattern of *l*(CPGC) matches the shape of pattern (negetive / positive / negetive) of *l*(CPFC) in TFE and is similar to the spectrum of *l*(CPFC) in bromoform/DMSO. (Figure 5-6). When it is in less polar solvent, two negative peaks were observed in its VCD spectrum. That spectrum resembles the spectrum of *l*(CPdFC) in D_2O/ DMSO. TFE brings about a similar pattern of *l*(CPGC) as it in case of *l*(CPFC), but with a weak signal level. Thus we may conclude that conformation of *l*(CPGC) in polar solvent is same as that of *l*(CPFC) in less polar solvent, whereas its conformation in less polar solvent resembles that of *l*(CPdFC) in more polar solvent. The

behavior of *l*(CPGC) in various solvents is expected and has been confirmed by other techniques.

The VCD spectra of *l*(CPdFC) in solvents of various polarity are quite different from those of other peptides. The common part of the VCD pattern of *l*(CPdFC) is the negative bias of the couplet produced by secondary carbonyls at high frequency (Figure 5-1,2,3,4).

5.3.2. IR absorption and VCD spectra of linear octamer:

This linear octamer is a peptide that is requested by Association of Biomolecular Resource Facilities (ABRF) to serve as a standard peptide for 1995's study [5-9]. ABRF member labortories were asked to synthesize and cyclize the following peptide by the method most frequently used in their facility:

H-Phe-Cys-Phe-Trp-Lys-Thr-Cys-Thr-NH_2

This peptide sequence was chosen for several reasons. It is homologous to octreotide, an eight-residue somatostatin analogue, which is also readily oxidized to its cyclical form. Cyclized peptides have been shown to be more effective than their linear counterparts in many biological systems. The presence of a Trp residue provided a site susceptible to modification. Finally, for our own reason, it fits very well in our research project: It not only expanded from trimer, tetramer to octamer, but also has a cyclical form which has a bigger ring size.

One of the most fascinating aspects of the living state is that organisms are capable of regulating their chemical processes. There are many facets to this regulation. In the animal kingdom one aspect involves hormones (from the Greek hormaein, "to rouse or excite"), substances produced in one type of cell and transported to other specific target cells. In mammals (including humans) a large number different hormones with different regulatory effects are produced by

various organs. The hypothalamus produces at least three peptide hormones, which in turn control the production of other hormones by pituitary. Somatostatin is one of the hypothalamus hormones which inhibits the pituitary's production of human growth hormon HGH. Somatostatin is also produced by the pancreas and has other regulatory actions in body. One such action is controlling the release from the pancreas of two other peptide hormones, insulin and glucagon. Insulin is responsible for lowering levels of blood glucose (sugar); glucagon acts to elevate blood sugar.

The stick model of this somatostatin analogue linear octamer H-Phe-Cys-Phe-Trp-Lys-Thr-Cys-Thr-NH_2 with a α-helix conformation is shown in Figure 5-7. Measured IR absorption and VCD spectra in TFE solvent along with NECO calculated IR and VCD spectra are shown in Figure 5-8 and 5-9. The calculated VCD spectrum which assume a α-helix structure assembles the observed VCD spectrum very well. This suggests that a helix conformation does exist for linear FCFWKTCT octamer in TFE which is a well known helix promoter. Comparing to the VCD results of tetramers in TFE which exhibited negetive / positive / negetive patterns in all three tetramers, clearly there are no helix structures in tetramer solutions. This might be explained by the following: First, the conformation of α-helix needs at least 3.6 residues (that is one hydrogen bond or one turn), tetramer has four residues, which is on board line, might form more like a turn structure instead of a helix structure. Second, the octamer might have enough residues to form a helix structure which is confirmed by the experiments results.

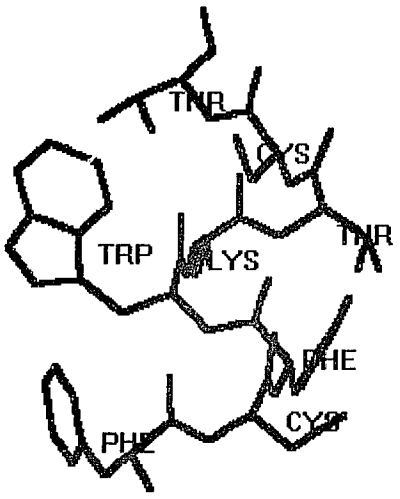

Fig.5-7 Alpha-helix structure of linear octamer FCFWKTCT.

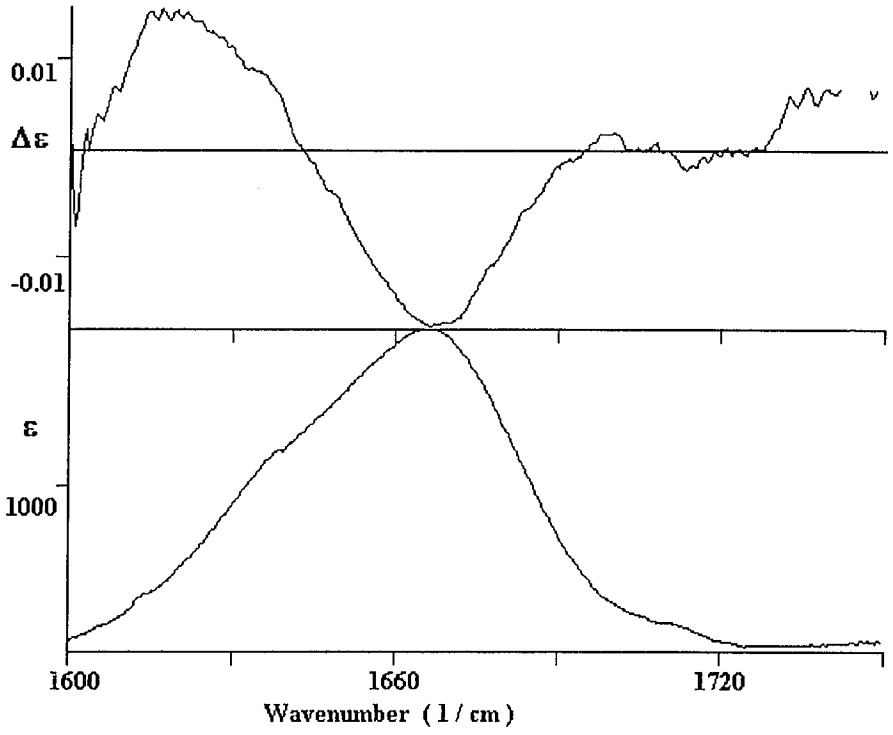

Fig. 5-8 Measured IR and VCD spectra of linear octamer in TFE .

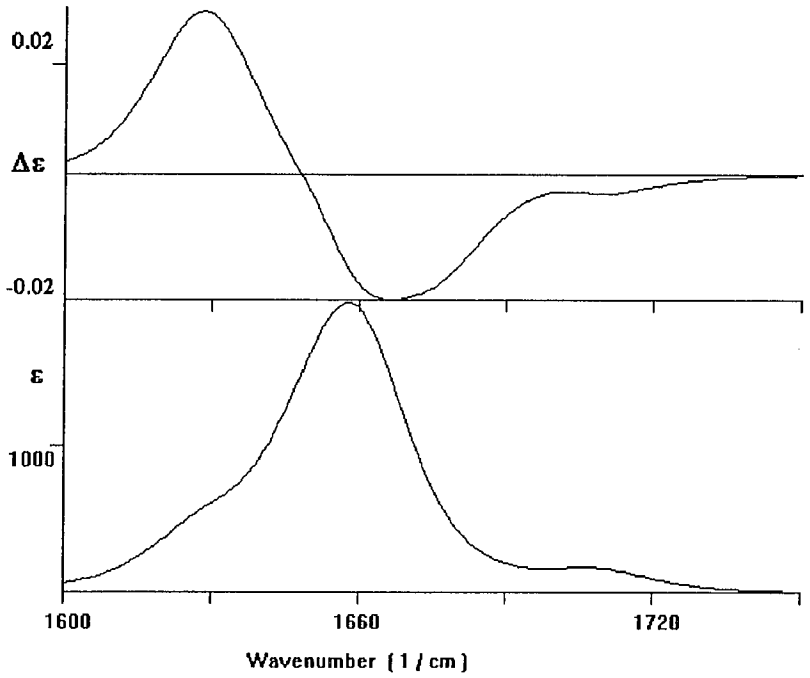

Fig. 5-9 Calculated IR and VCD spectra of octamer by NECO (assume α-helix).

Figure 5-10, 11 show the observed IR absorption and VCD spectra of linear peptide FCFWKTCT in water and in bromoform respectively. The VCD signal of the octamer in water is very weak which might suggest an ill-defined structure since the strong interaction between solvent water and octamer. The VCD spectrum of linear octamer in a low polarity solvent (bromoform) exhibit broad, monosignate (negative) features. We found previously that this spectral behavior is associated with low-order structures. The wavenumber range for the spectrum of octamer in bromofom is 1500 cm^{-1} to 1750 cm^{-1}. There are no IR absorption and VCD peaks between 1500 cm^{-1} to 1600 cm^{-1} which is why we always scan from 1600 cm^{-1} to 1750 cm^{-1} . A negative VCD peak in low frequency (around 1620 cm^{-1}) maybe due to the interaction of N and C terminals of the octapeptide. Overall, the three VCD patterns of this octamer in three different solvents exhibit large difference which means that different structures exist in different solvents. This is usually true in a lot of cases.

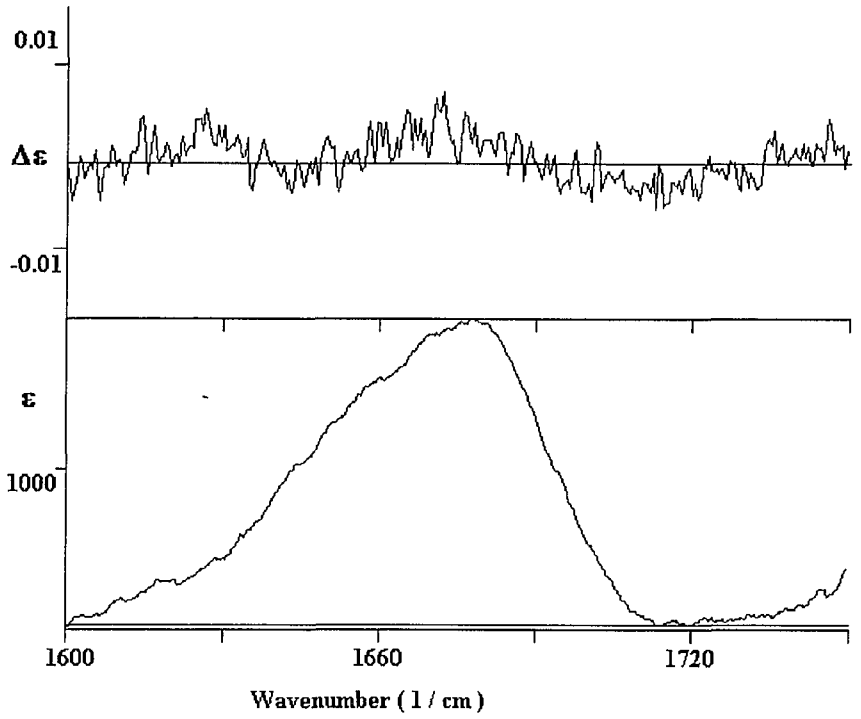

Fig. 5-10 Observed IR and VCD spectra of the octamer in water.

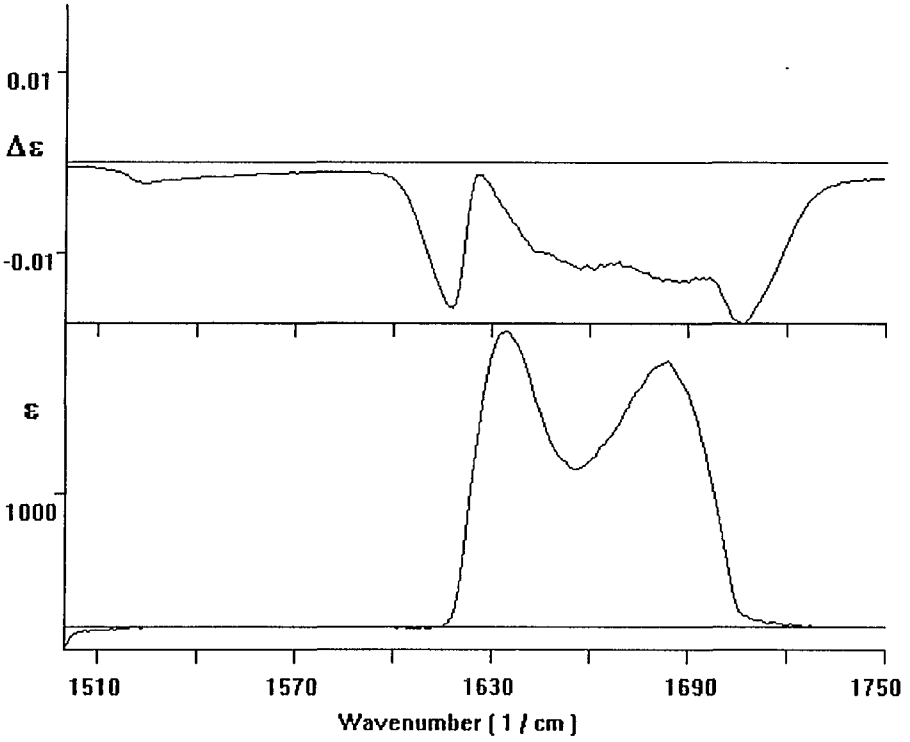

Fig. 5-11 Observed IR and VCD of octamer in bromoform.

5.4. DISCUSSION

Based on analysis of these VCD spectra from the three linear peptides, their conformations seem to have no features in common with their cyclic analogs, even though they have the same sequences and data we acquired under same conditions. This finding suggests two possibilities: One is that linear peptides are so flexible in those solvents that they may not form a stable conformation at all. Or they may create conformations other than a regular type I or type II β-turn, which were formed by their cyclic analogs. The strong VCD spectra of those peptides support the second interpretation, since lack of conformational stability will manifest itself by a lack of VCD.

The aim of the following discussion is to attempt to qualitatively interpret the changes in VCD spectra observed from linear tetrapeptides. In general, since there are three carbonyls with different vibrational frequencies (one at low frequency region and two at high frequency) in β-turn, which are fixed in geometry, coupling between carbonyls can occur in two ways: a low(tert.)- high (sec.) and a high (sec.) - high (sec.) coupling. We like to call the proposed interpretation " frequency strategy". It interprets the couplets between $C=O_{(i)}$ and $C=O_{(i+1)}$ or $C=O_{(i)}$ and $C=O_{(i+2)}$ as well as between $C=O_{(i+1)}$ and $C=O_{(i+2)}$, respectively. The typical pattern shown in those VCD spectra from 3 linear peptides are a negetive / positive for low- high couplet and a positive / negetive for high -high couplet with various ratios of negative and positive parts. Those patterns correspond to a certain geometry of carbonyls.

According to the exciton formalism, the dipolar coupling energy between interacting C=O groups depends on the distance and direction between dipoles of

C=O. The large rotational strengths are created for perpendicular geometry between the interacting groups. Such a geometry, however, produces the smallest coupling energy and splitting of the exciton components. Parallel or antiparallel geometry present maximum splitting, but minimal rotational strengths.

In *l*(CPFC), a simple negetive / positive couplet pattern in polar solvents (DMSO and DMSO/D_2O) covers the lower wavenumber region of absorption and can be classified as a low -high couplet. The zero-crossing of this VCD spectrum, located between the tertiary and secondary amide I', (1655 cm^{-1} in D_2O and 1668 cm^{-1} in DMSO, respectively) further supports this interpretation. In such a polar solvent, the 1 $\rightarrow$ 4 intra-hydrogen bond will be broken by solvent and the $NH_{(i+3)}$ would prefer H-bonding with solvent. $C{=}O_{(i+2)}$ will be situated at the position, at which it may be parallel or antiparallel to $C{=}O_{(i+1)}$. Since there is a L side-chain group at the third position, we believe that $C{=}O_{(i+1)}$ and $C{=}O_{(i+2)}$ are close to each other, and it is more reasonable to assume they may align parallel rather than anitiparallel. Consequently, they may not have any contributions to rotational strength. Therefore, the coupling of structure is between $C{=}O_{(i)}$ and $C{=}O_{(i+1)}$ or $C{=}O_{(i)}$ and $C{=}O_{(i+2)}$. The shape of couplet depends on the orientation of these dipoles.

In a less polar solvent, the driving force of folding is intra-molecular-hydrogen bonding. So the $C{=}O_{(i+2)}$ may turn to a position at which $C{=}O_{(i)}$ can hydrogen-bond with $NH_{(i+3)}$ and the orientation of $C{=}O_{(i+1)}$ and $C{=}O_{(i+2)}$ is no longer parallel any more. These two dipoles now can couple with each other. Therefore, a high-high couplet appears in the VCD spectrum of *l*(CPFC) in the high frequency region. Therefore, two couplets exist in this geometry of *l*(CPFC): A negetive / positive couplet at lower frequency (zero-crossing at 1665 cm^{-1}) for the low- high interaction between $C{=}O_{(i)}$ and $C{=}O_{(i+1)}$ or between $C{=}O_{(i)}$ and $C{=}O_{(i+2)}$, and a p / n couplet in the high frequency (zero-crossing at 1685 cm^{-1}),

for high-high coupling interaction between $C=O_{(i+1)}$ and $C=O_{(i+2)}$. To produce a 1 $\rightarrow$ 4 intra-hydrogen bonds in that conformation, it must form a different turn than type I and II β-turns, whose spectra were observed by previously VCD. Reviewing the three VCD spectra of *l*(CPFC) in various solvents, the low-high couplet shows up in each of the spectra with the same pattern (n / p) in frequency region between tertiary and secondary amide I linkage. It suggests that the conformation changes of *l*(CPFC) with solvent polarities is due to rotation of $C=O_{(i+2)}$.

Due to the absence of a side group in the third position of *l*(CPGC), it may assume structures similar to one of *l*(CPFC) and *l*(CPdFC) in various solvents. In fact, in D_2O/DMSO, the VCD spectrum of *l*(CPGC) is identical to that for *l*(CPFC) in the same solvent. We believe it has the same conformation as *l*(CPFC). We expect that the C=O groups in *l*(CPGC) are forming inter molecular H-bond with D_2O is a major driving force. In other words, hydrogen and the L side-chain group on $\alpha C_{(i+2)}$ would cause the same influence on peptide folding under this given condition.

It is not surprising that *l*(CPGC) in pure DMSO behaves like *l*(CPFC) in a less polar solvent and exhibits two couplets in the low and high frequency regions, respectively. The best description of those spectra of *l*(CPGC) in pure DMSO and *l*(CPFC) in a less polar solvent is that they are mirror images. The VCD spectrum of *l*(CPGC) contains a stronger couplet in the high frequency range than in the low frequency range. This indicates that $C=O_{(i+2)}$ of *l*(CPGC) can turn easily in less hydrogen bonded solvent than $C=O_{(i+2)}$ of *l*(CPFC) does in same solvent, because there are lower steric barriers at $\alpha C_{(i+2)}$ of *l*(CPGC), but L-side-chain group on $\alpha C_{(i+2)}$ of *l*(CPFC) blocks the motion of $C=O_{(i+2)}$. In other words, DMSO can not cause a movement of $C=O_{(i+2)}$ to the position where it was in D_2O in that case.

The couplet between $C=O_{(i+1)}$ and $C=O_{(i+2)}$ at higher frequency exists unchanged in spectra of *l*(CPdFC) in all three solvents. Based on the shapes of these couplets and their frequencies in *l*(CPdFC), we are assuming, that the D-side-chain group in the third position can more efficiently either limits the movement of the $C=O_{(i+2)}$ group or block the movement of both $C=O_{(i+2)}$ and $C=O_{(i+2)}$, keeping the distance and orientation of $C=O_{(i+1)}$ and $C=O_{(i+2)}$ constant. These two carbonyls can couple with each other in all conformations. With the changes of polarity of solvent, we believe that their conformational changes must exclusively relate to the variation of geometry of $C=O_{(i)}$. Actually, changes in VCD spectra of *l*(CPdFC) in the three solvents do only occur on the low frequency region. Reducing the polarity of solvent minimizes the a portion of the low- high coupling between $C=O_{(i)}$ and $C=O_{(i+1)}$ or $C=O_{(i+2)}$.

Another way to recognize that conformations of *l*(CPGC) are an intermediate state between states of *l*(CPFC) and *l*(CPdFC) in each solvent is the comparison of the VCD spectra of those peptides in the three solvents. We found, that a conformational state of *l*(CPGC) in the same solvent is a transition between the conformation of *l*(CPFC) and *l*(CPdFC).

In order to interpret the differences of VCD spectra between cyclic and linear tetrapeptides and among linear peptides, we refer to the structure of standard β-turns, which are confirmed by other techniques (Figure 4-1).

There exist three peptide linkages in β-turn conformations, which determine types of structure formed. The movement or rotation of such planes of peptide linkage depends on the nature of side-chains on each α-carbon, particularly, on situation of its adjacent α-carbon. Since $C=O_{(i)}$ is a tertiary peptide linkage, the proline ring fixed the angle of N- $\alpha C_{(i+1)}$. But the $C=O_{(i)}$ can easily form a cis peptide linkage with a small energy difference. The formation of a cis linkage in $C=O_{(i)}$ plane will largely depend on the movability of $\alpha C_{(i)}$. In order

to transform to the cis conformer, $\alpha C_{(i)}$ has to turn into β-turn core with a $C{=}O_{(i)}$ turning out. In cyclic peptide discussed in chapter 4, the distance between $\alpha C_{(i)}$ and $\alpha C_{(i+3)}$ is fixed by the S-S bond. In other words, the position of $\alpha C_{(i)}$ is fixed. Consequently, it is difficult to form a cis conformer in the cyclic tetrapeptides.

Movements of $C{=}O_{(i+2)}$ in the cyclic peptide are still possible, event though $\alpha C_{(i+3)}$ is less movable. It can be seen in cases of *c*(CPFC) and *c*(CPdFC). Such a movement depends on the size and location of the side-chain on $\alpha C_{(i+2)}$. Since $C{=}O_{(i)}$ can not move too much, the rotation of $C{=}O_{(i+2)}$'s plane also is affected by $NH_{(i+3)}$, which attempts to form an intra $1\rightarrow 4$ H-bond with $C{=}O_{(i)}$.

The movement of $C{=}O_{(i+1)}$ plane is restricted by the size and the position of side-chain on both $\alpha C_{(i+1)}$ and $\alpha C_{(i+2)}$. Since the L- proline is at second position, the effects of side-chain on $\alpha C_{(i+2)}$ become a sole factor in determining the types of turns formed in a cyclic peptide. Furthermore, since each C=O is closer to its own α-carbon, the steric effect from a side-chain on this α-carbon has a more influence on the movement of C=O instead other factors. Therefore, the geometry of $C{=}O_{(i+1)}$, in general, should be mainly terminated by the side-chain on $\alpha C_{(i+1)}$ rather than on $\alpha C_{(i+2)}$ except other primary constraints involved on forming a structure. In comparison each cyclic peptide with their linear analogs, the main difference between their structure is the limitation of distance between $\alpha C_{(i)}$ and $\alpha C_{(i+3)}$. In cyclic peptides, it is limited by the disulfide bond. Therefore, the variation of movement of $C{=}O_{(i)}$ and $C{=}O_{(i+2)}$ planes in cyclic peptides should be much smaller than in acyclic one.

There are two kinds of influences on folding of cyclic tetrapeptides, which arise from limitation of $\alpha C_{(i)}$ - $\alpha C_{(i+3)}$ distance. First, S-S bond brings two "arms" of turn together. Possibly, they are parallel to each other. This constraint on peptide chain might make that the side-chain's influence becomes a major factor in forming certain types of turn. Second, a fixed distance between $\alpha C_{(i)}$ and $\alpha C_{(i+3)}$

would efficiently limit rotations of $C=O_{(i)}$ and $C=O_{(i+2)}$ planes, particularly, for preventing $C=O_{(i)}$ into cis conformer.

In linear peptide, a limitation on $\alpha C_{(i)}$ - $\alpha C_{(i+3)}$ distance does not exist. The C=O planes have more freedom to rotate. For example, the cis conformer can be easily formed regardless of the position of $\alpha C_{(i)}$. Accordingly, the pattern of couplets between $C=O_{(i)}$ and $C=O_{(i+1)}$ or $C=O_{(i)}$ and $C=O_{(i+2)}$ must be different than cyclic analogs. So there exist more suitable geometries for $C=O_{(i)}$ in linear tetrapeptides.

Based on arguments above, the observed VCD spectra of three linear tetrapeptide can be interpreted in following way. According to the sequence strategy of β-turn[5-3a], the $C=O_{(i+1)}$ in *l*(CPFC) should prefer a position as it in the type I turn, since its energy would be lower. Therefore, the differences between the observed VCD spectra of *l*(CPFC) in various solvents must be due to movements of both $C=O_{(i)}$ and $C=O_{(i+2)}$. Since there is no limitation on the $\alpha C_{(i)}$ - $\alpha C_{(i+3)}$ distance , one can expect some reasonable structures other than type I structure for *l*(CPFC).

In the case of *l*(CPdFC), $C=O_{(i+1)}$ may be located in a position similar to a type II turn like *c*(CPdFC), because of the effect on D-side-chain in $\alpha C_{(i+2)}$. Without other constraints on peptide chains, this may not be a favorable position with respect to the L-side chain from proline residue. Such a higher energy geometry may not stable for linear peptide, particularly, in the case there is no limitation on the $\alpha C_{(i)}$ - $\alpha C_{(i+3)}$ distance. Therefore, some adjustment of its conformation have to be made with polarity of solvent. Following a same idea, the D-side chain on $\alpha C_{(i+2)}$ is an important factor for the movement of $C=O_{(i+2)}$ with various polarity of solvent.

Additionally, since the high-high couplet shows up in all case of *l*(CPdFC), thc orientation between $C=O_{(i+1)}$ and $C=O_{(i+2)}$ seems to be fixed. Consequently,

the possibility of cis conformer of $C{=}O_{(i)}$ is another reason for that *l*(CPdFC) will not form the structure as those in case of cyclic peptide.

In the case of linear octamer (shown in Fig. 5-8, 10, 11), the IR absorption spectra show a broad peak with a low frequency shoulder in the amide I' region. The shoulder becomes more obvious in solvent of bromoform. The main peak in IR spectra shift downwards from less polar solvent (bromoform), polar solvent (water), to strong polar solvent (TFE). Inspection of VCD spectra from the octamer in three different solvents, much difference can be seen. That implies that the different solution structures exist in three solvent for this octamer. The VCD spectrum of the octamer in water gives a weak signal across the spectrum region which might imply an ill-defined structure. One promising result is that the octamer in TFE exhibit a strong positive / negative pattern (as shown in Fig. 5-8) which perfectly reassemble the calculated α-helix pattern by NECO (see Figure 5-9). This is consistent with results from other techniques, which suggest that TFE can promote peptide to form α-helix conformation regardless of the peptide sequence.

5.5. REFERENCES:

5-1a B. N. Narrating Rae. (1983) *J. Am. Chem. Soc.*, 105,7423-28.

5-1b M.Hollosi and G.D.Fasman (1985), *Biopolymers* 24,211-241.

5-1c B. N. Rae,(1983), *J. Am. Chem. Soc.* 105,7423-7428.

5-2 Peter Y. Chou and G. D. Fasman. (1977) *J. Mol. Biol.* 115,135-175.

5-3a George D. Rose; Lila M. Gierash and John A Smith. *Adv. in Protein Chem.* (1985) 37,1-109.

5-3b K. Ramnarayam. (1994) *peptide research* 7, 270-278.

5-3c C.M. Wilmot and J. M. Thornton (1988) *J. Mol. Biol.* 203, 221-232.

5-3d H. J. Dyson. (1988) *J. Mol. Biol.* 201,161-200.

5-4 B. Imperiali. (1992) *J. Am. Chem. Soc.* 114, 3182-3188.

5-5 Andras Perczel. (1991) *J. Am. Chem. Soc.* 113,9772-9784.

5-6 M. Hollosi. G.D. Fasman. (1994) *Biopolymers* 34, 177-185.

5-7 Byler, M. and Susi, H. *Biopolymers.* (1986) 25, 269-287.

5-8 Kuntz, I. D. (1972) *J. Am. Chem. Soc.* 94, 4009-4012.

5-9 Angeletti, R. H. etc., (1995) *Techniques in Protein Chemistry VII*

CHAPTER SIX

IR CIRCULAR DICHROISM OF TURNS IN TRIMERS

6.1. INTRODUCTION:

IR (VCD) is a relatively new and structurally highly sensitive spectroscopic technique in which differential absorption of left and right circularly polarized light by vibrational transitions is monitored in the IR spectral region[6-1,2]. The conformational sensitivity of VCD can be visualized to originate from the dipolar coupling of (achiral) IR transitions, such as the various amide I stretching modes in a peptide, in analogy to the coupling of electronic transitions which gives rise to electronic CD (ECD). Thus, the exciton theory invoked for the interpretation of ECD spectral features may also be used for VCD.

VCD can be observed for many of the 3N-6 vibrational degrees of freedom of a molecule; however, the results here deal exclusively with the amide I vibration of peptides, since it appears to be the vibration most sensitive to solution conformation. This vibration, which can be described mostly as the carbonyl stretching motion of the amide moiety, occurs between 1630 and 1700 cm^{-1}, and has a dipole transition moment of 0.29 D. Conformation dependent VCD spectral features in aqueous and non-aqueous solution are relatively easily accessible for this band, and have been well documented [6-3,4]. Since the vibrational transition moment of the carbonyl stretching mode is smaller than that of electronic transitions, for example, the $\pi^* \leftarrow \pi$ or $\pi^* \leftarrow$ n transitions in a peptide linkage, the dipolar coupling extends over shorter distances in VCD than in ECD. Consequently, VCD is a superior technique to monitor short-range structural motifs, such as various turns in peptides. In addition, the better spectral resolution

of IR transitions, as compared with the often very broad and unstructured electronic transitions in the UV range, permit a better and more detailed assignment of spectral features.

6.2. RESULTS:

All data presented here were collected on the broadband (800-1800 cm^{-1} spectra range), dispersive VCD spectrometer at Hunter College described previously [6-5]. Several improvements were implemented since the earlier description of the instrument. Mostly, these improvements deal with further lowering the artifact levels. Thus, VCD spectra with amplitudes of about 3×10^{-7} ΔA units can now be measured reliably. Details of the modifications will be reported at a later date.

Sample handing in VCD is entirely analogous to that in IR spectroscopy. Samples are contained between CaF_2 plates, separated by Teflon spacers of appropriate thickness, typically between 15 and 25 μm. Sample volumes of 10-20 μl at peptide concentration of 5-20 mg ml^{-1} were utilized. The peptides Cys-Ala-Cys (CAC), cyclo-(-Cys-Ala-Cys-) (c-CAC), Cys-Pro-Cys (CPC), and cyclo-(-Cys-Pro-Cys-) were prepared by standard Fmoc solid phase peptide synthesis described in chapter two. All peptides were lyophilized from D_2O prior to dissolving them in the solvents discussed for each experiment. Thus, all reported C = O stretching vibrational frequencies will be for the deuteriated peptide linkage, referred to as the amide I' vibration. Molecular modeling, and the generation of structures shown, were carried out using program HyperChem running on a personal computer equipped with a 90 Mhz Intel Pentium processor. Nondegenerate extended coupled oscillator (NECO) method was used to calculate the VCD and absorption spectra.

Since turns are such frequent and important peptide structural motifs, a number of experimental and theoretical studies have been undertaken in order to identify their spectral characteristics. However, no single unique and prototypical feature of turns has been established via CD or vibrational spectroscopes, whereas for other peptide conformations (e.g. the α-helix) such unique identifiers do exit. The direct observation of turn structure is difficult because the CD features of the turns are generally weak and are masked easily by CD features of other parts of molecules, including S-S linkages often used to establish turn structures.

6.2.1 Models of γ -turns (CAC and c-CAC):

Cys-Ala-Cys, cyclo-(Cys-Ala-Cys) will be discussed in this section.

Figure 6.1 show the models of the cyclized c(CAC) and linear CAC trimers. Because of the cyclic nature of c-CAC, it appears to be an ideal model for a peptide γ -turn, in which a hydrogen bond between residues 1 and 3 stabilize turn. NMR studies have indicated that a number of tripeptides exist in a γ -turn conformation in solvents with low polarity [6-6]. The observed IR absorption and VCD spectra of c-CAC and its non-cyclic analogue in DMSO and DMSO-bromoform mixed solvents are shown in Fig.6.2.

The IR spectra are very similar in all cases, consisting of a main absorption peak with an unresolved low-frequency shoulder. The more polar solvent (DMSO) produces a higher frequency absorption (1689 cm^{-1}), whereas in the DMSO-bromoform mixture, the band maximum is observed at 1682 cm^{-1} . Aside from these relatively small frequencies shifts, the absorption spectra are very similar and would not indicate any major conformational differences between these molecules. The high frequencies observed, however, are typical for peptide-turn motifs.

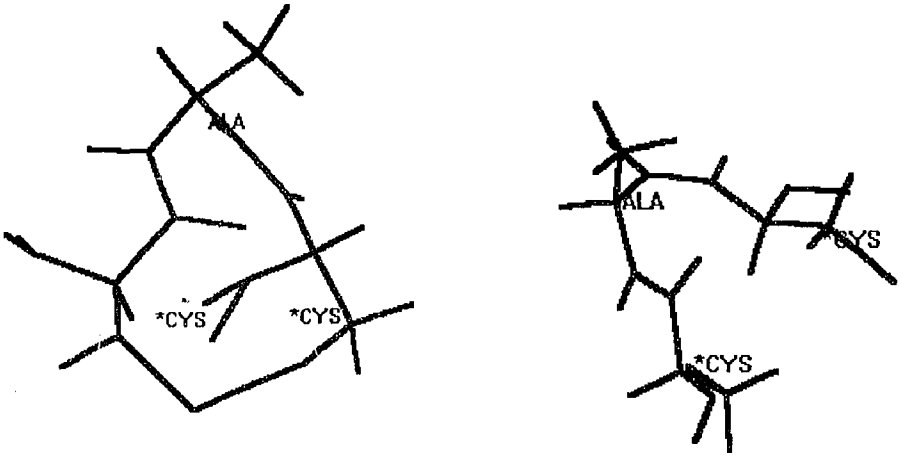

Fig.6.1 Stick models of cyclic c-CAC (left) and linear CAC (right).

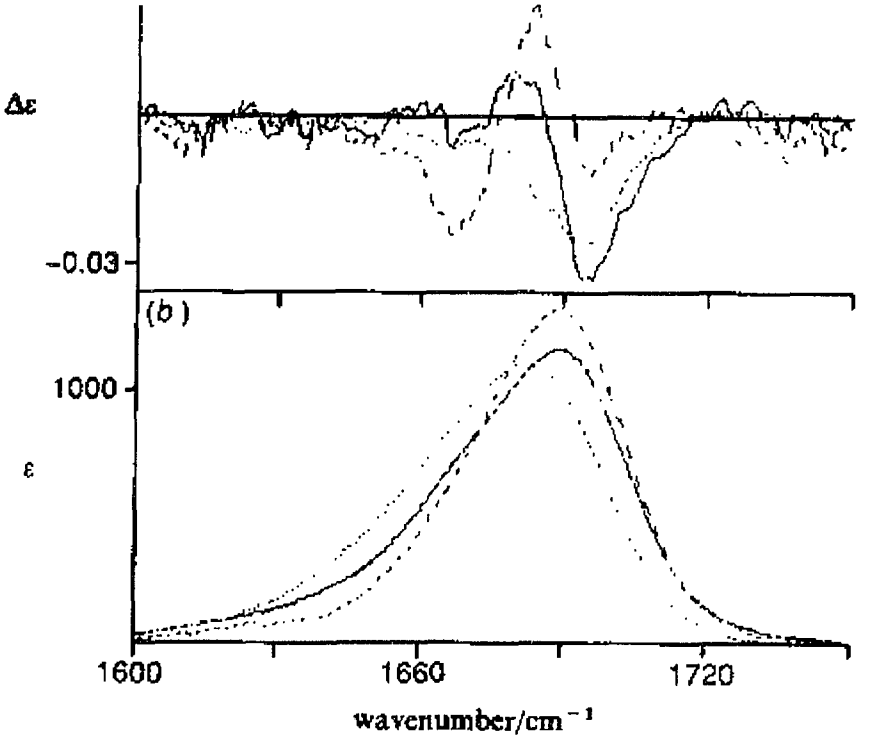

Fig.6.2 (a) VCD and (b) absorption spectra of c-CAC in DMSO (-), c-CAC in $CDBr_3$ -DMSO (...) and CAC in DMSO (---).

The VCD spectra of both CAC and c-CAC in a low polarity solvent (DMSO-bromoform mixture) exhibit broad, monosignate (negative) features. In a more polar solvent (DMSO), distinct VCD couplets are observed for both CAC and c-CAC (Figure 6-2). We believe that the none-conservative, positive VCD couplet (implying positive VCD intensity at lower wavenumber) of c-CAC in DMSO actually is representative of a γ-turn, since it is vey similar to the VCD of another molecule containing a γ-turn, to be discussed below.

At this point, the importance of the solvent on the observed VCD spectra needs to be pointed out. One might expect that in a relatively small and well defined ring system containing an intramolecular hydrogen bond, such as c-CAC, the conformational freedom would be sufficiently restricted as not to allow the solvent to influence the molecular conformation significantly. This is, obviously not the case, and similar observations will be discussed later for c-CPC. We find that the VCD spectral differences between c-CAC in different solvents are as pronounced as those between CAC and c-CAC, indicating that ring closure and solvent effects influence the turn conformation nearly equally. Furthermore, we find that even a linear tripeptide, such as CAC, will exhibit a distinct solution phase VCD spectrum, indicating that on the time scale of molecular vibrations, solution structures do exist. VCD spectra of tripeptides (Ala-Ala-Ala and Pro-Pro-Pro) have been reported in the literature [6-7, 8], but their VCD spectra (in water) are different from the one observed here for CAC.

Figure 6-3 shows the calculated spectra of CAC and c-CAC by NECO method. This is done by assuming a γ-turn structure for c-CAC and adjusted γ-turn for linear CAC (see Fig. 6-1). The structure of linear CAC is adjusted by breaking down the S-S linkage, but maintain the γ-turn structure. Meantime, energy minimization is don by rotating the now free carbonyl group of Cys on C-terminal.

Comparing the results between observed and calculated VCD spectra, one can see a reasonable fit between two of them, which imply γ-turn probably exist in tripeptide solutions.

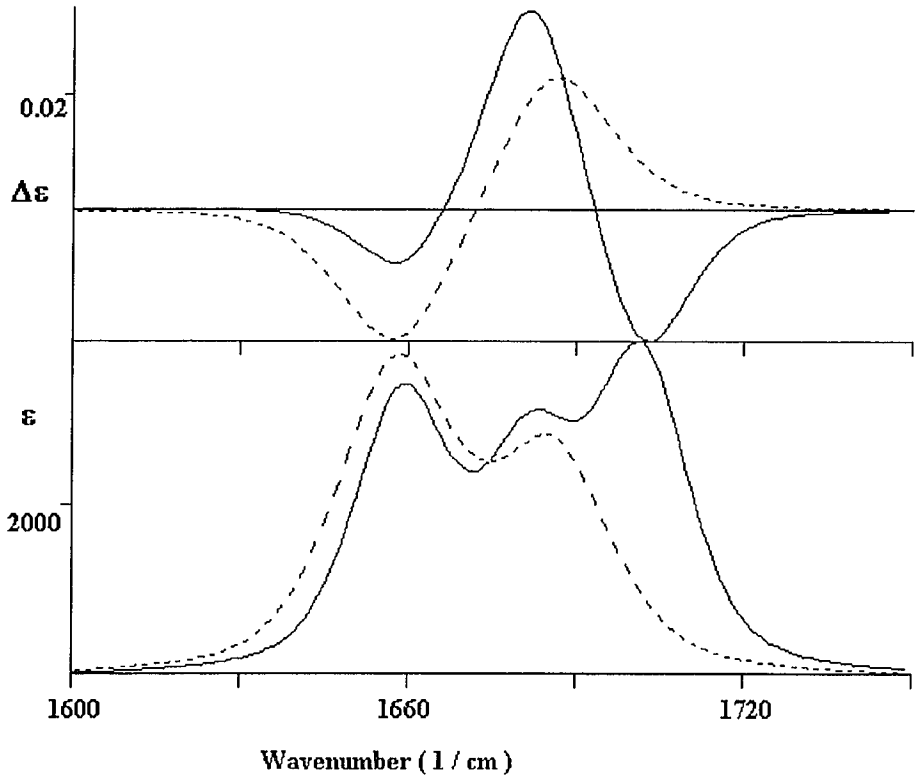

Fig.6.3 Calculated spectra of c-CAC (-) and CAC (---) by NECO.

6.2.2 Models of γ-turns (CPC and c-CPC)

Another pairs of tripeptides, linear Cys-Pro-Cys and cyclo-(Cys-Pro-Cys), are studied. The observed IR absorption and VCD spectra of c-CPC and its non-cyclic analogue CPC are shown in Figure 6-4 and 6-5.

The higher frequency absorption also observed in c-CPC in DMSO solution which is similar as in the c-CAC case. The VCD spectra of both CPC and c-CPC exhibit couplets at lower frequency comparing to CAC, which can be

explained that CPC contains a proline with a tertiary amine at the second position which usually produce a lower C=O stretching frequency. Furthermore, the CPC and c-CPC have similar IR absorption and VCD spectra with CAC and c-CAC, which might suggest that they have similar solution structures which is γ-turn.

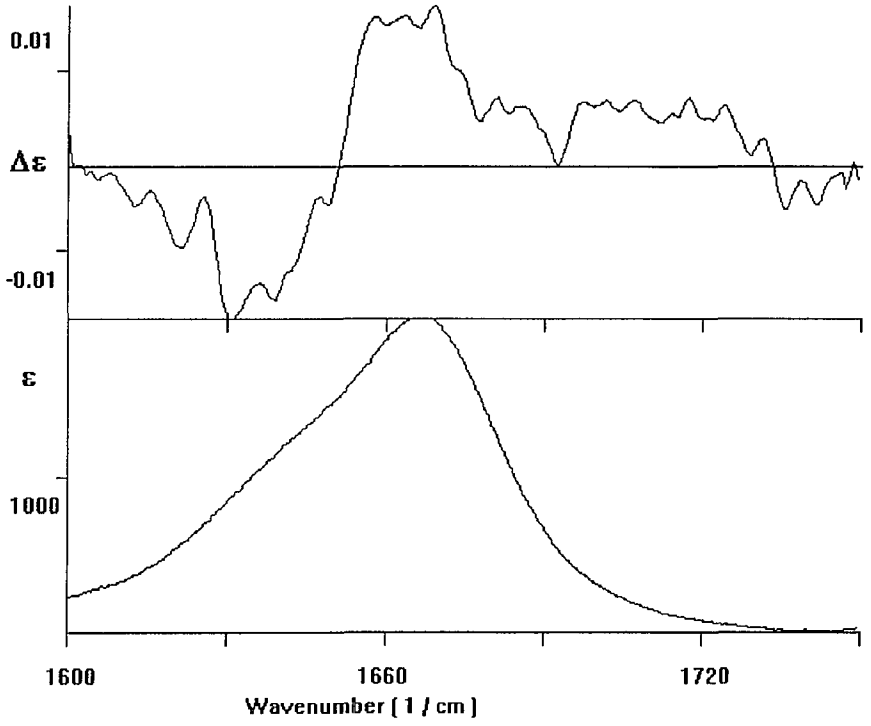

Fig.6-4 Linear tripeptide CPC in water; bottom, absorption and top, VCD.

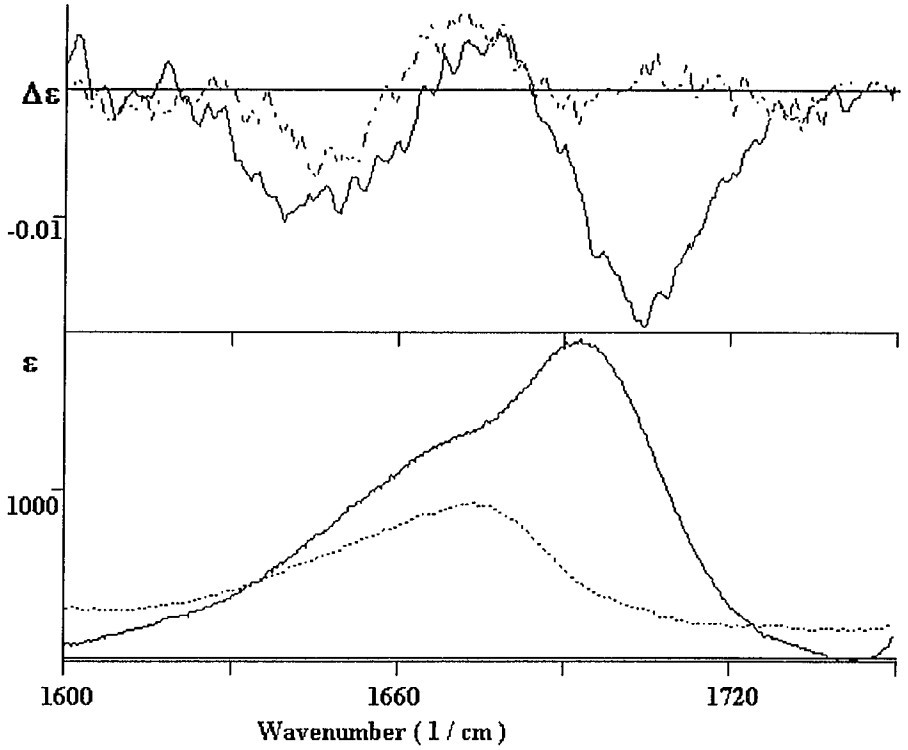

Fig.6-5 Observed IR (bottom) and VCD (top) of cyclized c(CPC) in DMSO (-) and in D_2O (--).

6.3 DISCUSSION:

VCD of polymeric models, such as homo-polyamino acids, has been reported previously [6-2, 3]. Thus, the spectral features of most of the major structural motif, such as α-helix, sheet and left-handed extended ("random coil") peptides, are well documented. Here, we discuss new spectral data on peptide turns observed in a selected small peptides, in which the peptide turns are caused by the formation of covalent linkages of S-S. Since VCD is a technique which monitors short distance interactions, its conformational sensitivity is particularly pronounced and useful in these small peptides. It offers the stereochemical sensitivity of chiroptical methods to the well established advantages of FTIR spectroscopy, which has been used extensively to investigate peptide and protein solution conformations.

γ-turn were studied in a number of peptides which were thought to be conformationally quite restricted, owing to the small ring size (in c-CAC), and the presence of proline residue (in CPC). In spite of its cyclic nature and the presence of the proline, c-CAC and c-CPC still exhibit flexibility in different polarity of solvents. This concludes that the interaction of the carbonyl groups with the solvent will produce minimum-energy conformations in which the alignment of the carbonyl groups may vary, even with the constraint of a relatively small (11 member) peptide ring [6-9].

Thus, two major conclusions may be drawn from these observations: first, even peptides termed " rigid " by some structural biochemists and biophysicists have enormous conformational freedom which manifests itself in slight changes of the equilibrium conformation when the peptide is subject to different surroundings. Second, VCD is a powerful method to monitor such changes in solution conformation.

6.4 REFERENCES:

6-1 M. Diem, (1994) in *Techniques and Instrumentation in Analytical Chemistry*, ed. N. Purdie and H. G. Brittain, Elsevier Amsterdam, pp. 91-130.

6-2 T. A. Keiderling, (1990) in *Practical Fourier Transform Infrared Spectroscopy: Industrial and Laboratory Chemical Analyses*, ed. J. R. Ferraro and K. Krishnan, Academic Press, New York, pp. 203-283.

6-3 S. C. Yasui, and T. A. Keiderling, (1986) *J. Am. Chem. Soc.*, 108, 5576.

6-4 S. S. Birke, I. Agbaje and M. Diem, (1992) *Biochemistry*, 31, 450.

6-5 M. Diem, G. M. Roberts, O. Lee and A. Barlow,(1988) *Appl. Spectrosc.*, 42, 20.

6-6 V. Madison and K. D. Kopple, (1980) *J. Am. Chem. Soc.*, 102,4855.

6-7 O. Lee, G. M. Robers and M. Diem, (1989) *Biopolymers*, 28, 1759.

6-8 R. K. Dukor, T. A. Keiderling and V. Gut, (1991) *Int. J. Pept. Prot. Research*, 38, 198.

6-9 P. Xie and M. Diem, (1995*), J. Am. Chem. Soc.*, 117, 429.

BIBLIOGRAPHY

Chapter One

1-1. *Thirteenth International School*, Erice, Sicily (1987). See: *Elemental and Molecular Clusters*, ed. by G. Benedek et al. (Springer-Verlag, New York).

1-2. *Fifth International Meeting on Small Particles and Metal clusters*, Konstanz, Germany, 1990. See: Zeits. Phys. D19, (1991); *Six International Meeting on Small Particles and Metal clusters*, Chicago, Illinois, 1992. See: *Zeits. Phys.* D26, (1993).

1-3. *International Symposium on the Physics and Chemistry of Small clusters*, NATO Advanced Workshop, Richmond, Virginia (1991). See: *Physics and Chemistry of Finit-Systems: From Clusters to Crystals*, edited by P. Jena and S. N. Khanna and B. K. Rao (Kluwer, Dordrecht, 1992).

1-4. *Symposium on Clusters and Cluster Assembled Materials Research Society Meeting*, Boston (1990). See: *MRS Symposium Series* 206, (1991).

1-5. *First International Conference on Nuclear and Atomic Clusters*, Turku, Finland (1991); *Second International Conference on Nuclear and Atomic Clusters*, Santorini, Greece (1993).

1-6. *Transition Metal Molecules*, W. Weltner and R. J. Van Zee, (1984) *Ann. Rev. Phys. Chem.* 35, 291.

1-7. *Clusters of Transition-Metal Atoms*, M. D. Morse, (1986) *Chem. Rev.* 86, 1049.

1-8. *Metal Clusters*, edited by M. Moskovits (Wiley, New York, 1986).

1-9. *Spectroscopy and Dynamics*, edited by M. A. Duncan, *Advances in Metal and Semiconductor Clusters* (JAI press, Greenwich CT, 1992).

1-10. T. H. Maugh, *Science*, (1983) 219, 474; 220, 592 (1983).

1-11. A. L. Robinson, *Science* 185, 772 (1974); 194, 1150 (1976).

1-12. J. H. Sinfelt, *Science*, (1977) 195, 641; *Acc. Chem. Res.* (1977) 10, 15.

1-13. J. Haggin, *Chem. & Eng. News*, page 32, Jan. 18 (1993).

1-14. J. F. Hamilton and P. C. Logel, *J. Catal.* (1973) 29, 253; *Photo. Sci. Eng.* (1974) 18, 507; *J. de Phys.* (1977) C2, 181.

1-15. G. A. Somorjai, *Acc. Chem. Res.* (1976) 9, 248.

1-16. C. Wang, S. Pollack, D. Cameron and M. M. Kappes, *J. Chem. Phys.* (1990) 93, 3787.

1-17. W. Harbich, S. Fedrigo, F. Meyer, D. M. Lindsay, J. Ligniers, J. C. Rivoal and D. Kreisle, *J. Chem. Phys.* (1990) 93, 8535.

1-18. E. C. Honea, A. Ogura, C. A. Murray, K. Raghavachari, W. O. Sprenger, M. F. Jarrold and W. L. Brown, *Nature* (1993) 366, 42.

1-19. M. E. Jacox, *J. Mol. Spectrosc.* (1985) 113, 286.

1-20. D. M. Lindsay, F. Meyer, and W. Harbrich, *Z. Phys.* (1989) D12, 15.

1-21. W. Harbich, S. Fedrigo, J. Buttet and D. M. Lindsay, *Optical Spectroscopy on Size Selected Gold Clusters Deposited in Rare Gase Solids, Z. Phys.* (1991) D19, 157.

1-22. W. Harbich, S. Fedrigo, J. Buttet and D. M. Lindsay, *Softlanding of Monodispersed Small Metal Clusters in Rare Gas Solids, Mater. Res. Soc. Symp. Ser.* (1991) 206, 369.

1-23. *R. Keller, in The Physics and Technology of Ion Sources*, edited by I. G. Brown (Wiley, New York, 1989), chap. 7.

1-24. K. Bescoke, S. Berger, W. O. Hofer and U. Littmark, *Radiat. Eff.* (1982) 66, 35.

1-25. W. Begemann, Ph. D. thesis, Universitat Bielefeld (1988).

1-26. E. M. Spain and M. D. Morse, *Int. J. Mass Spectrosc. Ion Phys.* (1990) 102, 183.

1-27. K. P. Huber and G. Herzberg, *Constants of Diatomic Molecules* (Van Nostrand, New York, 1979).

1-28. D. M. Cox, R. L. Whetten, M. R. Zakin, D. J. Trevor, K. C. Reichmann, and A. Kaldor, *Advances in Laser Science I*, edited by W. C. Stwalley and M. Lapp (Aip Conf. Proc. 146, 1986), pg. 527; *Z. Phys.* (1986) D3, 195.

1-29. M. Morse, *Chem. Rev.* (1986) 86, 1049.

1-30. Zhengdong Hu, Bo Shen, Qinwei Zhou, S. Deosaran, J. R. Lombardi, D. M. Lindsay and W. Harbich, *J. Chem. Phys.* (1991) 95, 2206.

1-31 C. Cosse, M. Fouassier, T. Mejean, M. Tranquille, D. P. DiLella and M. Moskovits, *J. Chem. Phys.* (1980) 73, 6076.

1-32. A. R. Gee, D. C. O'Shea and H. Z. Cummins, *Solid State Commun.* (1965) 4, 43.

1-33. P. R. R. Langridge-Smith, M. D. Morse, G. P. Hansen, R. E. Smalley and A. J. Merer, *J. Chem. Phys.* (1984) 80, 593.

1-34. W. Demtroder, *Laser Spectroscopy* (Springer-Verlag, Berlin, 1981).

1-35. T. A. Ford, H. Huber, W. Klotzbucher, E. P. Kunding, M. Moskovits and G. A. Ozin, *J. Chem. Phys.* (1977) 66, 524.

1-36. D. W. Green and D. M. Gruen, *J. Chem. Phys.* (1972) 57, 4462.

1-37. W. Klotzbucher and G. A. Ozin, *Inorg. Chem.* (1977) 16, 984.

1-38. M. Moskovits and W. Limm, *Ultramicroscopy,* (1986) 20, 83.

1-39. R. W. Wood, *Phil. Mag.* (1902) 4, 396.

1-40. R. J. H. Clark, *Raman, Resonance Raman and Electronic Raman Spectroscopy in Vibronic Processes in Inorganic Chemistry*, edited by C. D. Flint, NATO ASI Series (Kluwer Academic Publishers, 1989), page 301.

1-41. M. P. Andrews and G. A. Ozin, *J. Phys. Chem. Soc.* (1986) 90, 2852.

1-42. M. C. Manning and W. C. Trogler, *J. Amer. Chem. Soc.* (1983) 105, 5311.

1-43. F. A. Cotton and I, Shim, *J. Phys. Chem.* (1985) 89, 952.

1-44. S. P. Walch and C. W. Bauschlicher, *in Comparison of ab initio Quantum Chemistry with Experiment*, edited by R. J. Bartlett (Reidel, Boston, 1985).

1-45. Zhendong Hu, Bo Shen, Qinwei Zhou, S. Deosaran, J. R. Lombardi and D. M. Lindsay, *Proc. SPIE* (1992) 1599, 65.

1-46. We use units of nA-h (the product of the current times the deposition time in hours) where 1 nA-h = 2.25 x 10^{13} particles.

1-47. J. K. Bates and D. M. Gruen, *High Temp. Sci.* (1978) 10, 27; C. Steindruchel and D. M. Gruen, *J. Chem. Phys.* (1981) 74, 205.

1-48. W. Klotzbucher and G. A. Ozin, *Inorg. Chem*, (1980) 19, 3767.

1-49. *Handbook of Physics and Chemistry*, edited by R. C. Weast (chemical Rubber, Cleveland, 1975).

1-50. C. W. Bauschlicher, H. Partridge, S. R. Langhoff and M. Rosi, *J. Chem. Phys.* (1991) 95, 1057.

1-51. K. Balasubramanian and Ch. Ravimohan, *J. Chem. Phys.* (1990) 92, 3659.

Chapter Two

2-1 For a review of the early history of peptide synthesis, see Fruton, J.S. (1987) in *Peptides 1986*, Theodoropoulous, D. (ed.), Walter de Gruyte, Berlin, p. 25.

2-2 du Vigenaud, V., Ressler, C., Swann, J.M., Roberts, C.W. and Katsoyannis, P.G. (1954) *J. Amer. Chem. Soc.*, 76, 3115.

2-3 Bergmann, M. and Zervas, L. (1932) *Chem. Berichte*, 65, 1192.

2-4 Goddard, P., McMurray, J. S., Sheppard, R. C. and Emson, P. (1988) *J.Chem. Soc. Chem. Commun.*, 1025.

2-5 Merrifield, R. B. (1963) *J. Amer. Chem. Soc.*, 85, 2149.

2-6 Merrifield, R. B. (1964) *Biochemistry*, 3, 1385.

2-7 Kemp, D. S. (1973) in *Peptides 1971*. Nesvadba, H. (ed), North Holland, Amsterdam, p. 1.

2-8 Kemp, D. S., Choong, S. L. H. and Pekaar, L. (1974) *J.Chem. Soc.*, 4097.

2-9 Atherton, E., Logan, C. J. and Sheppard, R. C. (1981) *J. Chem. Soc., Perkin Trans.* 1, 538.

2-10 Carpino, L. A. and Han, G. Y. (1972) *J. Org. Chem.*, 37, 3404.

2-11 Kaiser, E., Colescott, R. L., Bossinger, C. D. and Cook, P. I. (1970) *Analyt. Biochem.*, 34, 595.

2-12 Sarin, V. K., Kent, S.B.H., Tam, J.P. and Merrifield, R.B. (1981) *Analyst. Biochem.*, 117. 147.

2-13 Kuhn, R., Winterstein, A. and Lederer, E. (1931) *Hoppe-Seyler's Z. Physiol. Chem.*, 197, 141.

2-14 Martin, A.J.P. and Synge, R.L.M. (1941) *Biochem. J.*, 35, 1358.

2-15 Consden, R., Gordon, A.H. and Martin, A.J.P. (1944) *Biochem. J.*,38, 224.

2-16 Howard, G.A. and Martin, A.J.P. (1950) *Biochem. J.*, 46, 532.

2-17 Hruby, V.J. (1993) *Proceedings of the Thirteenth American Peptide Symposium*, p. 3.

2-18 Norbert P.N. (1972) *Methods in Enzymology*, 25-6.

Chapter Three

3-1 Kuhn, W. (1958) *Ann. Rev. Phys Chem.* 9, 417.

3-2 L.Rosenfeld, (1929), *Z. Physik*, 52,161

3-3 E. U. Condon, (1937), *Rev. mod. Physics* 9, 432.

3-4 G. Holzwearth (1974) *J. Am. Chem. Soc.* 96, 252.

3-5 W. Moffitt and A. Moscowitz, (1959), *J. Chem. Physics* 30, 648

3-6 M. Diem, (1993), *Introduction to Modern Vibrational Spectroscopy*

3-7 L. A. Nafie (1976), *J. Am. Chem. Soc.* 98 2715.

3-8 L.A. Nafie and M. Diem (1979), *Accts. Chem. Res.* 12, 296.

3-9 L. A. Nafie and M. Diem (1979) *J. Am. Chem. Soc.* 101, 496.

3-10 M. Diem,. (1988), *Appl. Spectr.* 42, (1) 20-27.

3-11 O. Lee and M. Diem, (1992) *Analy. Instr.* 20(1) 23-43.

3-12 M. Diem, (1992), *SPIE Proceedings* 1681, 67-78.

3-13 Moffit, W., (1956) *J. Chem. Phys.*, 25, 467- 78.

3-14 C. W. Duetsche, (1969) *Ann. Rev. Phys. Chem.* 20 407-448.

3-15 Tinoco, I. (1963), *Radiation Research*, 20, 133-39.

3-16 Holzwarth, G. and Chabay, I. (1972), *J. Chem. Phys.* 57, 1632-1635.

3-17 T. R. Fraulkner (1977) *J. Chem. Chem. Soc.* 99, 8160-8168.

3-18 C. Marcott (1977) *J. Am. Chem. Soc.* 99, 8169-8175.

3-19 Birke, S. S. and Diem, M. (1992) *Biochemstry* 31, 450-455.

Chapter Four

4-1. Kabsch, W. and Sander, C., (1983) *Biopolymers*, 22, 2577-2637

4-2. Chou, P. Y. and Fasman, G.D., (1977) *J. Mol. Biol.*, 115, 135-175

4-3. Venkatachalam, C. M., (1968) *Biopolymers*, 6, 1425-1436

4-4. Lewis, P. N., Momany, F. A. and Scheraga, H.A., (1971)

Proc.Natl.Acad.Sci.USA, 68, 2293-2297

4-5. Zimmerman, S. S. and Scheraga, H.A., (1977) *Proc. Natl. Acad. Sci.USA*, 74, 4126-4129

4-6. Xie, P. and Diem, M., (1995) *J.Amer.Chem. Soc.*, 117, 429-437

4-7. Wyssbrod, H. and Diem, M., (1992) *Biopolymers*, 31, 1237 - 1242

4-8. Xie, P., Zhou, Q. and Diem, M., (1994) *Faraday Discussions.*, 99, in press

4-9. Xiang, T., Goss, D.J. and Diem, M., (1993) *Biophysical Journal*, 65, 1255-1261

4-10. Venkatachalapathi, Y.V. and Balaram, P., (1979) *Nature,* 281, 83-84.

4-11. Nair, C.M.K., Vijayan, M., Venkatachalapathi, Y.V. and Balaram, P., (1979) *J. Chem. Soc Chem.Commun.*, 1183-1184.

4-12. Venkatachalapathi, Y.V., Prasad, B.V.V and P. Balaram, (1982) *Biochemistry*, 21, 5502-5509

4-13. Hollosi, M., Kawai, M. K., Fasman, (1985) *Biopolymers,* 24, 211-242

4-14. Perczel, A., Hollosi, M., Foxman, B. M. and Fasman, G. D., (1991) *J.Amer.Chem.Soc.*, 113, 9772-9784

4-15. Hollosi, M., Majer,Z., Ronal, A.Z., Magyar, A., Medzihradsky, K., Holly, S. and Fasman, G.D., (1994) *Biopolymers*, 34, 177-185

4-16. Rose, G.D., Gierasch, L.M. and Smith, J.A., in Adv. Protein Chemistry, Anfinson, C.B., Edsall, J.T. and Richards, F.M., Eds., (1985), Academic Press, NY

4-17. Woody, R.W., in *Peptides, Polypeptides and Proteins,* E.R.Blout, F.A.Bovey, N.Lotan and M.Goodman, Eds., Wiley, New York, (1974) pp 338-350

4-18. Woody, R.W., in "*The Peptides: Analysis, Synthesis , Biology*", V.J. Hruby, Ed., Academic Press, New York, (1985) 15-113

4-19. Diem, M., Roberts, G.M., Barlow, A. and Lee, O., (1988) *Applied Spectrosc.*, 42, 20-28

4-20. Chandrasekaran, R., Lakshminarayana, A.V., Pandya, U.V. and Ramachadran, G.N.,
(1973). *Biochim. Biophys. Acta,* 303, 14-27

4-21. Rao, B.N.N., Kumar, A., Balaram, H., Ravi, A. and Balaram, P., (1983) *J.Am.Chem.Soc.*, 105, 7423-7428.

4-22. Imperiali, B. ,Fisher, S.L. Moats, R.I. and Prins, T. J., (1992). *J.Amer.Chem.Soc.* 114, 3182-3188.

4-23. Pease, L.G. and Watson, C., (1978), *J. Amer.Chem.Soc.*, 100, 1279-1286

4-24. Karle, I., (1978) *J. Amer.Chem.Soc.*, 100, 1286-1289

Chapter Five

5-1a B. N. Narrating Rae. (1983) *J. Am. Chem. Soc.*, 105,7423-28.

5-1b M.Hollosi and G.D.Fasman (1985), *Biopolymers* 24,211-241.

5-1c B. N. Rae,(1983), *J. Am. Chem. Soc.* 105,7423-7428.

5-2 Peter Y. Chou and G. D. Fasman. (1977) *J. Mol. Biol.* 115,135-175.

5-3a George D. Rose; Lila M. Gierash and John A Smith. *Adv. in Protein Chem.* (1985) 37,1-109.

5-3b K. Ramnarayam. (1994) *peptide research* 7, 270-278.

5-3c C.M. Wilmot and J. M. Thornton (1988) *J. Mol. Biol.* 203, 221-232.

5-3d H. J. Dyson. (1988) *J. Mol. Biol.* 201,161-200.

5-4 B. Imperiali. (1992) *J. Am. Chem. Soc.* 114, 3182-3188.

5-5 Andras Perczel. (1991) *J. Am. Chem. Soc.* 113,9772-9784.

5-6 M. Hollosi. G.D. Fasman. (1994) *Biopolymers* 34, 177-185.

5-7 Byler, M. and Susi, H. Biopolymers. (1986) 25, 269-287.

5-8 Kuntz, I. D. (1972) *J. Am. Chem. Soc.* 94, 4009-4012.

5-9 Angeletti, R. H., et. al. (1995) *Techniques in Protein Chemistry VII.*

Chapter Six

6-1 M. Diem, (1994) in *Techniques and Instrumentation in Analytical Chemistry*, ed. N. Purdie and H. G. Brittain, Elsevier Amsterdam, pp. 91-130.

6-2 T. A. Keiderling, (1990) in *Practical Fourier Transform Infrared Spectroscopy: Industrial and Laboratory Chemical Analyses*, ed. J. R. Ferraro and K. Krishnan, Academic Press, New York, pp. 203-283.

6-3 S. C. Yasui, and T. A. Keiderling, (1986) *J. Am. Chem. Soc.*, 108, 5576.

6-4 S. S. Birke, I. Agbaje and M. Diem, (1992) *Biochemistry*, 31, 450.

6-5 M. Diem, G. M. Roberts, O. Lee and A. Barlow,(1988) *Appl. Spectrosc.*, 42, 20.

6-6 V. Madison and K. D. Kopple, (1980) *J. Am. Chem. Soc.*, 102,4855.

6-7 O. Lee, G. M. Robers and M. Diem, (1989) *Biopolymers*, 28, 1759.

6-8 R. K. Dukor, T. A. Keiderling and V. Gut, (1991) *Int. J. Pept. Prot. Research*, 38, 198.

6-9 P. Xie and M. Diem, (1995*), J. Am. Chem. Soc.*, 117, 429.